Plasma enabled chemical value-product pathways from CO_2 and H_2, including methanol synthesis

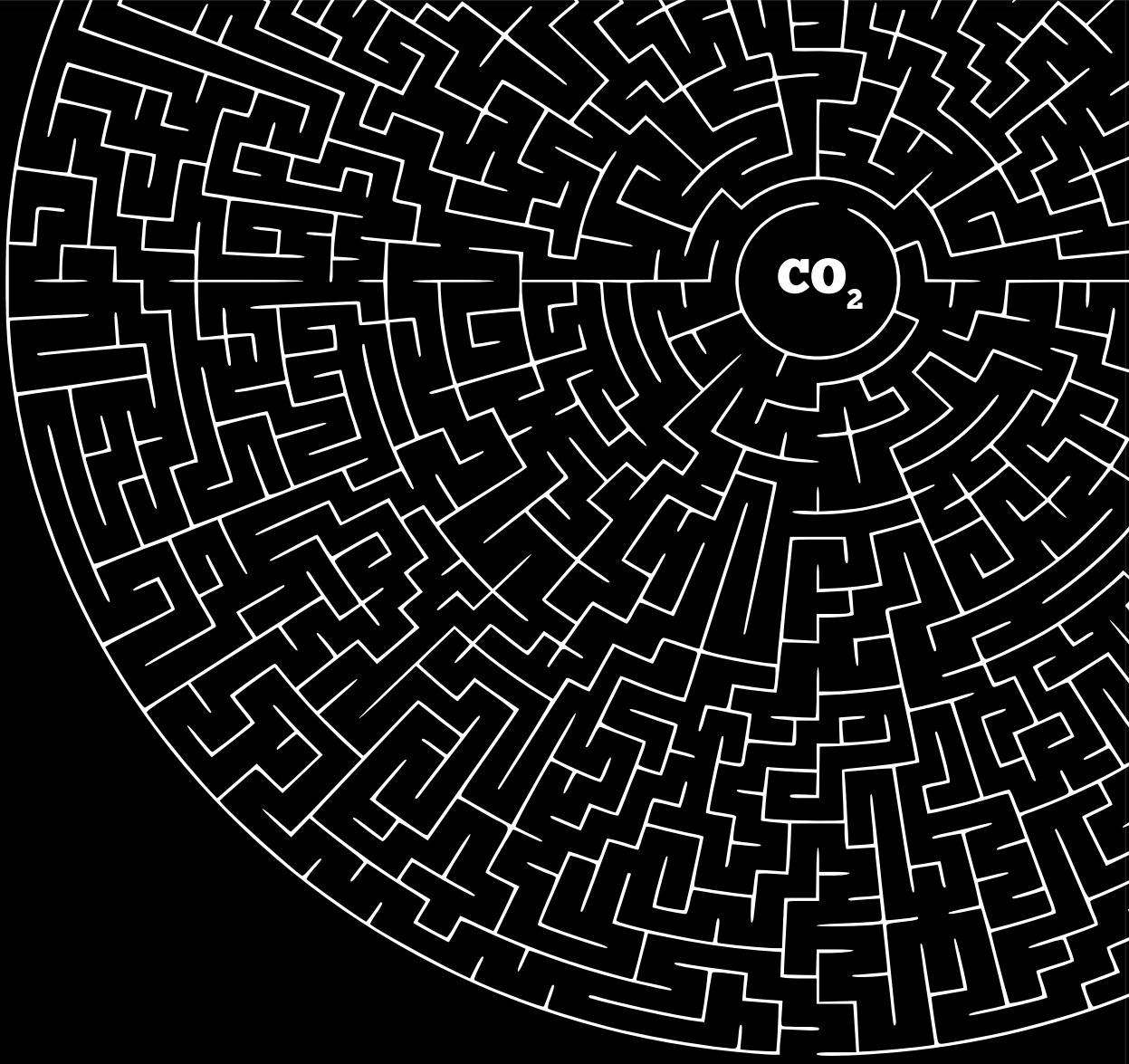

Plasma Enabled Chemical Value-Product Pathways from CO_2 and H_2, Including Methanol Synthesis

Rohit Chaudhary

Plasma enabled Chemical Value-Product Pathways from CO_2 and H_2, including Methanol Synthesis

PROEFSCHRIFT

ter verkrijging van de graad van doctor aan de Technische Universiteit Eindhoven, op gezag van de rector magnificus prof.dr.ir. F.P.T. Baaijens, voor een commissie aangewezen door het College voor Promoties, in het openbaar te verdedigen op donderdag 19 december 2019 om 16:00 uur

door

Rohit Chaudhary

geboren te Mumbai, India

Dit proefschrift van het proefontwerp is goedgekeurd door de promotoren en de samenstelling van de promotiecommissie is als volgt:

voorzitter:	prof.dr. F. Gallucci
1e promotor:	prof.dr. V. Hessel
2e promotor:	prof.dr.ir. G.J. van Rooij
leden:	prof.dr. J.C. Whitehead (The University of Manchester)
	prof.dr. A. Bogaerts (University of Antwerp)
	prof.dr.ir. M.C.M. van de Sanden
adviseur(s):	dr. L.J.P. van den Broeke (Tielo-Tech BV)
	dr. Q. Wang (SABIC)

Het onderzoek of ontwerp dat in dit proefschrift wordt beschreven is uitgevoerd in overeenstemming met de TU/e Gedragscode Wetenschapsbeoefening.

What we are today comes from our thoughts of yesterday,

and present thoughts build our life of tomorrow

- Gautama Buddha

This work was financially supported by STW (Foundation for Technical Sciences, the Netherlands)-Alliander Program on Plasma Conversion of CO_2, Project number: 13583.

Plasma enabled Chemical Value-Product Pathways from CO_2 and H_2, including Methanol Synthesis

Technische Universiteit Eindhoven, 2019

A catalogue record is available from the Eindhoven University of Technology Library

ISBN: 978-90-386-4935-1

Cover design by Rohit Chaudhary

Printed by GVO drukkers en vormgevers B.V, The Netherlands

This thesis is dedicated to my family and friends...

Table of Contents

Summary

S

Plasma enabled Chemical Value-Product Pathways from CO_2 and H_2, Including Methanol Synthesis

Relentless but periodic renewable green energy is available to humankind via solar source, and non-thermal plasma discharges offer a direct way to store this volatile green energy to chemical bonds. Converting CO_2 in this way can contribute to reducing the greenhouse effect, and provide additional opportunity for chemical processing, e.g. on-site production or decentralised, small scale production. CO_2 transformation includes a wide variety of applications from fuels to bulk and commodity chemicals mainly methanol. There are two possibilities to integrate CO_2 into methanol synthesis, viz. through syngas via reverse water-gas shift reaction and direct CO_2 hydrogenation to methanol. As an energy carrier, apart from methanol, methane, formaldehyde, formic acid, as well as higher hydrocarbons also offer attractive routes. The ozone production, analytical techniques, and surface treatment techniques have exploited plasma technology industrially. However, plasma technologies for synthesis of chemicals, bulk as well as fine, are underdeveloped for industrial applications. This PhD research as a part by STW (Foundation for Technical Sciences, the Netherlands)-Alliander Program on Plasma Conversion of CO_2, investigates and provides insight into different routes of plasma-assisted CO_2 hydrogenation to valuable products.

In this thesis, plasma-assisted hydrogenation of carbon dioxide is investigated by using Dielectric barrier Discharge (DBD) and a gliding arc (GA) reactor, as it has the potential for scale-up, evident from its industrial establishment in various fields. Three different routes have been investigated, reverse water-gas shift (RWGS), direct CO_2 methanation and methanol synthesis, via systematic reactor design and catalysts. The overall economic performance of the plasma-assisted CO_2 hydrogenation is assessed through techno-economic evaluation. This research aims to achieve higher energy efficiency, higher product yield, and a holistic

evaluation to give green and cheap solutions for the future industrialisation of plasma-assisted CO_2 valorisation. Moreover, the type of plasma source, different designs of plasma reactors and the influence of operation conditions are studied in pursuance of selectively forming desired products out of CO_2 hydrogenation. It is established that we can have the selective products from CO_2 depending on its further application.

The first part of the thesis we study the plasma-assisted non-catalytic reverse water-gas shift (RWGS) reactions to make syngas. The results and inferences of RWGS reaction carried out using a DBD reactor, are discussed in Chapter 2. In this chapter, a thorough optimisation of process and electrical parameters for the RWGS reaction in a DBD reactor is carried out. A burst mode operation is applied for the first time to the RWGS reaction in a DBD plasma reactor to improve the energy yield of the RWGS reaction. The outcome of this optimisation provides insight into the response of CO_2 hydrogenation reaction to the DBD plasma parameters, which proves beneficial in subsequent chapters to improve the process performance. The performance of the RWGS reaction in a DBD plasma reactor is reported in terms of CO_2 conversion, selectivity, yield and the energy efficiency by exploring a vast parameter space. The results of the RWGS reaction performed using a sinusoidal AC gliding arc reactor are presented in Chapter 3. The initial discussion revolves around the experiments performed to determine the operating regime of the gliding arc reactor. The burst mode (plasma on and off) function was used to control the gliding arc profile by manually inducing the termination of the arc. Once the operating regime of the gliding arc plasma is determined based on the reactor geometry and the electrical characterisation, then the effect study flow rate (residence time) and feed gas composition are explored. The bright light emitted from the gliding arc reactor was used to perform optical emission spectroscopy (OES) to identify species in the plasma. The results from the OES analysis were correlated with the reaction performance to postulate a plausible reaction mechanism. The selectivity of carbon monoxide is 100% with the gliding arc reactor

with the best value for the energy required to synthesise carbon monoxide as 4.8 moles/kWh.

In the second part of the thesis, we investigate the plasma-assisted catalytic hydrogenation of CO_2. Chapter 4 reports the direct methanation of CO_2 in a hybrid plasma-catalytic reactor using various packing materials including Rh/γ-Al_2O_3 catalyst. Their performances in the plasma discharge on the CO_2 hydrogenation are investigated and reported. The burst mode plasma operations were applied to improve energy efficiency. The first-time use of burst mode for plasma-catalytic CO_2 methanation is stated. The results for conversion, selectivity and energy yield are reported with a focus on methane formation. The Rh/γ-Al_2O_3 catalyst provided 97% methane selectivity. The characteristic behaviour of the Rh catalyst is used to speculate the reaction mechanism of the plasma-catalytic CO_2 methanation reaction. The higher fraction of hydrogen in the feed-gas mixture and the burst mode operation show a positive effect on methanation reaction in terms of improving methane selectivity as well as energy consumption. In the best-case scenario, 2.4 moles of methane is formed per kWh of energy consumed. Although DBD reactor demonstrates its ability to perform methanation at ambient pressure, it also highlights its limitation towards the formation of methanol or other hydrocarbon oxygenates. Hence, optimisation of the DBD plasma reactor design is done with the goal to achieve a controlled temperature profile in the reactor, as confirmed by thermal imaging. This has led to the design and fabrication of a water-electrode DBD plasma reactor, and its results are discussed in Chapter 5. A Pd-Au/γ-Al_2O_3 catalyst was synthesised and tested by this reactor under exposure to plasma. The selectivities of the liquid products formed by the chemical reaction, calculated based on total gas product composition, show substantial improvement in the selectivities of methanol and formaldehyde compared to that of a standard DBD reactor.

In the last part of the thesis, Chapter 6 presents the techno-economic assessment of the plasma-assisted CO_2 hydrogenation routes with the experimental data obtained from the preceding chapters. This method serves as a starting point to

make an estimate of the cost analysis to facilitate an ex-ante approach. The process designs based on plasma-assisted route for RWGS, methanol synthesis and methanation reactions are performed. The mass and energy flow data are obtained via Aspen simulations of the process models. Based on this data, capital and operating expenditures are calculated and reported. This study demonstrates the current state of plasma processes lacks competitiveness compared with the conventional technologies. This, however, helps to focus on the specific aspects that need to be addressed in order to improve the performance of the plasma processes.

The thesis is concluded with Chapter 7 where the outcomes of the aforementioned chapters are summarised with the future recommendations. In this thesis we adopt a holistic approach to studying plasma-assisted CO_2 hydrogenation reactions. The critical takeaway messages of this thesis can be summarised in simple words as buying selectivity with the expense of electricity. We recognise the potential of simple, flexible and environmentally green atmospheric pressure CO_2 hydrogenation plasma processes can prove to be an essential phase in the power to chemicals routes.

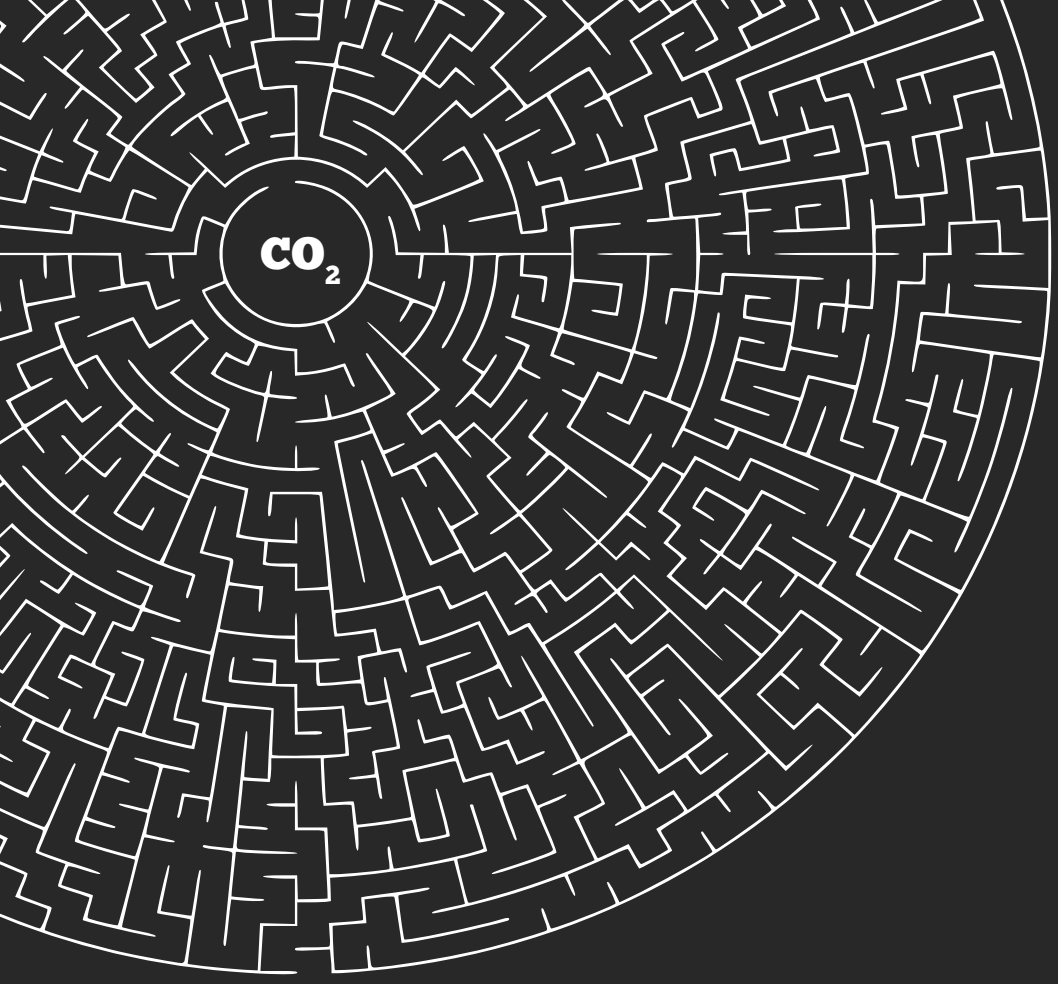
CO_2

Chapter 1

Introduction

1.1 Introduction

1.1.1 Carbon Capture and Utilisation

In recent years, the global consumption of energy has increased rapidly leading to a scarcity in the sources of energy, and also caused an increase in emission of thermodynamically stable greenhouse gases in the atmosphere [1]. One of the most significant contributors to greenhouse gas emission is CO_2 as it is the final product of all fossil fuels life-cycle. The CO_2 emission has been increasing exponentially over the past decades, 23 GT in 1990 to 36 GT in the year 2015 [2]. Figure 1.1 (a) and (b) show a clear correlation between CO_2 emission and average global surface temperature. It is evident that the use of non-renewable energy sources, such as coal, oil and gas dominate the contribution to CO_2 emissions, which is the result of ever-increasing global energy consumption.

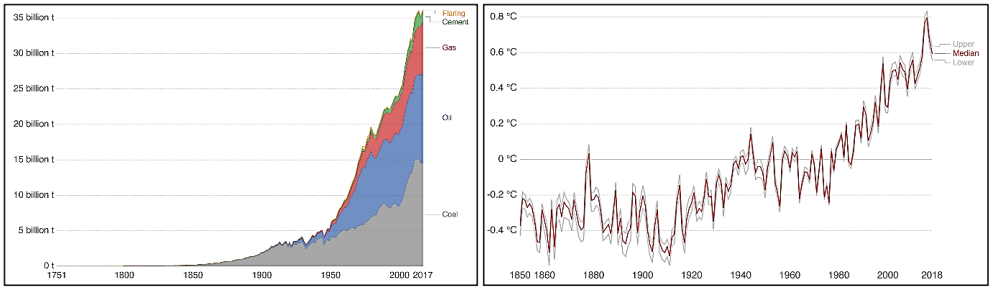

(a) (b)

Figure 1.1: *(a) Global CO_2 emission by fuel type, measured in tonnes per year [3], (b) Global average temperature anomaly, in °C. [4]*

To reduce CO_2 emissions, two strategies are being heavily explored today [5]. The working principle of these strategies gravitates towards the sequestration of CO_2. Sequestration is a process that entails separating CO_2 from emitting sources, moving it to a storage location, and isolating the compound permanently this pathway is known as carbon capture and storage (CCS). Whereas the other pathway

of carbon capture and utilisation (CCU) involves recycling the captured CO_2 directly in the industry, mainly as a raw material or converted it into chemicals and liquid fuels [6–8]. Currently, CCU has limited applications, and those can be roughly divided into two categories, the direct application (without an intermediate conversion process) and the indirect application. The direct applications consist of use as an inert agent for food packaging, in carbonated drinks, in refrigeration systems, in fire extinguishers, as a solvent, and for enhanced oil recovery (EOR). Moreover, the indirect applications comprise of the chemical production of urea, methanol and a wide variety of other products in small quantities [9,10]. Yet current the utilisation capacity is not sufficient and is eclipsed by the production capacity of CO_2 [11]. Hence realisation of industrially relevant CO_2 utilisation processes is necessary urgently. A few potential industrially relevant chemicals that can be synthesised from CO_2, and their market prices (in USD) are summarised in Figure 1.2, which underlines available fields of research to be explored.

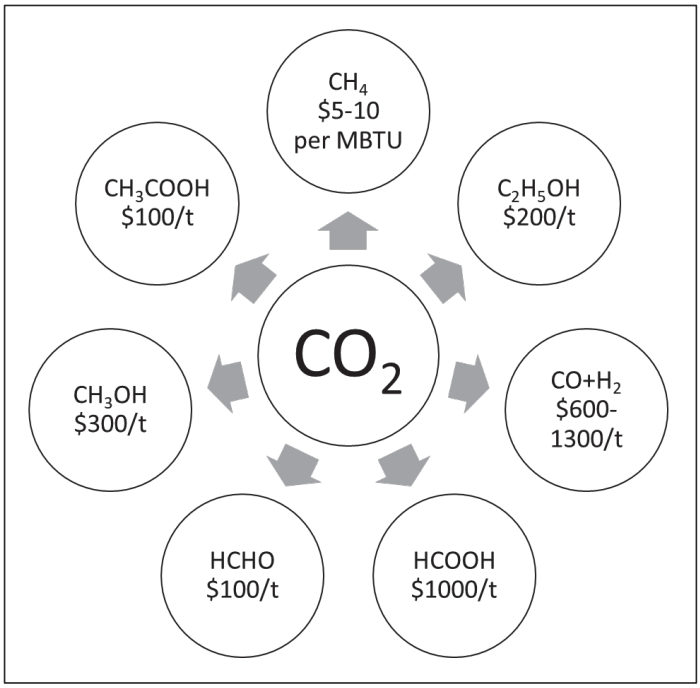

Figure 1.2: *CO_2 products and their current market price*

1.1.2 Surplus Energy to Chemicals

Energy is regarded as one of the most critical and fundamental requirements for human survival. The current trends in the consumption of energy have mostly been driven by the robust global economy and the ever-increasing global energy demand [12]. A report by McKinsey suggests that the share of renewable energy sources to satisfy the global energy demand is proliferating, and predicts that it will occupy 34% of the total primary energy demand in 2050 [13]. The sources of energy that are renewable in nature, such as wind and solar have been adopted by many countries worldwide currently and are set to become the dominant source of energy supply in the future [14]. With the higher share of renewable solar and wind energy in the electrical grid, the chances of temporal surplus are also immense, which causes the situations where the energy generation exceeds the demand. This temporal surplus resulting from intermittency of the renewable energy sources needs to be stored so that it can be used afterwards when the energy demand is higher or can be transported to the location of application [15,16]. Since renewable sources are available in nature, an endless supply of energy is evident, but there is a need to invent and use the advanced technologies which will maximise the supply for future demand.

The chemical route of the energy storage via the use of the recycled CO_2 provides a viable and sustainable solution along with the added benefit of CO_2 mitigation [17,18]. For instance, CO_2 can be converted into methanol using renewable energy, where the energy is stored. When this methanol is burned, the CO_2 is recaptured, thus, making the cycle CO_2-neutral [19]. The use of this waste CO_2 gas allows decreased spending in the conversion into chemicals, and this process complies with the environmental and green chemistry policy, given that the process used for such CO_2 conversions reaction itself is green [20]. If we look at the CO_2 hydrogenation reactions from a vantage point of Chemistry, then a variety of potential reactions are possible; however, the thermodynamic stability of CO_2 creates the significant restrictions to carry forward those reactions [21,22]. This

thesis explores a pathway via atmospheric pressure non-thermal plasma technology for CO_2 valorisation. Ozone production, analytical techniques, and surface treatment have exploited plasma technology industrially [23]. However, the plasma technologies for synthesis of chemicals, bulk as well as fine, are underdeveloped for industrial applications. The main reasons being lower product yield and energy inefficiency of plasma-assisted processes compared to that of conventional ones. Hence extensive research is required to investigate and optimise the plasma-assisted chemical synthesis processes.

1.1.3 Plasma-assisted Chemical Reactions

Plasma, considered as the fourth state of matter is generated via partially or entirely ionisation of a gas, and it consists of highly energetic electrons, neutral species, radicals, and excited atomic and molecular species [24]. The collisions of highly energetic electrons with other heavy species in the plasma assist ionisation and dissociation of CO_2, a thermodynamically stable molecule, via electronic, vibrational, or rotational excitation at ambient reaction conditions [25]. The CO_2 dissociation at low temperature with plasma was proven by numerous investigations of CO_2 in dielectric barrier discharge (DBD), corona, radio-frequency (RF), gliding arc (GA), and microwave (MW) plasmas [26–31]. Application of catalyst to such plasma system has shown improved activity through synergistic effect between plasma and catalyst [32–34]. When a catalytic reaction is carried out in plasma, these activated species by plasma generated in the gas phase or directly on the catalyst surface. Therefore, the role of energy supply to adsorb molecules on the catalyst surface is undertaken (partially) by plasma rather than heating in conventional reactions [35]. It is now well established from a variety of studies that the interaction within plasma and catalysts helps the reaction to take place even at ambient conditions [36–39]. The application of catalyst in plasma discharge leads to better selectivity of the desired products and suppression of unwanted by-products [40–42].

1.2 The Framework of the Thesis

The central theme of this thesis is to develop various routes of CO_2 valorisation with renewable H_2 activated by means of non-thermal plasma with a particular focus on the synthesis of methanol. Such an approach entails studies ranging from design and fabrication of plasma reactor, optimisation of plasma reactor performance with and without catalyst, studying active plasma species by optical measurements to postulate reaction mechanism and techno-economic study to understand the feasibility of industrialisation of studied plasma reactions for decentralised, small-scale production.

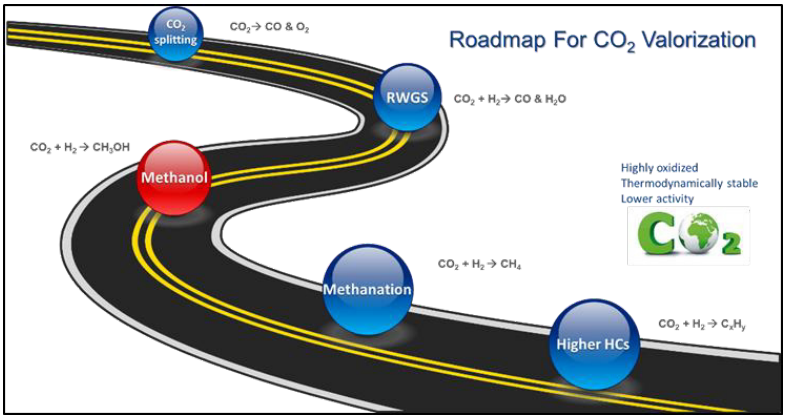

Figure 1.3: *Roadmap for CO_2 valorisation with H_2 through plasma reaction*

The roadmap has been created presenting the possible major products from CO_2 using plasma processes illustrated in Figure 1.3. Amongst all the schemes mentioned in the Figure CO_2 splitting is widely studied, but yet performed to benchmark and validate the performance of the dielectric barrier discharge (DBD) & gliding arc (GA) systems, compared to those reported in the literature (Appendix A1). As illustrated in the roadmap, the focus of the research has been dedicated towards the reverse water-gas shift (RWGS), direct methanation and methanol synthesis due to their significant industrial relevance and prospects of implementation.

Along with the investigation of chemical reaction processes by plasma, another focus of the research is on the continuous improvement of the plasma reactors design, to get maximum output for the reaction in consideration. In the present research, a setup (Appendix A2) to perform plasma catalytic CO_2 hydrogenation reactions was designed from scratch and built up, which allowed testing of various kinds of plasma reactors and their configurations. The best configuration for a DBD reactor was tested using CO_2 splitting as a probe reaction. The design and fabrication of two high capacity 3-D structured gliding arc reactors were done, and their preliminary tests were carried out in argon flow. However, their performance with the CO_2 hydrogenation reaction was not tested.

The techno-economic assessments were performed for new-window of opportunities for plasma-assisted CO_2 hydrogenation processes for small-scale decentralised production facility near the desired application location [43–45]. Small-scale decentralised production plants are advantageous over large-scale centralised production plants in new and emerging markets. Compared to full-scale plant decentralised small-scale plants have a lower investment entry point; as a result, investment risks are fewer. Small-scale plants adapt well with the flexible market as they have a fast reaction to the market situation, which can additionally benefit for the development of new markets. They can be installed directly at the site of product demand, or at the site of feedstock utilisation [46–49]. There is reduced commercial risk because although the cost-per-unit output of the first small-scale plant may be high, it will have and a reduced lag between investment and revenue generation. Technology is not mature; the process will need ongoing modifications and advancements. If the marketplace is volatile, there will need to be operational flexibility. If the feedstock is limited or isolated, there will need to be creative solutions to continue to meet demand.

The thesis is divided into three sections – non-catalytic reverse water-gas shift reaction (chapter 2 and 3), plasma-assisted catalytic CO_2 hydrogenation (chapter 4 and 5) and techno-economic evaluation of plasma-assisted CO_2 hydrogenation processes (Chapter 6).

The RWGS reaction was investigated using a DBD reactor, and the results are reported in Chapter 2. The optimisation of process and electrical parameters was performed for the RWGS reaction in a DBD reactor, and the outcome of this optimisation proved beneficial in subsequent chapters to improve the process performance. The performance of the RWGS reaction in a DBD plasma reactor is reported in terms of CO_2 conversion, selectivity, yield and the energy efficiency by exploring a vast parameter space. The burst mode was applied for the first time to the RWGS reaction in a DBD plasma reactor, and the findings are reported.

In Chapter 3, the RWGS reaction was carried using a sinusoidal AC gliding arc reactor. Firstly, the experiments were performed to determine the operating regime of the gliding arc reactor. The burst mode (plasma on and off) function was used to control the gliding arc profile by manually inducing the termination of the arc. The effect study flow rate (residence time) and feed gas composition were explored for particular electrical conditions fixed for this reactor geometry. The bright light emitted from the gliding arc reactor was used to perform optical emission spectroscopy (OES) to identify species in the plasma. The results from the OES analysis were correlated with the reaction performance to postulate a plausible reaction mechanism.

The direct methanation of CO_2 in a hybrid plasma-catalytic reactor was performed. For packing in the plasma discharge, different support materials and $Rh/\gamma\text{-}Al_2O_3$ catalyst were prepared, and their performances in the plasma discharge on the CO_2 hydrogenation were investigated and reported. The burst mode plasma operations were applied to improve energy efficiency. The first-time use of burst mode for plasma-catalytic CO_2 methanation is reported. The results for conversion, selectivity and energy efficiency were reported with a focus on methane formation. The intensity of the light emitted from the DBD plasma reactor was low, resulting in a very high signal to noise ratio, making it challenging to analyse the obtained spectra. Hence not all those results are reported in this thesis.

Optimisation of the DBD plasma reactor design was done with the goal to achieve a controlled temperature profile in the reactor, as confirmed by thermal imaging. This has led to the design and fabrication of a water-electrode DBD plasma reactor. Experiments were carried out to compare its performance with a standard DBD plasma reactor. A Pd-Au/γ-Al_2O_3 catalyst was synthesised and tested by this reactor under exposure to plasma. The selectivities of the liquid products formed by the chemical reaction were calculated based on total gas product composition. The effect of catalyst synergy with plasma was highlighted.

In Chapter 6, a techno-economic assessment of the plasma-assisted CO_2 hydrogenation routes was undertaken with the experimental data obtained from the preceding chapters. This was used as a starting point to make an estimate of the cost analysis to facilitate an ex-ante approach [50,51]. The process design based on plasma-assisted route for RWGS, methanol synthesis and methanation reactions was performed. The mass and energy flow data were obtained via Aspen simulations of the process models. Based on this data, capital and operating expenditures were calculated and reported.

In closing remarks of the thesis, Chapter 7 gives conclusions and outlook for the future.

References

[1] URI N D 1995 Energy Scarcity and Economic Growth Reconsidered *Energy Sources* **17** 277–94

[2] Olivier J and Peters J 2018 Trends in global CO_2 and total greenhouse gas emissions 2018 report *PBL Netherlands Environ. Assess. Agency* 53

[3] Quéré C 2018 Global Carbon Budget 2018 *Earth Syst. Sci. Data* **10** 2141–94

[4] Met Office Hadley Centre observations datasets (available at https://www.metoffice.gov.uk/hadobs/hadcrut4/data/versions/HadCRUT.4.6.0.0_release_notes.html, accessed on 28-08-2019)

[5] von der Assen N, Jung J and Bardow A A 2013 Life-cycle assessment of carbon dioxide capture and utilization: avoiding the pitfalls *Energy Environ. Sci.* **6** 2721

[6] Putting CO_2 to Use. *IEA,* 2019 (available at https://www.iea.org/publications/reports/PuttingCO2touse/ accessed on 28-08-2019)

[7] ENEA Consulting 2015 Energy and carbon for green chemistry **33** 8–9

[8] ENEA Consulting 2016 The Potential of Power-To-Gas **33** 51

[9] Aresta M 2010 Carbon Dioxide as Chemical Feedstock *Carbon Dioxide as Chem. Feed.* (Wiley-VCH Publishing)

[10] Benson S M and Orr F M 2008 *Carbon dioxide capture and storage* **33**

[11] Daza Y A and Kuhn J N 2016 CO_2 conversion by reverse water gas shift catalysis: comparison of catalysts, mechanisms and their consequences for CO_2 conversion to liquid fuels *RSC Adv.* **6** 49675–91

[12] Marchal V, Dellink R, Vuuren D Van, Clapp C, Château J, Lanzi E, Magné B and Vliet J Van 2011 OECD environmental outlook to 2050: Climate change chapter *OECD* 90

[13] McKinsey Global Institute 2019 Global Energy Perspective 2019 : Reference Case *Energy Insights* 31

[14] 2017 *Market Report Series: Renewables 2017 Analysis and Forecasts to 2022*

[15] Oberschmidt J, Klobasa M and Genoese F 2013 *Techno-economic analysis of electricity storage systems* (Woodhead Publishing)

[16] Rahman F, Baseer M A and Rehman S 2015 *Assessment of Electricity Storage Systems* (Elsevier)

[17] Goede A and van de Sanden R 2016 CO_2 -Neutral Fuels *Europhys. News* **47** 22–6

[18] Van Kranenburg K, Schols E, Gelevert H, De Kler R, Van Delft Y and Weeda M 2016 Empowering the chemical industry. Opportunities for electrification. 32

[19] Olah G, Prakash G K S and Goeppert A 2011 Anthropogenic chemical carbon cycle for a sustainable future *J. Am. Chem. Soc.* **133** 12881–98

[20] Słoczyński J, Grabowski R, Olszewski P, Kozłowska A, Stoch J, Lachowska M and Skrzypek J 2006 Effect of metal oxide additives on the activity and stability of $Cu/ZnO/ZrO_2$ catalysts in the synthesis of methanol from CO_2 and H_2 *Appl. Catal. A Gen.* **310** 127–37

[21] Müller K, Mokrushina L and Arlt W 2014 Thermodynamic constraints for the utilization of CO_2 *Chemie-Ingenieur-Technik* **86** 497–503

[22] Darensbourg D J 2010 Chemistry of carbon dioxide relevant to its utilization: A personal perspective *Inorg. Chem.* **49** 10765–80

[23] Kogelschatz U, Eliasson B and Egli W 1999 From ozone generators to flat television screens: history and future potential of dielectric-barrier discharges *Pure Appl. Chem.* **71** 1819–28

[24] Bittencourt J A 2004 *Fundamentals of Plasma Physics* (Springer)

[25] Fridman A 2008 *Plasma Chemistry* **48** (Cambridge University Press)

[26] Zheng G, Jiang J, Wu Y, Zhang R and Hou H 2003 The Mutual Conversion of CO_2 and CO in Dielectric Barrier Discharge (DBD) *Plasma Chem. Plasma Process.* **23** 59–68

[27] Yang R, Zhang D, Zhu K, Zhou H, Ye X, Kleyn A W, Hu Y and Huang Q 2019 In situ study of the conversion reaction of CO_2 and CO_2-H_2 mixtures in radio frequency discharge plasma *Acta Phys. -Chim. Sin.* **35** 292–8

[28] Heijkers S, Snoeckx R, Kozák T, Silva T, Godfroid T, Britun N, Snyders R and Bogaerts A 2015 CO_2 Conversion in a Microwave Plasma Reactor in the Presence of N_2 : Elucidating the Role of Vibrational Levels *J. Phys. Chem. C* **119** 12815–28

[29] Bongers W, Bouwmeester H, Wolf B, Peeters F, Welzel S, van den Bekerom D, den Harder N, Goede A, Graswinckel M, Groen P W, Kopecki J, Leins M, van Rooij G, Schulz A, Walker M and van de Sanden M C M

2017 Plasma-driven dissociation of CO_2 for fuel synthesis *Plasma Process. Polym.* **14** 1600126
[30] Wang W, Mei D, Tu X and Bogaerts A 2017 Gliding arc plasma for CO_2 conversion: Better insights by a combined experimental and modelling approach *Chem. Eng. J.* **330** 11–25
[31] Wen Y and Jiang X 2001 Decomposition of CO_2 using pulsed corona discharges combined with catalyst *Plasma Chem. Plasma Process.* **21** 665–78
[32] Wang L, Yi Y, Guo H and Tu X 2017 Atmospheric Pressure and Room Temperature Synthesis of Methanol through Plasma-Catalytic Hydrogenation of CO_2 *ACS Catal.* **8** 90–100
[33] Kyriakou V, Vourros A, Garagounis I, Carabineiro S A C, Maldonado-Hódar F J, Marnellos G E and Konsolakis M 2017 Highly active and stable TiO_2-supported Au nanoparticles for CO_2 reduction *Catal. Commun.* **98** 52–6
[34] Holzer F, Kopinke F D and Roland U 2005 Influence of ferroelectric materials and catalysts on the performance of Non-Thermal Plasma (NTP) for the removal of air pollutants *Plasma Chem. Plasma Process.* **25** 595–611
[35] Whitehead J C 2010 Plasma catalysis: A solution for environmental problems *Pure Appl. Chem.* **82** 1329–36
[36] Wang Q, Yan B H, Jin Y and Cheng Y 2009 Dry reforming of methane in a dielectric barrier discharge reactor with Ni/Al_2O_3 Catalyst: Interaction of catalyst and plasma *Energy and Fuels* **23** 4196–201
[37] Nozaki T and Okazaki K 2013 Non-thermal plasma catalysis of methane: Principles, energy efficiency, and applications *Catal. Today* **211** 29–38
[38] Vidal A B, Feria L, Evans J, Takahashi Y, Liu P, Nakamura K, Illas F and Rodriguez J A 2012 CO_2 activation and methanol synthesis on novel Au/TiC and Cu/TiC catalysts *J. Phys. Chem. Lett.* **3** 2275–80
[39] Ma X, Li S, Ronda-Lloret M, Chaudhary R, Lin L, van Rooij G, Gallucci F, Rothenberg G, Raveendran Shiju N and Hessel V 2019 Plasma Assisted Catalytic Conversion of CO_2 and H_2O Over Ni/Al_2O_3 in a DBD Reactor *Plasma Chem. Plasma Process.* **39** 109–24
[40] Liu C, Eliasson B, Xue B, Li Y and Wang Y 2001 Zeolite-enhanced plasma methane conversion directly to higher hydrocarbons using dielectric-barrier discharges *React. Kinet. Catal. Lett.* **74** 71–7
[41] Zhang K, Eliasson B and Kogelschatz U 2002 Direct Conversion of Greenhouse Gases to Synthesis Gas and C4 Hydrocarbons over Zeolite HY Promoted by a Dielectric-Barrier Discharge *Ind. Eng. Chem. Res.* **41** 1462–8
[42] Aghamir F M, Matin N S, Jalili A H, Esfarayeni M H, Khodagholi M A and Ahmadi R 2004 Conversion of methane to methanol in an AC dielectric barrier discharge *Plasma Sources Sci. Technol.* **13** 707–11
[43] Anastasopoulou A, Butala S, Patil B, Suberu J, Fregene M, Lang J, Wang Q and Hessel V 2016 Techno-Economic Feasibility Study of Renewable Power Systems for a Small-Scale Plasma-Assisted Nitric Acid Plant in Africa *Processes* **4** 54
[44] Anastasopoulou A, Hessel V and Rooij G J van 2018 *Conceptual process design of plasma-assisted nitrogen fixation through energy, environmental and economic assessment* (Eindhoven University of Technology)
[45] Hessel V, Anastasopoulou A, Wang Q, Kolb G and Lang J 2013 Energy, catalyst and reactor considerations for (near)-industrial plasma processing and learning for nitrogen-fixation reactions *Catal. Today* **211** 9–28
[46] Hessel V 2014 Special Issue: Design and Engineering of Microreactor and Smart-Scaled Flow Processes *Processes* **3** 19–22
[47] Li S, Medrano J A, Hessel V and Gallucci F 2018 Recent progress of plasma-assisted nitrogen fixation research: A review *Processes* **6** 248
[48] GE Oil and Gas report 2014, The definitive guide to small-scale liquefied natural gas (lng) plants helping you harness the energy of opportunity
[49] ARPA-E 2017 Funding Opportunity Announcement Advanced Research Projects Agency – Energy Macroalgae Research Inspiring Novel Energy
[50] Wang Q, Spasova B, Hessel V and Kolb G 2015 Methane reforming in a small-scaled plasma reactor - Industrial application of a plasma process from the viewpoint of the environmental profile *Chem. Eng. J.* **262** 766–74
[51] Roes A L, Alsema E A, Blok K and Patel M K 2009 Ex-ante environmental and economic evaluation of polymer photovoltaics *Prog. Photovoltaics Res. Appl.* **17** 372–93

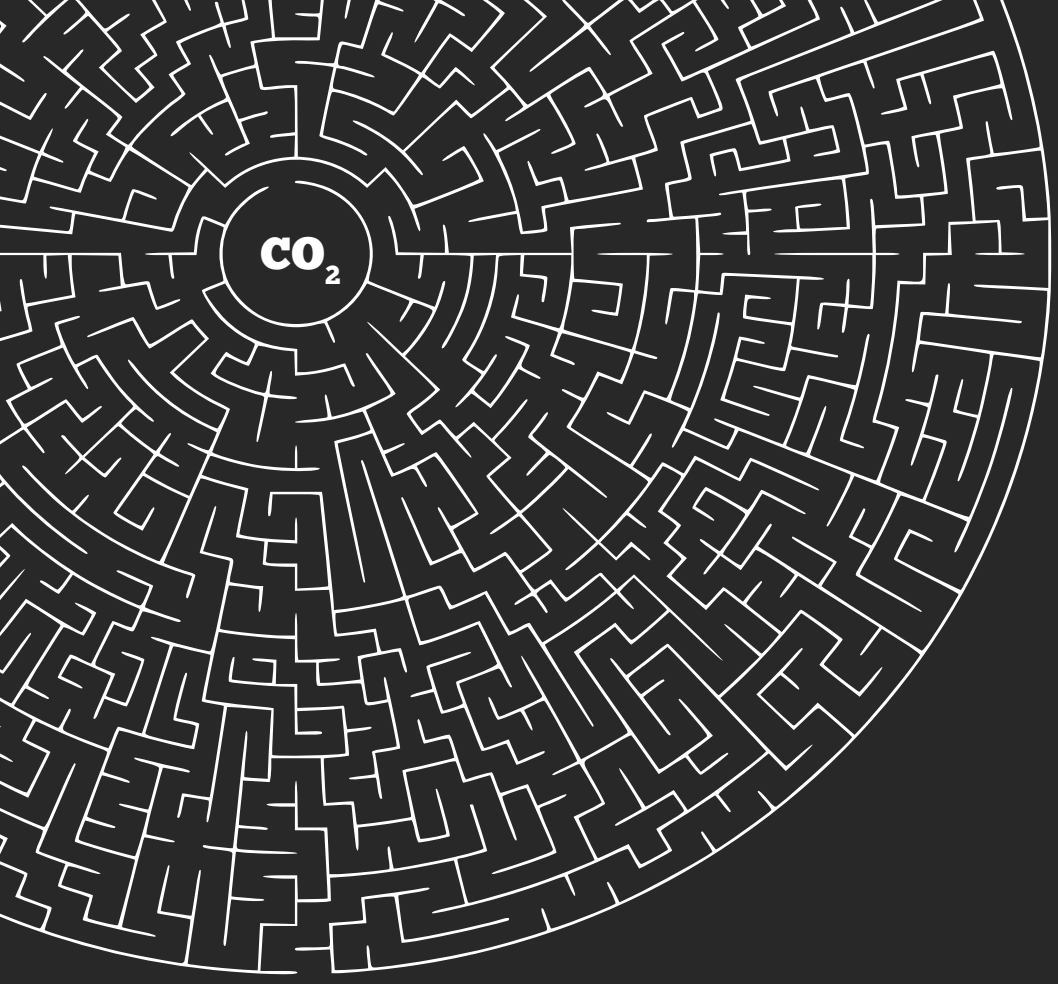
CO_2

Chapter 2

CO_2 to CO - Reverse water-gas shift reaction in dielectric barrier plasma discharge, with view on practical uses

This chapter is based on:

Low-temperature, atmospheric pressure reverse water-gas shift reaction in dielectric barrier plasma discharge, with outlook to use in relevant industrial processes, Chaudhary, R., van Rooij, G., Li, S., Wang, Q., Hensen E., Hessel, V., Submitted to Chemical Engineering Science.

Abstract.

Plasma discharges offer a direct way to convert electrical to chemical energy and to store volatile renewable energy sources. Converting CO_2 in this way can contribute to reducing the greenhouse effect, and provide additional opportunity for chemical processing, e.g., on-site or on a small scale. The CO_2 hydrogenation to CO via the reverse water-gas shift reaction (RWGS) generates synthesis gas for use as feedstock to different fuels and chemicals. The RWGS reaction carried out in a Dielectric Barrier Discharge (DBD) plasma reactor benefits from operation at ambient pressure and mild temperature, as compared to the harsher conditions of conventional RWGS processing. To develop that with outlook to real-life uses key performances need to be achieved; that is, i.a., a threshold CO_2 conversion, a high CO selectivity at low impurity (low CH_4 selectivity), and a high (H_2 – CO_2)/(CO + CO_2) ratio (favourable for high reaction rates) as well as tolerable energy efficiency. Central plasma process parameters for this are the feed gas ratio, residence time, and uniformly distributed microdischarges. The optimisation of an individual key performance can be adverse to the other so that the process exploration is a task. This gives room to introduce new plasma operation types, and the burst mode was applied for the first time to the RWGS reaction in the present work. By this fast (millisecond) periodic switching on and off the plasma, the process temperature can be reduced as well as a better microdischarge distribution can be achieved. The residence time is not only set by the flow rate, as commonly done, but also by taking the discharge gap as an additional parameter of freedom, which also impacts the reducing distribution. As a result of relevant process conditions, a CO_2 conversion of 50%, a CO selectivity of 99%, a CH_4 selectivity <3%, and a (H_2 –CO_2)/(CO + CO_2) ratio of 2, and energy yield of 337 mmol/kWh is obtained.

2.1 Introduction

The pressing global concern over the last decades has been climate change to which the emission of greenhouse gases, mainly carbon dioxide (CO_2), greatly contributes. In 2016 the amount of anthropogenic CO_2 release was 36 Gt, and in 2050 it is projected to be 55 Gt in a business as usual scenario. This greenhouse effect has caused an increase in global surface temperature with all its negative impacts [1]. The rate of natural recycling of CO_2 is unable to compensate for the rate of CO_2 emissions due to human activities [1,2]. Various approaches have been developed to decrease CO_2 release. Among them is the use of CO_2 as a feedstock for the synthesis of chemicals and fuels, which creates value products with the option for renewable energy storage. The demand for CO_2 is estimated to reach 140 Mtpa by 2020. However, its availability is 150 times higher, leaving much room for new, innovative process solutions [3]. This makes the CO_2 feedstock also interesting as alternative bio-based feedstock, when that use is not practical, leads to environmental concerns, or competes with the primary use as food [2,4–11].

Many of the chemical process technologies proposed to involve the splitting of the CO_2 molecule to generate CO with O_2 as a by-product (equation 2.1).

$$CO_2 \leftrightarrow CO + \tfrac{1}{2}\, O_2 \qquad \Delta H_{25°C} = 283\ \mathrm{kJ/mol} \tag{2.1}$$

Undergoing a reaction with CO_2 is a challenge, as it is highly oxidised, thermodynamically stable and relatively unreactive. Hence, huge energy input is required to transform CO_2 into other chemicals. For example, a temperature in excess of 2000 K is required to perform its thermal decomposition to CO.

CO can be classically produced by the Boudouard reaction of CO_2 with carbon [12,13]. It is further produced by partial oxidation of carbon-containing compounds from various sources such as coal gas or biomass. Significant amounts of by-products are also formed during oxidative processes for the production of chemicals, or during iron smelting as part of steel manufacture. For safety reasons, there is a request for on-site and on-demand production of CO to fully replace tube trailer or

cylinder supply. This eliminates transportation and storage of the toxic gas and no hazardous handling of gas during cylinder or trailer exchange. Haldor Topsoe's carbon monoxide generator (eCOs™) allows safe and efficient on-demand CO production from food or beverage grade CO_2 through electrolysis at the site where the gas is needed. The standard purity is 99.0%, with modifications as high as 99.999 vol% [14]. This serves environmental, metallurgical, pharmaceutical, industrial hygiene and safety, and laboratory applications. It has found an industrial entry at a scale of 96 Nm^3/h; Gas Innovations Company, US [15].

Synthesis gas (syngas), the mixture of CO with H_2, is a crucial industrial reactant for producing many significant bulk and speciality chemicals. One prime example is the Fischer–Tropsch process yielding hydrocarbons, which can be used as fuel. Besides, a broad product reach is given towards, e.g., methanol, formaldehyde, or dimethyl ether, which are considered the backbone of chemical, dyes, food and even pharmaceutical industry

The oxygen content in the syngas, however, can harm the chemical synthesis by oxidation of the products or poisoning of the catalysts. Therefore, the oxygen content of the syngas is commonly eliminated before use in a chemical transformation [16]. Yet, there is a possibility to synthesise oxygen-free CO directly from CO_2, as given for the reverse water gas shift (RGWS) reaction (equation 2.2). In RWGS, CO_2 undergoes hydrogenation to CO on the expense of some H_2 which is converted to H_2O.

$$CO_2 + H_2 \leftrightarrow CO + H_2O \qquad \Delta H_{25°C} = 42.1\ \mathrm{kJ/mol} \tag{2.2}$$

The RWGS reaction is an endothermic reaction and thus favoured at high temperatures. At atmospheric pressure, the RWGS reaction requires more than 1000 K to achieve 50% conversion of CO_2. Therefore, to overcome the thermodynamic barrier in this reaction, it is always carried out at a high temperature and high pressure [17–21]. Industrial applications of the syngas produced by RWGS were already mentioned above and are similar to the CO_2 splitting. The manufacture of methanol in two steps by syngas (e.g. from RWGS) and directly in one step from

RWGS have been compared by Aspen process modelling [22–24]. There is a considerable difference in process equipment, operating conditions, economics, and seemingly it can target selectivity as a key performance parameter. Interestingly and as now more a curiosity, the RWGS reaction might be used with prime intention to generate water which is then split by electrolysis into O_2 and H_2. The latter is recycled. This so-called *in situ* resource utilisation (ISRU) is considered to produce oxygen on the planet Mars, where CO_2 availability is abundant (95% in the atmosphere) [25,26].

Current techniques for RWGS require high temperature and/or high pressure resulting in high material and operating costs. Kusama et al. obtained 88% CO selectivity and 52% CO_2 conversion at 200 °C using Rh/SiO_2 as the catalyst but needed a high pressure of 50 bar [27]. Lu et al. reported the performance of RWGS at atmospheric pressure, but the higher temperature of 900 °C, i.e. they obtained 100% CO selectivity at 55% CO_2 conversion using Nickel-based catalyst [28].

It would be more desirable to perform the reaction at lower temperature and atmospheric pressure. This has encouraged researchers to explore alternative processing featuring mild reaction conditions such as electrochemical, photocatalytic [29–32] and non-thermal plasma processes. Amongst them, non-thermal plasma is being extensively researched for many applications of CO_2 valorisation, viz. CO_2 splitting, dry methane reforming and direct CO_2 hydrogenation [33–36]. A striking advantage, as compared to conventional catalytic processes, is the ability to activate CO_2 at ambient conditions. In non-thermal plasma, the energy provided through electricity is used to generate high-temperature electrons with cold ions and neutral gas molecules, causing a state of non-equilibrium. These highly energetic electrons collide with cold molecules leading to dissociation reactions, consequently forming reactive radicals.

Atmospheric-pressure, non-thermal plasmas produced via barrier discharge are known for their high energy input (~1-10 eV/molecule) [37]. Dielectric Barrier Discharge (DBD) plasmas have been reported to carry out such CO_2 valorisation

reactions [34,38–44]. But till this date very limited work has been reported on the RWGS reaction carried out with non-thermal plasma. Eliasson et al. showed that it is possible to hydrogenate CO_2 in a non-thermal DBD plasma reactor and reported CO_2 conversions of 12% without catalyst, producing mainly CO [45]. Zeng and Tu obtained 7.5% conversion of CO_2 in a DBD for the non-catalytic case with CO selectivity of 45% which was enhanced to 10.2 and 77.7% respectively, by using Mn/Al_2O_3 catalyst when using 1:1 ratio of CO_2 to H_2 [46]. They report improvement in the reaction performance to 55% CO_2 conversion with 92% CO selectivity when using 1:4 ratio of CO_2 to H_2 [47]. Dobrea et al. achieved about 76% CO_2 conversion for 1:1 ratio of CO_2 and H_2 in a low-pressure microwave discharge but at the expense of very high power input of 600W [48]. Kano et al. reported a CO_2 conversion of 20–30% by hydrogenation of CO_2 in low-pressure radio frequency (RF) impulse discharge with CO selectivity between 80–90% [49].

The research presented in this article involves the experimental investigation of the non-catalytic plasma-assisted RWGS reaction to obtain oxygen-free CO, in a DBD reactor operated at ambient pressure and low temperature (100 °C). To reduce the total power consumption while increasing the productivity, the burst mode DBD technique has been implemented, and the principle is explained below [50]. With an outlook on the industrial perspective of using the technique, e.g. toward methanol synthesis, key performances need to be reached, which are specified in the discussion below. Those are a threshold CO_2 conversion, a high CO selectivity at low impurity (low CH_4 selectivity), and $(H_2 - CO_2)/(CO + CO_2)$ ratio about 2 (favourable for high reaction rates) as well as tolerable energy efficiency [51].

Previous research of our group has used such process target specifications (given by the industrial partner Evonik Industries) to guide experimental investigations for nitrogen fixation (NO_x from air) [43,52] towards a ‘window of opportunity’ (a conceptual business case), which Evonik had further developed and marketed [53]. Based on those achieved target specifications and realistic trajectories to improved outcome, a full-process scenario (with up- and down-stream processing) was developed at relevant industrial scale, by Aspen process modelling [54,55].

The sustainability of that was assessed by cost calculations and environmental impact check through the life-cycle assessment to study the impact of using different options of renewable sources, available at different countries, simulated as energy system (microgrid, energy source, battery) [56]. Those studies could give insight in the validity of new business models such as small-scale and distributed production, used for industry transformation, e.g. in the field of agriculture ('Green fertiliser; Fertilizing with Wind') [53,57].

2.2 Experimental Section

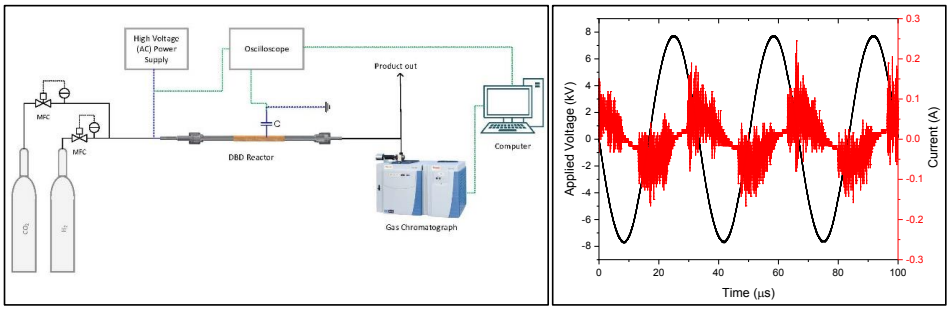

(a) (b)

Figure 2.1 *(a) Schematic representation of the experimental setup (b) A typical voltage-current waveform*

The schematic of the experimental setup is shown in Figure 2.1 (a). The plasma experiments were carried out in a cylindrical quartz reactor. Here, the quartz serves as the reactor wall as well as a dielectric barrier that is required for the generation of the plasma discharge. The outer diameter of the quartz reactor is 13 mm, and the inner diameter is 10 mm, giving a dielectric barrier thickness of 1.5 mm. The discharge zone in the reactor is 100 mm long. The diameter of the stainless steel axial inner electrode was set to 7, 8 or 9 mm corresponding to discharge gaps of 1.5, 1.0 and 0.5 mm with 16.0, 11.3 and 5.9 ml of reactor volume, respectively. A conductive silver coating on the outside of the quartz cylinder serves as a ground electrode (Appendix A1). An oven is used for heating the DBD reactor to avoid condensation of

liquid products inside the reactor. The DBD reactor is powered by an AC high voltage power supply (AFS G15S-150K). All electrical signals were recorded by a 4 channel oscilloscope (Picoscope® 3405D). The applied voltage (U) across the DBD reactor is measured with a 1:1000 high voltage probe (Tektronics P6015A). An external capacitor (100nF) is connected between the ground electrode and the grounding point, and the voltage across this capacitor is measured using a 1:10 voltage probe. The typical discharge signal is shown in figure 2.1(b), where the small spikes in red correspond to the microdischarges in the discharge. The voltage measured by this probe gives information regarding the generated charges (Q) in the plasma. Plotting Q as a function of the applied voltage (U) gives a Q-U Lissajous plot which is further used to calculate the power consumed by the DBD reactor. The power is calculated by multiplying the area obtained by Lissajous plot with the operating frequency (equation 2.3), where P (W) is the power consumption by the DBD, A_{Lissa} (J/cycle) is area measured by Lissajous plot and f is operating frequency (kHz).

$$P = A_{Lissa}\, x\, f \tag{2.3}$$

The reactant gases, hydrogen and carbon dioxide (Linde Gases) were supplied to the reactor via mass flow controllers (Bronkhorst). The product gas containing mainly CO, CH_4, unreacted CO_2/H_2 and some traces of CH_3OH and C_2H_6, was analysed by an online gas chromatograph (Thermo Scientific) consisting of two thermal conductivity detectors (TCD) and a flame ionisation detector (FID). For each measurement, the results are reported with 95% confidence interval calculated from three repetitions of an experiment. Performance of the reaction is characterized by the following set of parameters.

The conversion, X, of CO_2 is defined as:

$$X\,(\%) = \frac{CO_{2,\text{in}} - CO_{2,\text{out}}}{CO_{2,\text{in}}} x100 \tag{2.4}$$

The selectivity, S_i, where i can be CO, CH_4 or CH_3OH is defined as:

$$S_i\ (\%) = \frac{i_{\text{produced}}}{CO_{2,\text{in}} - CO_{2,\text{out}}} x100 \tag{2.5}$$

The yield, Y_i, where i can be CO, CH_4 or CH_3OH is defined as:

$$Y_i\ (\%) = X\ x\ S_i \tag{2.6}$$

The energy yield of CO production, E_{CO}, is defined as:

$$E(mmol/kWh) = \frac{Molar\ flowrate\ of\ CO(\frac{mmol}{h})}{Power\ (kW)} x100 \tag{2.7}$$

The Specific Energy Input (SEI) is defined as:

$$SEI\ \left(\frac{J}{ml}\right) = \frac{Power\ (W)}{Flow\ rate(ml/min)x(\frac{1}{60})} \tag{2.8}$$

The reactor used in this study was operated at atmospheric pressure, and the reactor wall temperature was maintained at 100 °C to avoid any condensation in the reactor and pipelines. The temperature of the outer wall of the reactor was monitored by an infrared thermal imaging camera (FLIR One Pro, and the temperature of discharge zone (from the exterior) was found to be within 100 to 150 °C (Appendix A). The highest value of 170 °C was observed at the edge of the discharge zone. The total gas flow was varied from 40 to 200 ml/min. The high voltage power supply was set to different frequencies viz. 12, 15, 20 and 30 kHz. The voltage across the reactor was maintained at 15 $kV_{p\text{-}p}$ (peak-to-peak) for all experiments. For the burst mode operation, the time of voltage applied (T_{on}) and voltage switched off (T_{off}) was kept constant at 1 ms each, and a frequency of 30 kHz was fixed.

2.3 Result and Discussion

2.3.1 Effect of Feed Ratio

The ratio of H_2:CO_2 is an important parameter, as it determines the exhaust plasma gas composition. For this, high conversion and high selectivity towards CO the RWGS reaction must be achieved. This results in a high CO level, which allows an exploitation of technology. Thus, process parameters were varied which likely impact those key performance parameters. First of all, the H_2:CO_2 ratio was varied from 1:4 to 4:1, including 0 (meaning no hydrogen added). The H_2:CO_2 ratio was investigated as the key to obtaining compositional freedom. This was done for two different discharge gaps, 1 and 1.5 mm, as this is a simple, direct way of changing the residence time and the plasma itself. The residence times were 16.95 and 24.00 s for the 1 and 1.5 mm discharge gaps, respectively, at a total feed gas flow rate of 40 ml/min. A voltage of 15 kV_{p-p} and 30 kHz frequency were applied throughout this set of experiments.

In the absence of H_2, the feed stream contains pure CO_2 which is dissociated into CO and O_2. A conversion of 22.0 and 24.5% CO_2 conversion is observed, when using 1 and 1.5 mm discharge gaps, respectively. Introduction of H_2 to the feed stream is expected to promote CO_2 dissociation by a shift of the equilibrium through the reaction of H_2 with the active O species, forming water. Indeed, the conversion rises from about 20 to about 50%, when the H_2:CO_2 ratio over the full range as given above, see Figure 2.2 (a). The only exception for this trend is observed when H_2:CO_2 ratio was 1:4, where conversion of CO_2 is at a minimum in this study; this is even more evident in the energy yield given in Figure 2.2 (b). In this scenario, energy supplied is distributed among CO_2 and H_2 gases for ignition of plasma, hence CO_2 molecules receive lesser energy for their splitting compared to pure CO_2 scenario reflecting negatively in total CO_2 conversion. This effect is assumed not to scale with higher CO_2 content, so leaving the energy to induce conversion. Moreover, the population of H_2 molecules is not significantly high at the 1:4 ratio to have substantial

collisions with CO_2 or O species present in the plasma, causing lower conversion as compared to higher H_2 content. It was also observed that not all oxygen was removed from the product stream, leaving behind traces up to 400 ppm.

The CO selectivity is high, as to be expected, and close to 100% at low H_2:CO_2 ratios. Increasing the latter reduces selectivity, and likely explanation is the onset of hydrogenation reactions, competing with the RWGS reaction. Amongst them, methanation of CO_2 is a major one, as shown by equation (2.9), with maximum selectivity for methane obtained as 6.6%.

$$CO_2 + 4H_2 \leftrightarrow CH_4 + 2H_2O \quad \Delta H_{25^\circ C} = -165\ \text{kJ/mol} \tag{2.9}$$

The direct hydrogenation of CO_2 is more favoured thermodynamically than the RWGS reaction as evident from the ΔH values of the two. Excess of H_2 has shown a positive effect on the RWGS reaction, increasing conversion of CO_2 at atmospheric pressure (figure 2.2 (a), Appendix A).

The energy yield of CO formation decreases with excess H_2 over CO_2, as to be expected, since hydrogen competes with the CO_2 molecules in absorbing the energy provided through plasma. Due to the change of gas composition, discharge characteristics and absorbed plasma power also change, affecting as well the energy yield of CO formation. From figure 2.2 (b), in the RWGS regime where the ratio is up to 1:2, the applied power did not vary much (hence SEI as the flowrate is constant), but the conversion of CO_2 was improved, reflecting in improved energy yield. This phenomenon appears to be inverted for the ratios higher than 1:2. The trend towards increasing CO_2 conversion with the high ratio is much smaller than the trend towards decreasing the corresponding applied power (and SEI as well), which is eventually reflected in reduced energy yield at higher ratios. The highest energy yield of CO formation is obtained at feed gas ratio of 1:2 (H_2:CO_2), having values of 229 and 192 mmol/kWh for 1 and 1.5 mm discharge gap respectively.

As said fine-tuning, the exhaust plasma gas composition is a motivation of the study presented so far. One key performance parameter is the (H_2 - CO_2):(CO + CO_2)

ratio. The ratio of 2 found when converting CO_2 at a ratio 3:1 of H_2:CO_2 matches the feed gas in industrially operated methanol synthesis plants by conventional catalysis [58]. Hence, the RWGS reaction using plasma can be applied directly to create a suitable feed gas for methanol with the only need to remove water content and no other further processing. Since the ratio of 3:1 of H_2:CO_2 is industrially relevant, it was kept constant for all the following experiments.

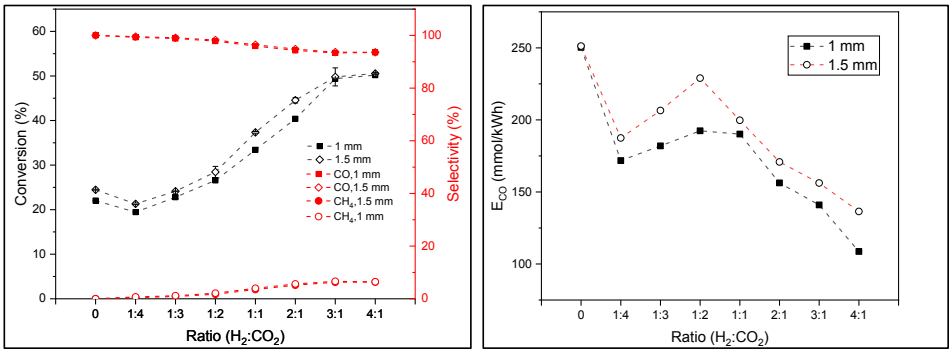

(a) (b)

Figure 2.2: *Effect of the H_2:CO_2 ratio with respect to discharge gap on (a) CO_2 conversion and CO selectivity; (b) energy* yield *of CO formation; voltage: 15 kV; frequency: 30 kHz, total flow rate: 40 ml/min, barrier thickness: 1.5 mm*

2.3.2 Effect of Discharge Frequency

Figure 2.4 (a) illustrates the effect of discharge frequency on the performance of the RWGS reaction. The applied voltage is kept constant at 15 kV_{p-p} in all experiments while changing the operating frequency viz. 12, 15, 20 and 30 kHz. Hence the applied power and specific energy input were also changed accordingly. The feed gas flow rate was kept constant at 40 ml/min with H_2:CO_2 ratio maintained at 3:1. The temperature is set to 100 °C.

As evident from the similar Lissajous diagrams, the charge transferred from a single wave of applied voltage does not change when the frequency was changed; see Figure 2.3. However, it changes the corresponding applied power as it is calculated by multiplying area obtained by Lissajous figure with frequency (equation 2.3). Hence the applied power is higher when the frequency is higher while keeping the applied voltage constant. This is relevant, as a higher frequency (hence higher power) will give higher CO_2 conversion. For the 0.5 mm discharge gap, the CO_2 conversion is found to increase from 20% at 12 kHz to 38% at 30 kHz. A similar trend is followed in the cases of 1 mm and 1.5 mm discharge gap, where it increases from 27 and 27% to 49 and 50%, respectively. The experiment with 0.5 mm discharge gap shows a lower conversion compared to the experiments with 1 and 1.5 mm discharge gap at the same operating frequency. This is due to the change in residence time of the feed gas and discussed in detail in section 2.3.3.

However, it is also observed that with higher power consumption, the selectivity of CO decreases. The higher energy efficiencies at low frequencies give higher selectivity of CO, as evident from Figure 2.4 (a). This is in accordance with the results on CO_2 splitting in a DBD plasma reactor [59]. At a constant frequency of operation, it was found that the energy yield of CO formation decreased with increasing discharge gap, as shown in Figure 2.4 (b). This can be attributed to the fact that higher discharge gaps lead to the formation of high energy microdischarges, increasing overall power consumption [37]. Such change to higher power consumption is not proportionally compensated by an increase in CO_2 conversion so that the energy yield of the CO formation in a negative way. Hence to have a narrow discharge gap is desirable for enhancing the energy yield of the RWGS reaction at lower frequency amongst the measured range.

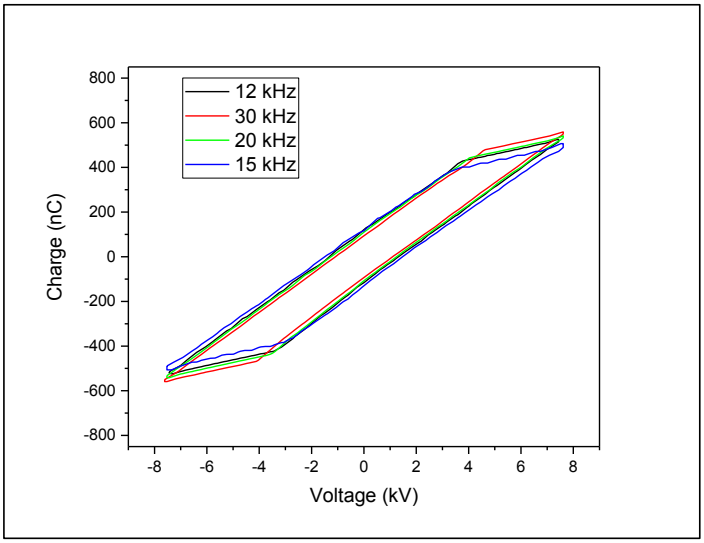

Figure 2.3: *Lissajous diagrams obtained at different operating frequencies voltage: 15kV, barrier thickness: 1.5 mm, total flow rate: 40ml/min, ratio of H_2 to CO_2: 3:1*

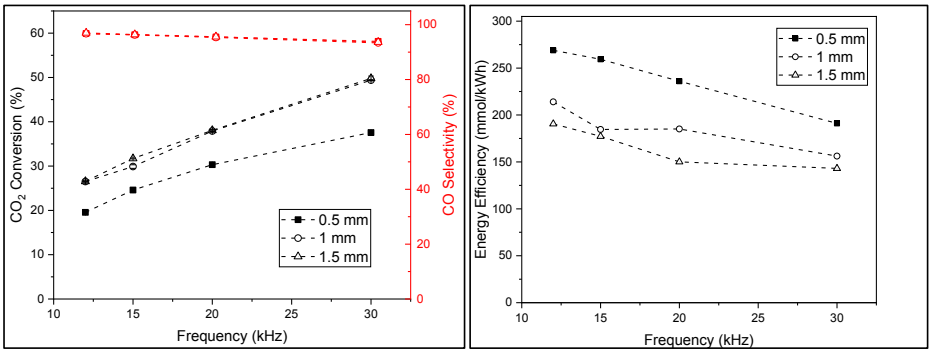

(a) **(b)**

Figure 2.4: *Effect of operating frequency on (a) CO_2 conversion and CO selectivity; (b) energy* yield *of CO formation voltage: 15 kV, barrier thickness: 1.5 mm, total flow rate: 40ml/min*

2.3.3 Effect of Discharge Gap with Respect to the feed Gas Flow Rate and Residence Time

Figure 5(a) shows the flow rate variation of the feed gas at different discharge gaps (0.5, 1 and 1.5 mm) and constant other relevant parameters (frequency: 15 kV_{p-p}; voltage: 30 kHz; H_2:CO_2 ratio 3:1). The idea of the experiment is to test for the effect of residence time, by varying the flow rate and the discharge gap; their combined effect allows for varying in a broader range of residence times (noting that the discharge gap also impacts the electric field and plasma, as said). The CO_2 conversion decreases with increasing flow rate, as to be expected, for all kinds of discharge gaps. At 40 ml/h, the change from 1 to 1.5 mm discharge gap (24.00 and 16.95 s residence time) has hardly any impact on the conversion, just changing from 49 to 50%, respectively. On the contrary, the conversion drops to 38%, when using a discharge gap of 0.5 mm 8.85 s). At the other flow rates (85, 100, 200 ml/h), the conversion drops with decreasing flow rate. Thus, residence time has a significant impact, and only for the lowest flow rate provided, the additional benefit of increasing residence by the discharge gap has seemingly no impact, i.e. enough reaction time is provided (about 17 s).

The CO selectivity does not change significantly in the above experiments, varying flow rates and discharge gaps. An investigation from van der Wiel et al. shows that low residence times are favourable for accomplishing high CO selectivity over methane [60]. This is also found in our investigations. The CO selectivity drops from 98 from 93% as feed gas flow rate is changed from 200 ml/min to 40 ml/min (1.5 mm discharge gap). Among all discharge gaps used, the highest energy yield is found for a gap of 0.5 mm, and that is found at any flow rate measured (Figure 2.5 (b)). The best energy yield of CO formation of 337 mmol/kWh is obtained at 200 ml/min of feed gas flow rate with the 0.5 mm discharge gap.

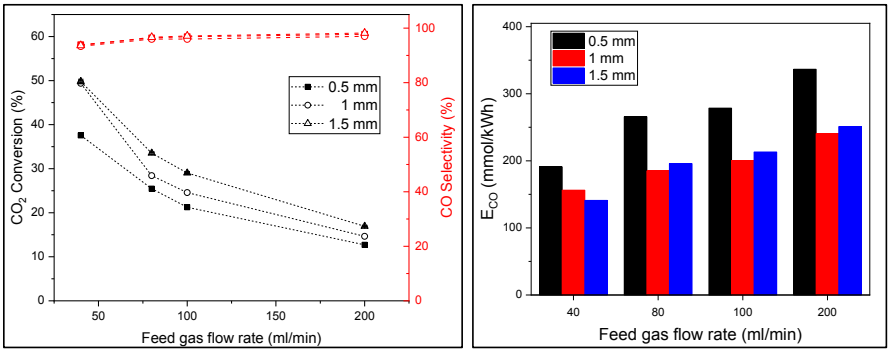

(a) (b)

Figure 2.5: *Effect of discharge gap at the same flow rate on (a) CO_2 conversion and CO selectivity; (b) energy* yield *of CO formation; applied voltage: 15 kV, frequency: 30 kHz, barrier thickness 1.5 mm*

In Table 2.1, CO_2 conversions are compared for all discharge gaps at the same residence time. This was achieved by adjusting to compensate for the residence-time differences caused by the discharge gap. With the exception of the experiment using the longest residence time (24 s), conversion of CO_2 is always highest when using the lower discharge gap. At 24 s reaction time, the conversion of the experiments with all discharge gaps is almost the same. This outcome is explained by the correlation of the CO_2 conversion to the number and energy of microdischarges formed in the plasma volume. A large discharge gap creates only a few microdischarges of high energy, while a small discharge gap increases the number of microdischarges on the expense of their energy [61–64]. Therefore if plasma exposure time per unit volume is the same, more conversion is due to the higher number of microdischarges (assuming that the single discharge energy is above the threshold for chemical conversion). As found earlier, a higher residence time promotes methanation of CO_2; hence CO selectivity is decreased significantly. Thus, at any residence time investigated, experiments using the 0.5 mm discharge gap show two-faced result, i.e. highest conversion, yet lowest CO selectivity and also overall lowest energy yield.

Table 2.1: *Effect of discharge gap with respect to residence time on RWGS key parameters*

Discharge gap (mm)	Residence time (s)	CO_2 conversion (%)	Selectivity (%)		E_{CO} (mmol/kWh)
			CO	CH_4	
0.5	4.8	27.6	96.1	3.8	244.2
	6.4	32.5	95.1	4.8	217.3
	9.6	39.4	93.5	6.4	159.7
	24	48.4	87.5	12.2	80.2
1	4.8	23.7	97.4	2.6	274.0
	6.4	28.8	96.9	3.1	253.2
	9.6	37.6	95.8	4.2	213.7
	24	48.9	92.3	7.6	110.9
1.5	4.8	16.9	98.2	1.8	251.1
	6.4	22.0	97.8	2.2	244.2
	9.6	33.5	97.1	2.9	246.1
	24	49.8	94.0	6.0	141.4

2.3.4 Burst Mode

In the plasma-assisted RWGS reaction, the energy absorbed by the gas inside the reactor generates heat as well. This leads to an expansion of the gas, which decreases the gas density and thus increases the space velocity of the molecules, influencing the conversion, respectively. The ambition thus is to focus discharge power entirely on the chemical reaction without heating the whole gas. Therefore, in this study, the concept of 'burst mode' introduced by Okzan et al. for CO_2 splitting in a DBD was studied [50]. Electric energy is not supplied continuously but intermittently at high frequency. Figure 2.6 represents the electrical signals of the discharge during burst mode. The burst mode is also acclaimed, due to intermediate quenching of products, to allow control over product formation and curb undesirable reaction pathways. The burst mode has a second advantage - the microdischarges are widely spread in the discharge zone [50]; thus an enhanced distribution of microdischarges is expected over the continuous operation.

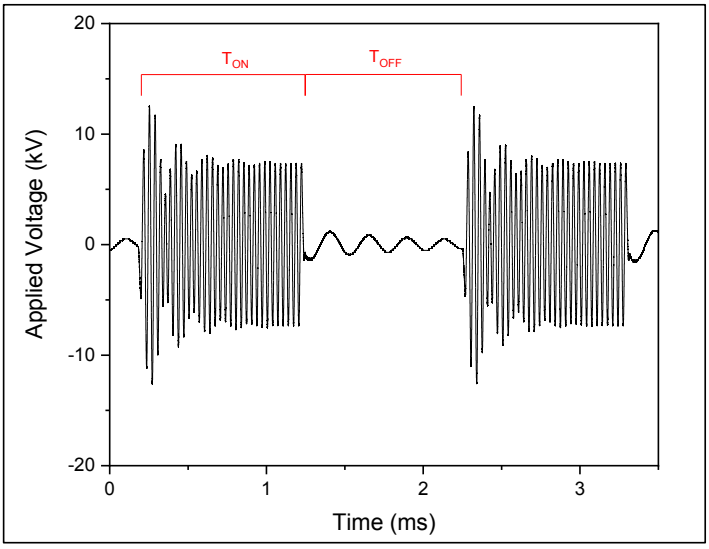

Figure 2.6: *Burst mode waveform, applied voltage: 15 kV_{p-p}, frequency: 30k Hz, barrier thickness 1.5 mm, discharge gap: 1 mm, operating frequency: 30 kHz*

In the burst mode investigations frequency and applied voltage are kept constant as given for the continuous mode while applying 1ms as the time period ((T_{on}) between the start of a 'plasma discharge wave' and its stop (T_{off}) time respectively (Figure 2.7). As the capacitive characteristics remain the same, the average energy supplied via a single wave remains the same as for the continuous mode making power consumption in the burst mode to be half of the power consumed in continuous AC mode.

Table 2.2 shows the comparison of the CO_2 conversion, CO selectivity and energy yield in continuous and burst modes. For all flow rates investigated, the CO_2 conversion in the burst mode dropped not to the same extent, as compared to the halving of the residence time and power consumption as given for the continuous operation. This means that the 'burst-mode corrected' conversion is higher. More remarkably, the CO selectivity can be increased for the best operation points by 2-3%, which means at best an almost halving of the CH_4 impurity load. In all experiments made, the burst mode has higher selectivity towards CO as compared

to experiments in continuous AC mode. The combined effect leads to a notable improvement in energy yield through the application of burst mode. Table 3 presents the summary of a few critical results from literature and this work highlighting mainly CO_2 conversion and energy yield of CO formation. As evident from the table, this work demonstrates the best energy yield along with the highest CO selectivity amongst other results.

Table 2.2: *Effect of the burst mode on the RWGS reaction*

Discharge gap (mm)	Power supply mode	Flow rate (ml/min)	CO_2 conversion (%)	Selectivity (%) CO	Selectivity (%) CH_4	E_{CO} (mmol/kWh)
1	Continuous AC	40	49.4	93.4	6.6	156.2
		80	28.4	96.0	3.8	184.9
		100	24.6	96.0	3.9	199.8
		200	14.7	97.0	3.0	240.7
	Burst mode	40	30.1	96.0	3.9	195.9
		80	20.3	97.6	2.4	268.4
		100	17.1	97.9	2.1	283.7
		200	9.7	98.5	1.4	324.9
1.5	Continuous AC	40	49.8	93.7	6.3	141.0
		80	33.5	96.7	3.3	195.9
		100	29.0	97.1	2.9	213.1
		200	16.9	98.2	1.8	251.1
	Burst mode	40	29.7	96.0	0.3	172.6
		80	18.4	97.9	2.1	217.7
		100	16.2	98.1	1.9	239.9
		200	9.1	98.7	1.3	270.3

Table 2.3: *Comparison of CO_2 conversion and energy* yield *of CO formation, E_{CO} for reverse water-gas shift reaction via plasma*

Type of plasma	Power (W)	CO_2 conversion (%)	CO Selectivity (%)	H_2:CO_2	E_{CO} (mmol/kWh)	Reference
DBD	500	13.3	96	3:1	78	[45]
DBD	35	10.2	77.7	1:1	96	[46]
DBD	30	55	92	4:1	229	[47]
MW	600	77	-	1:1	58	[48]
RF	10	26	75	4:1	96	[65]
DBD	45	12.7	97.8	3:1	337	This work
DBD (burst mode)	36	9.7	98.5	3:1	325	This work

2.4 Outlook on Business Implementation

The RWGS technology has the highest readiness level aiming towards the use of recycled CO_2 coupled with local renewable energy resources and renewable hydrogen [66,67]. Through such effective RWGS reaction, a $CO_2/CO/H_2$ mixture can be obtained having $(H_2 - CO_2)/(CO + CO_2)$ ratio equal to 2, to find direct use in methanol synthesis.

Even though the non-catalytic reaction pathway chosen provides ease of operation, the by-products are still not completely abridged, which may not be desired in subsequent chemical processes. Therefore future investigations may aim in the direction of tailored catalyst development specific for the RWGS reaction towards improved productivity, especially focusing towards depletion of the by-products. Following the last paragraph of the introduction, the achieved process performance may be taken as a guide to developing a 'window of opportunity' for a future industrial business case. That would need to develop a full-process scenario at relevant industrial scale and to determine its sustainability by cost calculations and life-cycle assessment. That would include for a check of suited renewable sources, and giving an energy system vision for the aforementioned scenario.

Such forecasts are typically not done as a retrofit (i.e. simple replacement) of existing technologies or their parts. The view is rather on industry transformation, and that might mean in this case to have the plasma plant next to the chemical plant of intended follow-up use (e.g. methanol) or even more far-fetching to have the plasma reactor integrated into the follow-up plant. Such an ensemble on a small scale, decentralised manner opens new windows of opportunities for CO_2 capture and utilisation.

2.5 Conclusions

The supply of pure CO streams is essential for several industrial processes such as Fischer-Tropsch and methanol synthesis. The Reverse-Water-Gas-Shift (RWGS) reaction is a viable option here and suits a plasma process. It is based on adding hydrogen to CO_2, since the pure CO_2 splitting, i.e. in the absence of H_2, results in lower CO_2 conversion and also produces an equivalent amount of oxygen which is undesirable for further hydrogenation of CO/CO_2 mixture. The results of this study confirm this. The introduction of H_2 into CO_2 feed stream has a significant effect on the CO_2 conversion as it forms stable water molecules, which suppresses the backward reactions from intermediate species and facilitates the forward RWGS reaction.

This chapter shows the feasibility of the RWGS reaction carried out in a DBD plasma reactor operated at ambient pressure and mild temperature. A maximum CO_2 conversion of 50% was achieved. The benefits of plasma operation are seen in the low-temperature operation as compared to conventional operation, overcoming harsh process conditions and lower yields. The paper adds to the literature the use of a burst mode which demonstrated the opportunity for further reducing temperature and increasing energy yield. The article also adds to literature the process simplification of not adding a catalyst, with a few other papers have already demonstrated that. The CH_4 selectivities are the lowest reported in the literature, to our best knowledge. That provides an opportunity to use the CO plasma exhaust gas streams of this study as feed to industrial processes, which use syngas for chemical synthesis. That renders the plasma process as a pre-processing step with the aim to replace a costly, harmful reactant (CO) by a better candidate (CO_2). That at-site feed provision allows making the CO at the site, with sustainability advantages such as better energy yield and reduced global warming.

This chapter focuses on the CO selectivity obtained and explores opportunities to increase that. Important reactor asset is the decoupling of the direct dependence of residence time to the flow rate. Using different discharge gaps, and thus

miniaturisation provides another opportunity to set residence time to the best value. As demonstrated, CO selectivity is best for small discharge gaps and short contact times, then an efficient plasma is required. The burst mode provided the additional advantage of utilizing more and more homogeneously distributed microdischarges. As a result, a higher normalised conversion is achieved, and more importantly, a higher CO selectivity and purity of the CO product gas stream (with low CH_4 selectivity). In this way, also the critical process parameter energy yield of CO formation was optimised. 337 mmol/kWh is the optimum value achieved in this study.

References

[1] Marchal V, Dellink R, Van Vuuren D, Clapp C, Château J, Lanzi E, Magné B and Vliet J Van 2011 OECD environmental outlook to 2050: Climate change chapter *OECD* 90

[2] Olah G, Prakash G K S and Goeppert A 2011 Anthropogenic Chemical Carbon Cycle for a Sustainable Future 12881–98

[3] Global CCS Institute 2011 Accelerating the Uptake of CCS: Industrial Use of Captured Carbon Dioxide *Technology*

[4] von der Assen N, Jung J and Bardow A A 2013 Life-cycle assessment of carbon dioxide capture and utilization: avoiding the pitfalls *Energy Environ. Sci.* **6** 2721

[5] Perathoner S and Centi G 2014 CO_2 recycling: A key strategy to introduce green energy in the chemical production chain *ChemSusChem* **7** 1274–82

[6] Centi G, Iaquaniello G and Perathoner S 2011 Can we afford to waste carbon dioxide? Carbon dioxide as a valuable source of carbon for the production of light olefins *ChemSusChem* **4** 1265–73

[7] Quadrelli E A, Centi G, Duplan J L and Perathoner S 2011 Carbon dioxide recycling: Emerging large-scale technologies with industrial potential *ChemSusChem* **4** 1194–215

[8] Barbato L, Centi G, Iaquaniello G, Mangiapane A and Perathoner S 2014 Trading Renewable Energy by using CO_2 : An Effective Option to Mitigate Climate Change and Increase the use of Renewable Energy Sources *Energy Technol.* **2** 453-461

[9] Darensbourg D J 2010 Chemistry of carbon dioxide relevant to its utilization: A personal perspective *Inorg. Chem.* **49** 10765–80

[10] Olah G, Goeppert A and Prakash G K S 2009 Chemical recycling of carbon dioxide to methanol and dimethyl ether: From greenhouse gas to renewable, environmentally carbon neutral fuels and synthetic hydrocarbons *J. Org. Chem.* **74** 487–98

[11] van Rooij G, Akse H N, Bongers W A and van de Sanden M C M 2018 Plasma for electrification of chemical industry: a case study on CO_2 reduction *Plasma Phys. Control. Fusion* **60** 014019

[12] Higman C and van der Burgt M 2008 *Gasification* (Elsevier)

[13] Lahijani P, Zainal Z A, Mohammadi M and Mohamed A R 2015 Conversion of the greenhouse gas CO_2 to the fuel gas CO via the Boudouard reaction: A review *Renew. Sustain. Energy Rev.* **41** 615–32

[14] Get CO on-demand at the touch of a button (available at https://www.topsoe.com/processes/carbon-monoxide/site-carbon-monoxide, accessed on 29-01-2019)

[15] CO from CO_2: On-site carbon monoxide generation takes the next step (available at https://www.gasworld.com/co-from-co2-on-site-carbon-monoxide-generation-takes-the-next-step/2011884.article, accessed on 29-01-2019)

[16] Wang D, Wright H A, Ortego B C, Trinh S, Espinoza R, US Patent 6992112-B2 (2006)

[17] Oshima K, Shinagawa T, Nogami Y, Manabe R, Ogo S and Sekine Y 2014 Low temperature catalytic reverse water gas shift reaction assisted by an electric field *Catal. Today* **232** 27–32

[18] Park S-W, Joo O-S, Jung K-D, Kim H and Han S-H 2001 Development of ZnO/Al_2O_3 catalyst for reverse-water-gas-shift reaction of CAMERE (carbon dioxide hydrogenation to form methanol via a reverse-water-gas-shift reaction) process *Appl. Catal. A Gen.* **211** 81–90

[19] Chen C S, Cheng W H and Lin S S 2004 Study of iron-promoted Cu/SiO_2 catalyst on high temperature reverse water gas shift reaction *Appl. Catal. A Gen.* **257** 97–106

[20] Ginés M J L, Marchi A J and Apesteguía C R 1997 Kinetic study of the reverse water-gas shift reaction over $CuO/ZnO/Al_2O_3$ catalysts *Appl. Catal. A Gen.* **154** 155–71

[21] Goguet A, Meunier F C, Tibiletti D, Breen J P and Burch R 2004 Spectrokinetic investigation of reverse water-gas-shift reaction intermediates over a Pt/CeO_2 catalyst *J. Phys. Chem. B* **108** 20240–6

[22] Wiesberg I L, de Medeiros J L, Alves R M B, Coutinho P L A and Araújo O 2015 Carbon dioxide management by chemical conversion to methanol: hydrogenation and bi-reforming *Energy Convers. Manag.* **125** 320-335

[23] Ghasemzadeh K, Sadati Tilebon S M, Nasirinezhad M and Basile A 2017 *Economic Assessment of Methanol Production* (Elsevier)

[24] Machado C F R, Medeiros J L De, Araújo O F Q and Alves R M B 2014 A comparative analysis of methanol production routes : synthesis gas versus CO_2 hydrogenation *2014 Int. Conf. Ind. Eng. Oper. Manag.* 2981–

90
[25] Zubrin R 2009 How to go to Mars-right now! *IEEE Spectr.* **46** 48–9
[26] Frankie B and Zubrin R 1999 Chemical engineering in extraterrestrial environments *Chem. Eng. Prog.* **95** 45–54
[27] Kusama H, Bando K K, Okabe K and Arakawa H 2001 CO_2 hydrogenation reactivity and structure of Rh/SiO_2 catalysts prepared from acetate, chloride and nitrate precursors *Appl. Catal. A Gen.* **205** 285–94
[28] Lu B and Kawamoto K 2013 Preparation of monodispersed NiO particles in SBA-15, and its enhanced selectivity for reverse water gas shift reaction *J. Environ. Chem. Eng.* **1** 300–9
[29] Hu B, Guild C and Suib S L 2013 Thermal , electrochemical , and photochemical conversion of CO_2 to fuels and value-added products *Biochem. Pharmacol.* **1** 18–27
[30] Schneck F, Schendzielorz F, Hatami N, Finger M, Würtele C and Schneider S 2018 Photochemically Driven Reverse Water-Gas Shift at Ambient Conditions mediated by a Nickel Pincer Complex *Angew. Chemie - Int. Ed.* **57** 14482–7
[31] Ioannidou E, Neophytides S and Niakolas D K 2019 Experimental clarification of the RWGS reaction effect in H_2O/CO_2 SOEC co-electrolysis conditions *Catalysts* **9** 1–19
[32] Karagiannakis G, Zisekas S and Stoukides M 2003 Hydrogenation of carbon dioxide on copper in a H^+ conducting membrane-reactor *Solid State Ionics* **162**–**163** 313–8
[33] Lebouvier A, Iwarere S A, D'Argenlieu P, Ramjugernath D and Fulcheri L 2013 Assessment of carbon dioxide dissociation as a new route for syngas production: A comparative review and potential of plasma-based technologies *Energy and Fuels* **27** 2712–22
[34] Bogaerts A, Kozák T, van Laer K and Snoeckx R 2015 Plasma-based conversion of CO_2 : current status and future challenges *Faraday Discuss.* **183** 217-232
[35] Bacariza M C, Biset-Peiró M, Graça I, Guilera J, Morante J, Lopes J M, Andreu T and Henriques C 2018 DBD plasma-assisted CO_2 methanation using zeolite-based catalysts: Structure composition-reactivity approach and effect of Ce as promoter *J. CO_2 Util.* **26** 202–11
[36] Zhang K, Eliasson B and Kogelschatz U 2002 Direct Conversion of Greenhouse Gases to Synthesis Gas and C4 Hydrocarbons over Zeolite HY Promoted by a Dielectric-Barrier Discharge *Ind. Eng. Chem. Res.* **41** 1462–8
[37] Kogelschatz U, Eliasson B and Egli W 1997 Dielectric-Barrier Discharges. Principle and Applications *Le J. Phys. IV* **07** C4-47-C4-66
[38] Tu X and Whitehead J C 2012 Plasma-catalytic dry reforming of methane in an atmospheric dielectric barrier discharge: Understanding the synergistic effect at low temperature *Appl. Catal. B Environ.* **125** 439–48
[39] De Bie C, van Dijk J and Bogaerts A 2016 CO_2 Hydrogenation in a Dielectric Barrier Discharge Plasma Revealed *J. Phys. Chem. C* **120** 25210–24
[40] Brehmer F, Welzel S, Van De Sanden M C M and Engeln R 2014 CO and byproduct formation during CO_2 reduction in dielectric barrier discharges *J. Appl. Phys.* **116** 123303
[41] Aerts R, Somers W and Bogaerts A 2015 Carbon Dioxide Splitting in a Dielectric Barrier Discharge Plasma: A Combined Experimental and Computational Study *ChemSusChem* **8** 702–16
[42] Hessel V, Anastasopoulou A, Wang Q, Kolb G and Lang J 2013 Energy, catalyst and reactor considerations for (near)-industrial plasma processing and learning for nitrogen-fixation reactions *Catal. Today* **211** 9–28
[43] Patil B S, Cherkasov N, Lang J, Ibhadon A O, Hessel V and Wang Q 2016 Low temperature plasma-catalytic NOx synthesis in a packed DBD reactor: Effect of support materials and supported active metal oxides *Appl. Catal. B Environ.* **194** 123–33
[44] Yan B H, Wang Q, Jin Y and Cheng Y 2010 Dry reforming of methane with carbon dioxide using pulsed DC arc plasma at atmospheric pressure *Plasma Chem. Plasma Process.* **30** 257–66
[45] Eliasson B, Kogelschatz U, Xue B and Zhou L 1998 Hydrogenation of carbon dioxide to methanol with a discharge-activated catalyst *Ind. Eng. Chem. Res.* **37** 3350–7
[46] Zeng Y and Tu X 2017 Plasma-catalytic hydrogenation of CO_2 for the cogeneration of CO and CH_4 in a dielectric barrier discharge reactor: effect of argon addition *J. Phys. D. Appl. Phys.* **50** 184004
[47] Zeng Y and Tu X 2016 Plasma-Catalytic CO_2 Hydrogenation at Low Temperatures *IEEE Trans. Plasma Sci.* **44** 405–11

[48] Dobrea S, Mihaila I, Tiron V and Popa G 2014 Optical and Mass Spectrometry Diagnosis of a CO_2 Microwave Plasma Discharge *Rom. Reports Phys.* **66** 1147–54
[49] Fridman A, Nester S, Kennedy L A, Saveliev A and Mutaf-Yardimci O 1999 Gliding arc gas discharge *Prog. Energy Combust. Sci.* **25** 211–31
[50] Ozkan A, Dufour T, Silva T, Britun N, Snyders R, Reniers F, Bogaerts A and Antwerpen U 2016 DBD in burst mode : solution for more efficient CO_2 conversion? *Plasma Sources Sci. Technol.* **25** 055005
[51] Ribeiro A M, Santos J C, Rodrigues A E and Rifflart S 2012 Syngas Stoichiometric Adjustment for Methanol Production and Co-Capture of Carbon Dioxide by Pressure Swing Adsorption *Sep. Sci. Technol.* **47** 850–66
[52] Patil B S, Rovira Palau J, Hessel V, Lang J and Wang Q 2016 Plasma Nitrogen Oxides Synthesis in a Milli-Scale Gliding Arc Reactor: Investigating the Electrical and Process Parameters *Plasma Chem. Plasma Process.* **36** 241–57
[53] Green Fertilizer - Eco Trainer, Evonik (https://www.youtube.com/watch?v=bR9cLJNQQOE, accessed on 29-01-2019)
[54] Anastasopoulou A, Wang Q, Hessel V and Lang J 2014 Energy Considerations for Plasma-Assisted N-Fixation Reactions *Processes* **2** 694–710
[55] Anastasopoulou A, Butala S, Lang J, Hessel V and Wang Q 2016 Life Cycle Assessment of the Nitrogen Fixation Process Assisted by Plasma Technology and Incorporating Renewable Energy *Ind. Eng. Chem. Res.* **55** 8141–53
[56] Anastasopoulou A, Butala S, Patil B, Suberu J, Fregene M, Lang J, Wang Q and Hessel V 2016 Techno-economic feasibility study of renewable power systems for a small-scale plasma-assisted nitric acid plant in africa *Processes* **4** 54
[57] Fertilizing with wind, (http://ecotrainer.evonik.com/, accessed on 29-01-2019)
[58] Cheng W H and Kung H 1994 *Methanol Production and Use* (CRC Press)
[59] Ozkan A, Dufour T, Silva T, Britun N, Snyders R, Bogaerts A and Reniers F 2016 The influence of power and frequency on the filamentary behavior of a flowing DBD – Application to the splitting of CO_2 *Plasma Sources Sci. Technol.* **25** 025013
[60] Vanderwiel D P, Wang Y, Tonkovich a Y, Wegeng R S Carbon Dioxide Conversions in Microreactors *IMRET 4: Proceedings of the 4th International Conference on Microreaction Technology, Topical Conference Proceedings, AIChE Spring National Meeting, March 5-9, 2000 Atlanta, GA* pp 187–93
[61] Kogelschatz U 2003 Dielectric-barrier discharges: Their History, Discharge Physics, and Industrial Applications *Plasma Chem. Plasma Process.* **23** 1–46
[62] Chirokov A, Gutsol A and Fridman A 2005 Atmospheric pressure plasma of dielectric barrier discharges *Pure Appl. Chem.* **77** 487–95
[63] Bruggeman P and Brandenburg R 2013 Atmospheric pressure discharge filaments and microplasmas: physics, chemistry and diagnostics *J. Phys. D. Appl. Phys.* **46** 464001
[64] Buser R G and Sullivan J 1970 Initial Processes in CO_2 Glow Discharges *J. Appl. Phys.* **41** 472–9
[65] Kano M, Satoh G and Iizuka S 2012 Reforming of Carbon Dioxide to Methane and Methanol by Electric Impulse Low-Pressure Discharge with Hydrogen *Plasma Chem. Plasma Process.* **32** 177–85
[66] Daza Y A and Kuhn J N 2016 CO_2 conversion by reverse water gas shift catalysis: comparison of catalysts, mechanisms and their consequences for CO_2 conversion to liquid fuels *RSC Adv.* **6** 49675–91
[67] Van Kranenburg K, Schols E, Gelevert H, De Kler R, Van Delft Y and Weeda M 2016 Empowering the chemical industry. Opportunities for electrification. 32 (https://www.tno.nl/media/7514/voltachem_electrification_whitepaper_2016.pdf, accessed on 29-1-2019)

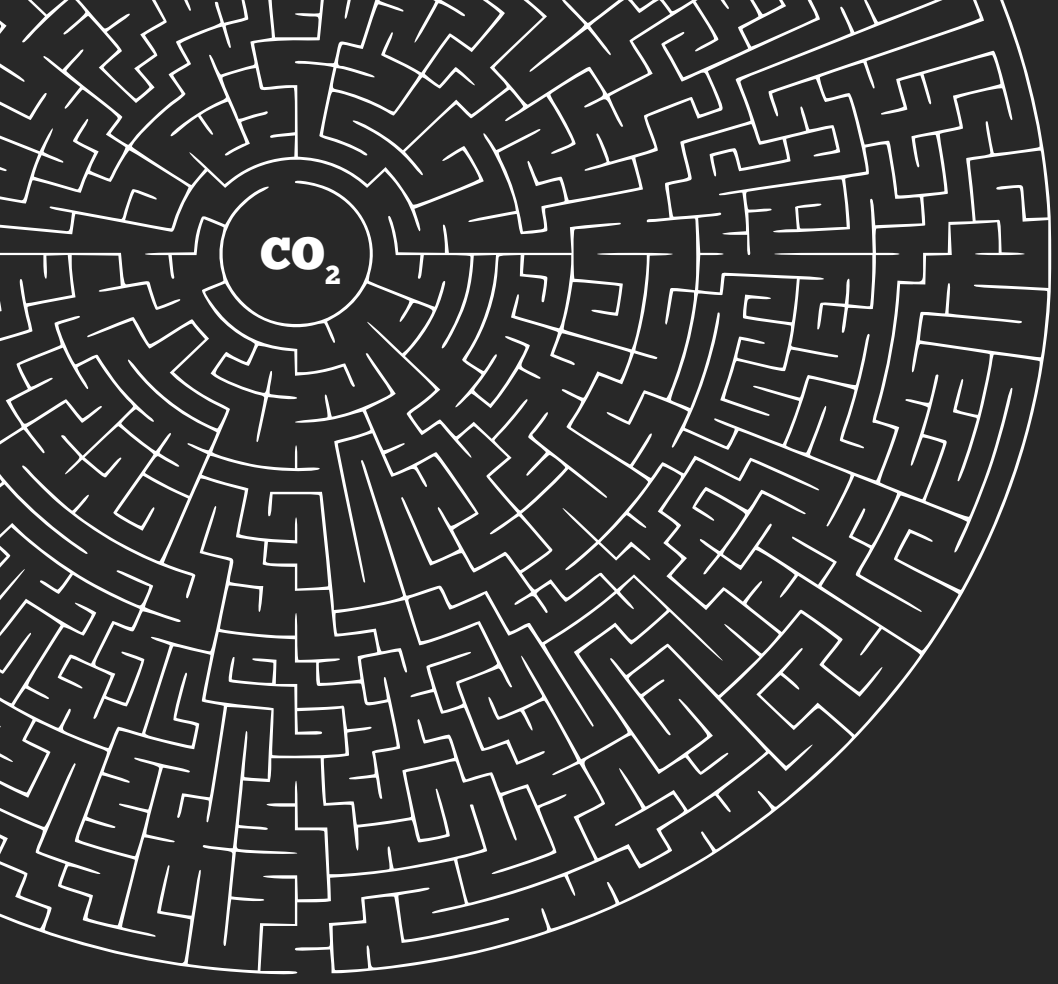
CO_2

Chapter 3

CO_2 to Syngas - Reverse water-gas shift reaction via atmospheric pressure gliding arc process

This chapter is adapted from

Chaudhary R., Peeters F.J.J., Li S., van Rooij G.J., Hessel V., Reverse Water-gas Shift reaction via ambient condition gliding arc plasma, in preparation

Abstract.

The reverse water-gas shift reaction is being realised as an essential process to produce syngas via recycled CO_2 and renewable energy, which serves for the dual purpose of CO_2 mitigation and storage of excess electricity from renewable energy sources. The use of plasma to carry out chemical reactions is attracting interest globally. This research focuses on plasma-assisted Reverse Water Gas Shift (RWGS) reaction by means of a gliding arc reactor. This investigation is carried out by planar two electrodes gliding arc reactor with two planar electrodes. The feed gas composition and total flow rate are optimised to get maximum output from the reaction, in terms of better conversion as well as energy efficiency. A maximum of 54% CO_2 conversion is obtained when feed gas contains 75% hydrogen. At equal content of H_2 and CO_2 in the feed gas, the maximum energy efficiency of 11% is obtained. The same condition also yields the best value of energy required to synthesise CO, which is 4.8 mol/kWh. Optical emission spectroscopy is employed to calculate plasma parameters. The calculation of electron density (~10^{16} cm^{-3}) and rotational temperature (3250K) confirmed the classification of gliding arc as a warm plasma. Supported by optical emission spectroscopy data, a plausible reaction mechanism is proposed.

3.1 Introduction

Reverse water-gas shift (RWGS) reaction, discovered in the 19th century denotes the reversible hydrogenation of CO_2 (Eq. 3.1) to form water and CO (syngas). RWGS reaction in conjunction with the Fischer Tropsch (FT) process to produce synthetic liquid hydrocarbon fuels and with CAMERE (carbon dioxide hydrogenation to form methanol via a reverse-water-gas-shift reaction) process to produce methanol seems to be a joint solution for CO_2 capture and valorisation [1,2].

$$CO_2 + H_2 \leftrightarrow CO + H_2O \quad \Delta H°_{298K} = 41\ \mathrm{kJ/mol} \tag{3.1}$$

Traditional methods of the production of syngas are via Pt-catalyzed partial oxidation of methane, Ni-catalyzed steam reforming of methane and light hydrocarbons or gasification of heavy hydrocarbons and coal as carbon feedstock, which have a substantial environmental impact in terms of CO_2 emissions [3–6]. However, an alternate strategy to use CO_2 as renewable raw material to produce syngas via RWGS reaction provides chances to be environmentally benign. The use of recycled CO_2 also makes the whole upstream sustainable via bringing the renewable raw material in the chain. Additionally, the significance of RWGS over other methods can be explained through looking at the carbon footprint of the processes. Traditional methods of syngas production have significant carbon footprint, as the synthesis and the separation of CO emit approximately from 1.396 to 2.322 kg of carbon dioxide equivalent (kg CO_2-eq) per kg of CO. On contrary; if syngas is produced from CO_2 directly at near ambient pressures, this value comes out to be –0.2 kg CO_2-eq/kg. This indicates that the CO_2 consumption in this process is more than what it emits, bringing down the carbon footprint [7]. Besides, valorising CO_2 with renewable energy sources to chemicals and fuels mitigates about 20-40 times more CO_2 than sequestration over 20 years [8–10]. Theoretically, recycling only 30% of emitted CO_2, can fulfil the total global fuel requirements [11]. The FT process also requires H_2 and CO without any oxygen content in the presence of a catalyst to yield straight-chain alkanes [12]. Although the formation of small

amounts of alkenes and alcohols is unavoidable, the higher alkanes can be used as fuels. The temperature range for both reactions differs significantly and hence provides a strong motivation to achieve the RWGS reaction at lower temperatures, apart from making it energy feasible [13].

In the interest of achieving this goal, the use of plasma techniques has been explored in the last few years. Amongst them, dielectric barrier discharge (DBD), microwave discharge (MW), spark discharge and radiofrequency discharge (RF) have been reported for CO_2 hydrogenation [14–20]. Plasma processes are much less investigated for RWGS reaction, and RWGS specifically using an AC gliding arc plasma has not been reported on at all. The gliding arc plasma has both thermal and non-thermal working regimes. During the ignition, a thermal arc is observed, which is subsequently quenched to non-thermal conditions due to its sudden expansion caused by the gas flow. Therefore, it couples benefits from both thermal and non-thermal plasma and is classified as warm plasma [21–23]. Typical plasma characteristics of a gliding arc plasma are electron temperature in the range of 1–3 eV, rotational temperature of the arc between 2000–4000 K, and electron density of 10^{12}–10^{15} cm^3 [24–26]. Direct current (DC) power supply or pulsed power supply is typically used for generation of gliding arc plasma, but alternating current (AC) power supply can also be used [27–35].

By use of a dielectric barrier discharge (DBD) plasma reactor (chapter 2) we obtained about 50% CO_2 conversion for RWGS reaction. However, in DBD, along with CO, CH_4 and some higher hydrocarbons (in traces) were also formed, bringing down the quality of syngas produced. The energy consumption of the DBD reactor was also very high; hence, we decided to explore the gliding arc reactor for the RWGS reaction. In this work, the RWGS reaction carried out by an AC gliding arc plasma is presented.

3.2 Experimental Section

3.2.1 Setup

The plasma-assisted RWGS reactions were carried out at atmospheric pressure using a gliding arc reactor. Figure 3.1(a) illustrates the experimental setup. A unique ceramic called Macor® is used in making the gliding arc reactor body with a quartz window. Two identical triangular Tungsten blades are used as electrodes, one as a high voltage and one as a ground. They are 2.5mm thick, 80 mm high and have a 2 mm gap between their narrowest points.

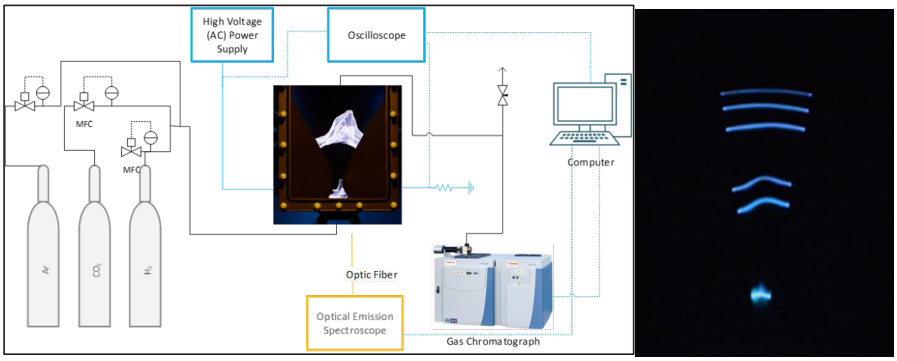

(a) (b)

Figure 3.1: *(a) Schematics of the experimental setup, (b) progression of a gliding arc: superimposed image*

A sinusoidal AC high voltage power supply (AFS G15S-150K) is used to power the gliding arc reactor. All electrical signals were recorded by a 4 channel oscilloscope (Picoscope® 3405D). The applied voltage (U) across the DBD reactor is measured with a 1:1000 high voltage probe (Tektronics P6015A). An external resistor (5 Ω) is connected between the ground electrode and the grounding point, and the voltage (V) across this resistor is measured using a 1:10 voltage probe. The typical V-I signal is shown in Figure 3.2. The following equations (3.2, 3.3) are used to calculate the current (I) and dissipated power (P).

$$I = \frac{V}{R} \tag{3.2}$$

$$P = \frac{1}{T}\int_{t=0}^{t=T} V.I.dt \tag{3.3}$$

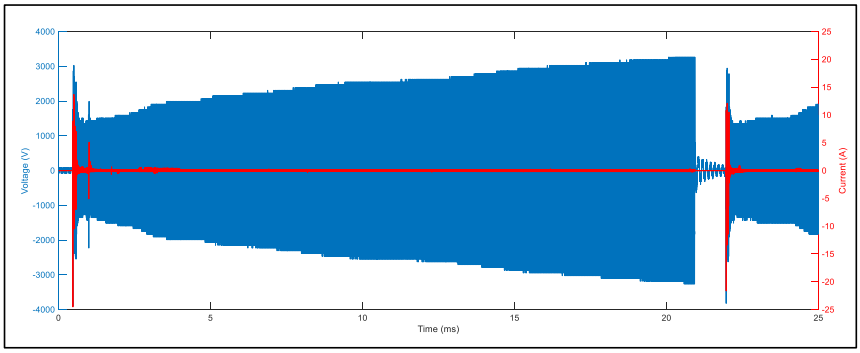

Figure 3.2: *V-I signals of a gliding arc plasma*

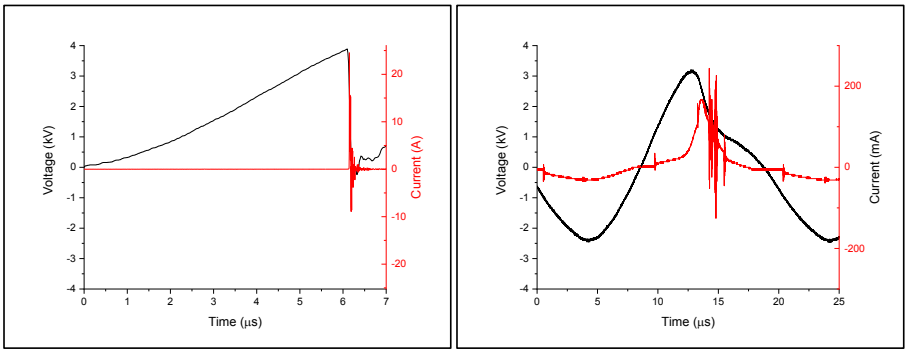

Figure 3.3: *V-I signals (a) Ignition region (b) Propagation region*

The reactor used in this study was operated at atmospheric pressure and temperature without any external heating. The temperature of the outer wall of the reactor was monitored by an infrared thermal imaging camera (FLIR One Pro), and the highest value was found to be 37 °C. The temperature of the outlet gas stream was measured with a thermocouple and found to be below 45 °C. The total gas flow was varied from 200 to 1600 ml/min. Mass flow controllers (Bronkhorst) were used to supply the reactant gases, hydrogen and carbon dioxide (Linde Gases >99.9) to

the reactor. The product gas was analysed by an online gas chromatograph (Thermo Scientific) consisting of two thermal conductivity detectors (TCD) and a flame ionisation detector (FID). In the product gas, only CO and unreacted CO_2/H_2 were measured, and no other products (such as methane) were found. For each measurement, the results are reported with 95% confidence interval calculated from three repetitions of an experiment. Performance of the reaction is characterised by the following set of parameters.

The conversion, X, of CO_2 is defined as:

$$X\ (\%) = \frac{CO_{2,\text{in}} - CO_{2,\text{out}}}{CO_{2,\text{in}}} x100 \tag{3.4}$$

The energy yield of CO production, E_{CO}, is defined as:

$$E(mol/kWh) = \frac{Molar\ flowrate\ of\ CO(mol/h)}{Power\ (kW)} \tag{3.5}$$

The energy efficiency (η) is defined as:

$$\eta\ (\%) = \frac{X\ x\ \Delta H\ (kJ/mol)}{SEI\ (kJ/L) x 22.4 (L/mol)} \tag{3.6}$$

Where the Specific Energy Input (SEI) is defined as:

$$SEI\ (kJ/L) = \frac{Power\ (W) x 60}{Flow\ rate(ml/min)} \tag{3.7}$$

Where ΔH is enthalpy of the RWGS reaction as per the equation 3.1.

The photos of the arc plasma are taken by a camera (Nikon, D5200) with a lens of (Tamron 18-200mm f/3.5-6.3). Moreover, a superimposed image of gliding arc plasma showing arc progression with respect to time is presented in figure 3.1 (b).

3.2.2 Controlling Gliding arc

The gliding arc plasma was operated without any noble gas dilution, and only with the reactant gases. In the gliding arc reactor, the plasma is ignited at the shortest discharge gap between the electrodes, which eventually glides up along the electrode length until a point where the gap between the electrodes is too wide to sustain the arc. Once the arc is extinguished at this point, a new arc is ignited at the lowest discharge gap, and this cycle is repeated. However, the gliding arc does not always form a stable arc cycle. To obtain a stable gliding arc cycle across all the flow parameters, the operational frequency was scanned from 10 to 100 kHz. The operating regime of the gliding arc was found to be between 47-55 kHz. Therefore, an operating frequency of 50 kHz was set for all experiments, for which a stable gliding arc cycle could be established at all the process parameters examined.

3.2.3 Optical Emission Spectroscopy

Optical Emission Spectroscopy (OES) was employed to identify the main active species in the plasma. The emission spectra of the gliding arc plasma were recorded via an optical emission spectrometer (HR2000+ES, Ocean Optics). A calibrated D_2 lamp for UV region and a halogen lamp for the visible region were used to calibrate the wavelength and relative intensity of the spectrometer (Appendix A5). The slit width of the instrument was set at 10 μm, resulting in 0.88 nm resolution. A 600 μm diameter optical fibre was used in combination with a UV/VIS collimating lens to collect the emission spectra. The location of sample collection was set just above the lowest discharge gap point, i.e. the ignition zone of the gliding arc. The recorded spectra were used to obtain plasma parameters such as rotational temperature, electron number density, and ground-state atomic oxygen density. The OH radical ($A^2\Sigma^+$-$X^2\Pi\gamma$ transition) spectra were used to calculate the rotational temperature of the plasma with the help of LIFBASE simulation software. This software includes transition moments, rotational Hönl-London factors and the emission coefficients as a function of vibrational and rotational quantum numbers,

which are essential for the spectroscopic computation of rotational and vibrational temperatures, even with low-resolution spectroscopic data [36]. Stark broadening (λ_s) of H_α emission spectra (656.27.nm) is used to calculate electron density [37].

3.3 Results and Discussion

3.3.1 Operating Regime

The voltage and current waveforms (figure 3.2) roughly adhere to the in-phase sinusoidal form except for a few instances in between. During such instances, the voltage waveform shows a rapid drop and the current waveform presents a sharp pulse. This is associated with a plasma arc, or spark, which develops inside the plasma channel [38]. Plasma arcs can occur randomly at sufficiently high voltages, when electron multiplication between the electrodes is high enough to create a self-propagating avalanche of high electron density plasma, creating a channel of low resistivity between the electrodes (a sort of short-circuit). It is evident from the current waveform that the sharp pulse does not regularly occur at every half-cycle period. However, when such a sharp pulse in the current signal occurs, it is observed that the voltage signal at the same instance shows a rapid drop in voltage. The current through the plasma arc channel is significant enough to affect the voltage being generated, i.e. the voltage source cannot supply the current required to maintain the voltage between the electrodes. Similar behaviour is observed during the ignition phase, where the voltage collapses almost entirely.

Nevertheless, a gliding arc survives over thousands of AC cycles. This behaviour of the gliding arc voltage-current waveforms is consistent with the prior findings in the literature [39–41]. However, a distinction needs to be made between short-lived (10 ns), high-current (20 A) arcs and the long-lived (10 μs), low-current (200 mA) gliding 'arc' plasma. As evident from Figure 3.3, a high-current arc is first ignited at the closest gap when the applied voltage reaches the value equal to V_{ign}, which drops suddenly while attempting to sustain this arc. After the high-current arc has passed, the voltage recovers, but along with it a broad low-current signal can be

observed developing almost in phase with the voltage. This low-current signal returns every half-cycle and can be identified as the part of the discharge that actually glides, and it has a sufficiently long lifetime to move progressively upwards over many AC cycles. As the plasma glides through the electrode, the maximum voltage magnitude in each half-cycle is observed t0 increase with the height (V_h). When V_h reaches the value of V_{ign}, then the plasma extinguishes, and a new arc is ignited at the bottom where the discharge gap is lowest.

The picture that emerges is that, initially, when there are no free charges in the gas (no pre-ionization), the bottom of the electrodes with the lowest discharge gap is the likeliest location for a discharge to occur. This discharge comes in the form of an arc, rapidly creating much ionisation in a small plasma channel. While this arc disappears quickly due to a rapidly falling voltage, the ions and free electrons survive. Once the voltage starts to increase again, this cloud of ions and free electrons conduct current while simultaneously moving upwards due to buoyancy and gas flow. In the next half-cycle, the same cloud of ions and free electrons still forms the path of least resistance for current to follow, and so on, until some maximum height is reached. Progressively less current can be conducted by this gliding plasma (since it becomes longer), allowing the voltage to reach a higher and higher magnitude with each half-cycle. At some point, the maximum voltage magnitude V_h becomes high enough to allow the ignition of a new high-current arc at the position of lowest discharge gap. The height at which $V_h = V_{ign}$ is termed as gliding arc height (H_{arc}), which is greatly affected by the flow of gas surrounding the plasma discharge. The H_{arc} was observed to be inversely proportional with the gas flow rates. The specific power dissipated from the discharge per unit length increases when the gas flow rate increases, hence V_h approaches V_{ign} faster making H_{arc} shorter than that of lower gas flow gliding arc [42].

In some cases, when the gas flow rate is low, the rate of increase of V_h ($\delta V_h/\delta_t$) is not sufficiently high, resulting in a situation where V_h does not reach V_{ign}. In these situations, the current drawn by the plasma during a half-cycle is high enough to prevent the generator from recovering back to a maximum voltage magnitude.

Here, the plasma gets stationary at a particular height, providing a path of least resistance for the electrons to transfer between the electrodes and preventing new arc formation at the bottom of the electrodes. Due to this phenomenon, progressively more current is drawn from the power supply to the point when the power supply is forced to switch itself off. To avoid such circumstances altogether, and to have uniform electrical characteristics in all gliding arc cases, we introduced a manual pause of 1 ms in the applied voltage. This allows time for any residual ions and free electrons to flow out of the reactor, so that each gliding cycle can start fresh, with an arc ignition at the lowest discharge gap. Depending on the gas composition and the flow rate, we adjusted the applied voltage time and the pause time in order to get an optimum H_{arc} for each case. Applying such technique ensured a long running time of the plasma discharge in the reactor.

3.3.2 Effect of H_2 Fraction in Feed Ratio

The amount of H_2 in the feed gas mixture has an apparent effect on the CO_2 conversion, as illustrated in Figure 3.4. The fraction of H_2 was varied from 0.25 to 0.75 in the feed gas mixture. The total flow rate of the feed gas mixture was maintained at 200 ml/min in all the cases to ensure the same residence time of the reactants. The higher amount of hydrogen in the feed enhances the total CO_2 conversion as depicted in the literature [ref], from 21% at 0.25 hydrogen fraction to 54% at 0.75 hydrogen fraction. With an increasing fraction of H_2 in the feed gas, the probability of interaction of oxygen species with the hydrogen species increases, leading to the formation of water and pushing the reaction forward. It also helps to limit the CO back-reaction to CO_2. This is explained in detail in section 3.3.4.2. Another interesting point to note is that although direct hydrogenation of CO_2 to CH_4 is favoured thermodynamically compared to the RWGS reaction as evident from the ΔH values of the two, the product gas did not contain any amount of CH_4, and only CO was formed, hence in all the cases CO selectivity obtained was 100%.

$$CO_2 + 4H_2 \leftrightarrow CH_4 + 2H_2O \quad \Delta H°_{298K} = -165\ \mathrm{kJ/mol} \tag{3.8}$$

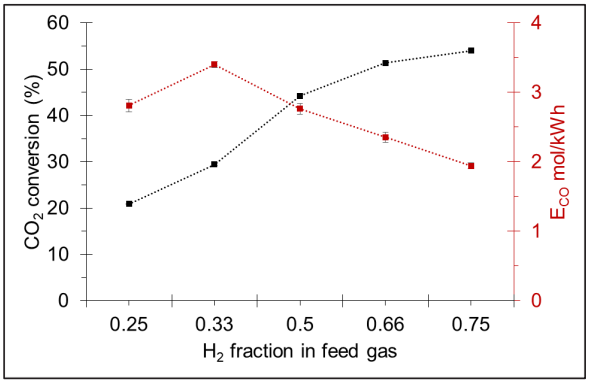

Figure 3.4: *Effect of the H_2 fraction in feed gas on the total CO_2 conversion and energy* yield *for the CO formation*

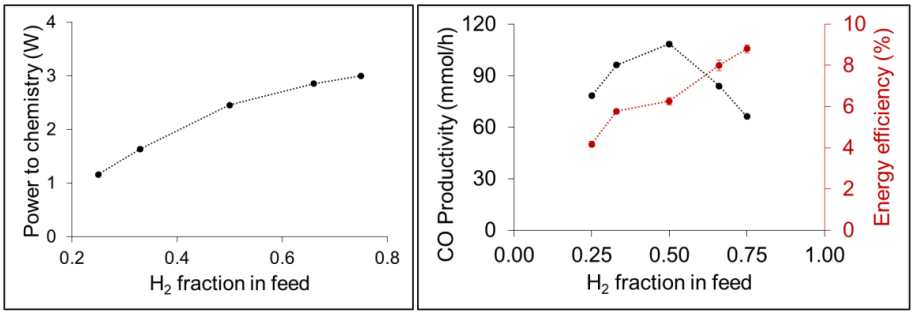

Figure 3.5: *(a) Power to chemistry and (b) CO productivity, as a function of the H_2 fraction in the feed gas*

The power consumed by the gliding arc plasma changes as the composition of the feed gas mixture changes. Correspondingly, the specific energy input varied, and their values were found to be between 8 to 10 kJ/L. Higher hydrogen fraction dissipates more power. H_2 has a higher ionisation potential than CO_2 (15.45 eV vs 13.78 eV), which makes it so that a higher hydrogen fraction requires a higher electric field, and hence a higher voltage V_{ign}, to ignite. Related to this, a higher ionisation potential also means a higher T_e to sustain the discharge, hence a higher T_e for higher H_2 fractions [43]. A higher T_e at same gas density provides more reactivity via electron-impact dissociation, signifying that more of the input power

is spent on these reactions and explaining the corresponding higher conversion of CO_2. This is illustrated in Figure 3.5 (a) as actual power delivered towards useful chemistry out of total power dissipated. Therefore, less power is required to sustain a discharge at low H_2 content, but the corresponding lower T_e also gives less conversion, and as H_2 content increases, more power is needed to sustain the discharge, resulting in a higher T_e but also more conversion (Appendix A6). It is observed in Figure 3.4 that the energy required to form a mole of CO generally decreases when H_2 fraction in the feed is increased, with an exception at a fraction of 0.33 of H_2. At this composition, 3.4 moles of CO are formed with the expense of 1 kWh of energy, which is the highest value among all the feed gas compositions. Furthermore, at highest CO_2 conversion this energy yield was found to be 1.9 mol/kWh. However, the energy efficiency improves with a higher amount of hydrogen, from 4% to almost 9% (Figure 3.5 (b)). The productivity of CO is plotted against the H_2 fraction in the feed gas in Figure 3.5(b). It is evident that overall, less CO is produced with increasing H_2, despite CO_2 conversion going up, because there is less CO_2 passing through the reactor. The maximum 108 mmol/h CO productivity is observed when feed gas contains 50-50% H_2 and CO_2 stoichiometrically.

3.3.3 Reactor Performance Evaluation at a Different Flow Rate

The effect of gas flow rate was studied at two different inlet gas compositions having 0.5 and 0.75 H_2 fractions. From both cases, it is established that the flow rate has a strong effect on the overall CO_2 conversion. High flow rates require high power to sustain the gliding arc plasma. Moreover, with an increase in the flow rate, the CO_2 conversion decreases in both the cases. For the case of 50% H_2 in the feed, the flow rate was varied from 200 to 800 ml/min, and for 75% H_2 case it was varied from 200 to 500 ml/min. The maximum flow rate was limited by the capacity of the mass flow controller used.

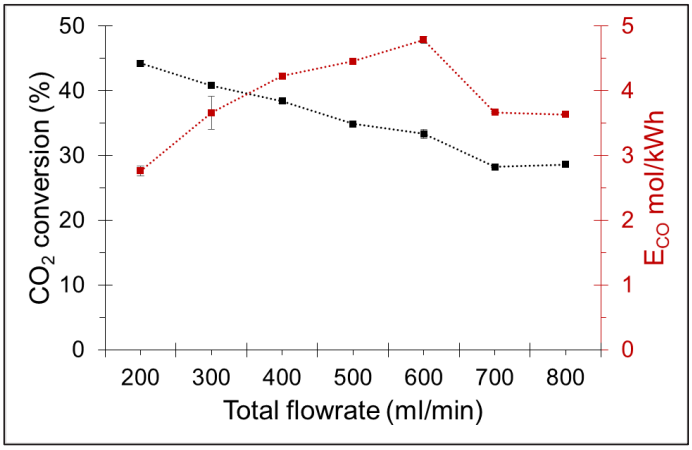

Figure 3.6: *Effect of the flow rate on the CO_2 conversion and the energy* yield *(at 0.5 H_2 fraction)*

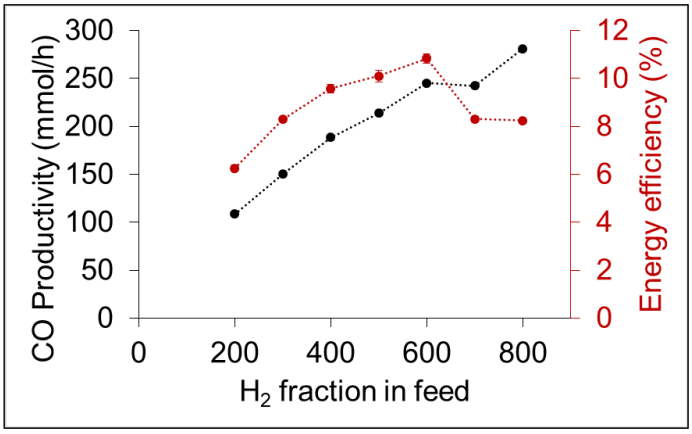

Figure 3.7: *CO productivity and energy efficiency as a function of the flow rate (0.5 H2 fraction)*

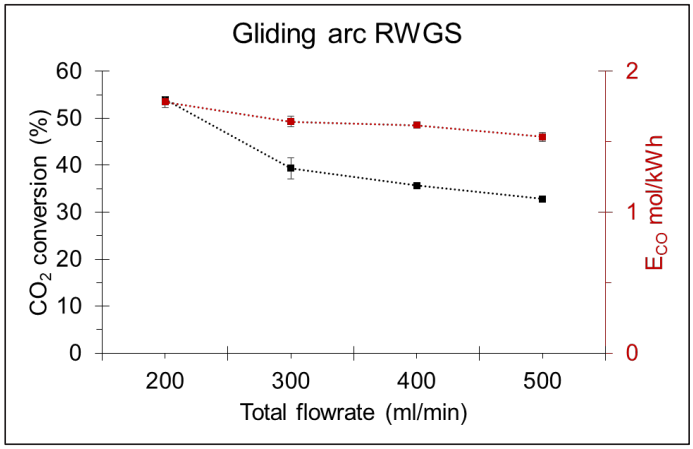

Figure 3.8: *Effect of the flow rate on the CO_2 conversion and the energy* yield *(at 0.75 H_2 fractions)*

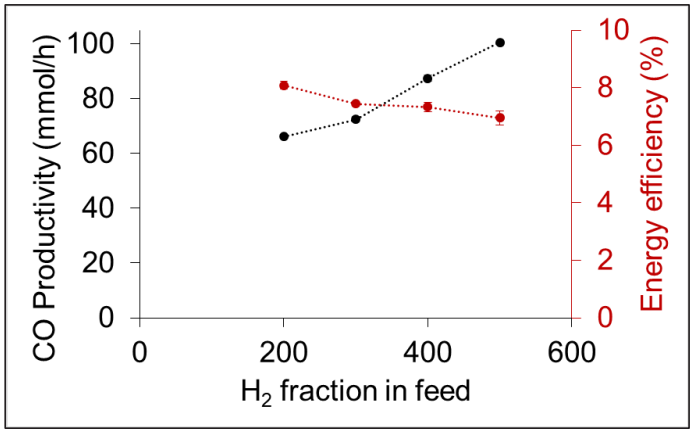

Figure 3.9: *CO productivity and energy efficiency as a function of the flow rate (0.75 H_2 fraction)*

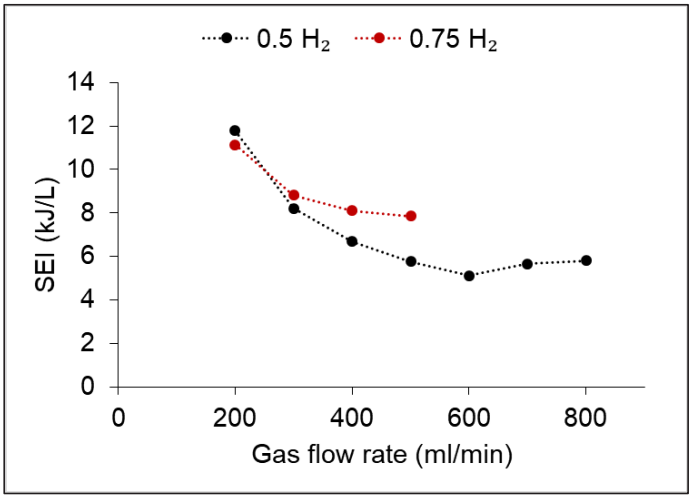

Figure 3.10: *Effect of the flow rate on the SEI*

In the case of 50% H_2, the CO_2 conversion at 200 ml/min was 45% which decreases to 28% at 700 and 800 ml/min (Figure 3.6). As the amount of CO_2 flowing through the plasma reactor increases with the high flow rates, the CO productivity also increases correspondingly, from 108 mmol/h to 281 mmol/h (Figure 3.7). Similarly, in the case of 75% H_2 in the feed gas, the CO_2 conversion decreases from 54% at 200 ml/min to 32% at 500 ml/min (Figure 3.6), and the CO productivity increases from 66 mmol/h to 100 mmol/h respectively.

As more molecules flow per unit time through the plasma zone, the gliding arc plasma requires more power to sustain. Although power increase with the flow rate, the SEI decreases as seen in Figure 3.10, which corresponds to the lower conversions at high flow rates. The energy required to form CO sees a maximum value at 600 ml/min with the value of 4.8 mol/kWh, and that corresponds to the highest energy efficiency of 11%, in case of 0.5 H_2 fractions. On occasion of 0.75 H_2 fractions in the feed, the energy required to form CO decreases with increase in the flow rate with the maximum value of 1.8 mol/kWh, corresponding to an energy efficiency of 8%. Comparing these values with the values of a DBD reactor, it is seen that the gliding arc plasmas produce more conversion with higher energy efficiencies. Similar

conclusions are reported in the literature[17]. The values of energy required to synthesise CO are 10-12 times more than that of a DBD reactor.

3.3.4 Optical Emission Spectroscopy Analysis

The electron density (N_e) and rotational temperature are important parameters which define the plasma characteristics. To calculate these parameters, the light emission of the plasma was recorded through optical emission spectroscopy. Various atomic and molecular spectra were identified in these OES measurements. Amongst those, the molecular band of OH radical at 306 nm ($A^2\Sigma^+$-$X^2\Pi_\gamma$ transition) was used to calculate the rotational temperature of the plasma, and H_α spectral line (656.27 nm) was used to calculate the electron density of the plasma. Furthermore, atomic O spectral lines at 777 nm were used to check the atomic oxygen concentration. The protuberance in the measured spectra was found to be caused by chemiluminescence phenomenon of the CO species, which explains the extent of CO backreaction and its effect on the reaction mechanism. This outcome is essential to propose a reaction mechanism for the RWGS reaction using a gliding arc reactor.

3.3.4.1 Calculation of factors

3.3.4.1.1 Electron Density (N_e)

N_e is calculated by the Stark broadening ($\Delta\lambda_S$) of H_α spectral emission. The Stark broadening of H_α spectral line in the plasma allows quick determination of the electron density [44,45]. To determine the Stark broadening, the measured H_α spectra were fitted with the Voigt function, which is a convolution of Gaussian and Lorentzian profiles (Figure 3.11). Doppler broadening ($\Delta\lambda_{Dop}$) and instrumental broadening ($\Delta\lambda_{Inst}$) mechanisms contribute to the Gaussian profile, whereas, natural broadening ($\Delta\lambda_n$), resonance broadening ($\Delta\lambda_r$), van der Waal's broadening ($\Delta\lambda_{van}$), and Stark broadening ($\Delta\lambda_S$) are responsible for the Lorentzian component of experimentally measured emission atomic emission lines [46–48]. The total FWHM

$\Delta\lambda_L$ for all Lorentzian contributions is directly the sum of each individual contribution.

$$\Delta\lambda_L = \Delta\lambda_{van} + \Delta\lambda_n + \Delta\lambda_r + \Delta\lambda_S$$

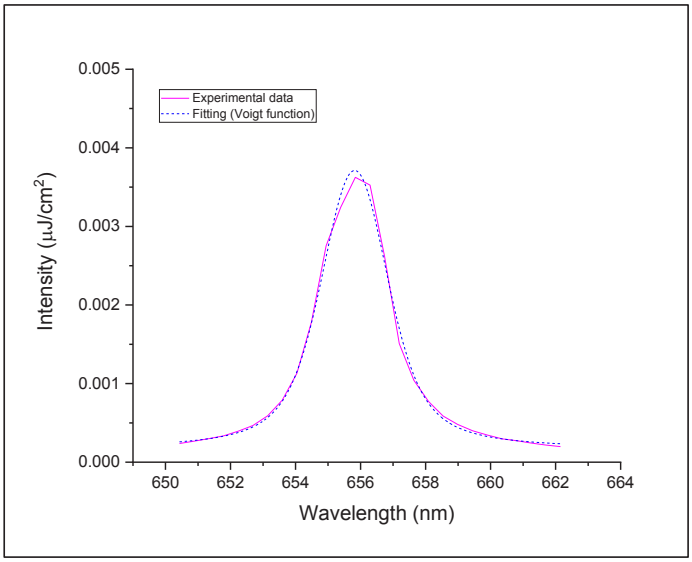

Figure 3.11: *Example of the Voigt function fitting and experimentally measured H_α spectral lines to calculate Lorentzian width (R^2 = 0.995) for 0.75 H_2 in feed mixture*

At our experimental operating conditions, $\Delta\lambda_n$ and $\Delta\lambda_r$ are negligible; hence, they are left out of the equation to calculate $\Delta\lambda_S$. The van der Waals broadening was calculated using the Griem's correlation; the literature mentions that at high density (atmospheric pressure) plasmas, the value of $\Delta\lambda_{van}$ can be ~ 30 to 35% of the total FWHM of Lorentzian profile [46]. Having both the values of $\Delta\lambda_{van}$ gives us a range of minimum and maximum values of $\Delta\lambda_{van}$, hence also the range of $\Delta\lambda_S$ and subsequently N_e. The Stark broadening correlation with electron density is given by Griem as follows [49]:

$$\lambda_S = 0.549\ nm\ x\ \left(\frac{N_e}{10^{23} m^{-3}}\right)^{0.67965} \tag{3.9}$$

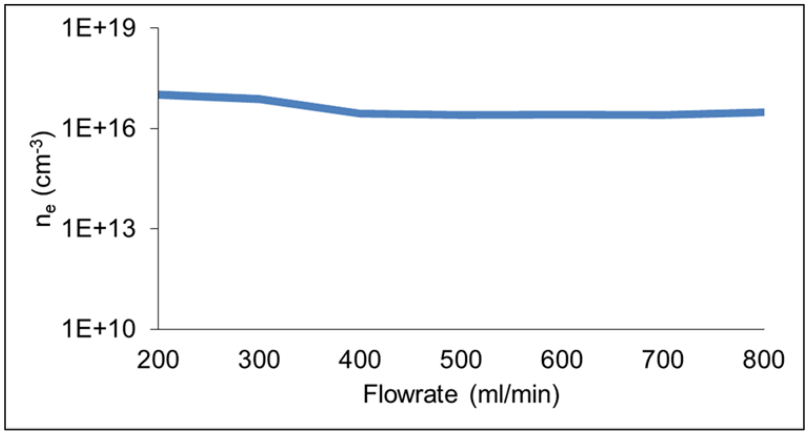

(a)

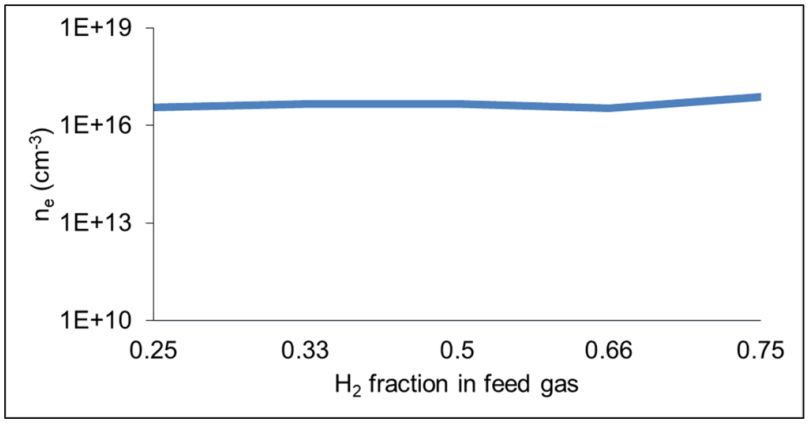

(b)

Figure 3.12: *Effect on the electron density with respect to (a) the gas flow rate, (b) feed gas composition*

The results suggest that the values of N_e are in the range of 10^{16} to 10^{17} cm^{-3}, which is typical for a gliding arc plasma [24]. Figure 3.12 (a) and 3.12 (b) shows the effect on the electron density with respect to the different feed gas composition and the flow rate. It is apparent from the Figures that the conditions where we have observed, namely high conversions (Figure 3.4 and 3.7), correspond to higher electron density. The electron densities at 200 and 800 ml/min flow rate are found

to be 1.3 x 10^{17} and 3.9 x 10^{16} cm^{-3}. Whereas, at 25% and 75% H_2 in feed these values were 4.6 x 10^{16} and 9.7 x 10^{17} cm^{-3}.

3.3.4.1.2 Rotational Temperature

The spectra recorded via OES are compared with simulated spectra to determine rotational temperature, assuming that the population of rotational levels follows a Boltzmann distribution. The OH (A-X) transition was used to determine the rotational temperature in this study [47,50]. The rotational temperature can be calculated either by fitting the entire rotational band of OH (A-X) or simple by fitting R and P branches of the OH spectra. R and P branch occur at 307 and 309 nm respectively. Figure 3.13 shows the simulated and experimental spectra of OH (A-X) band. The rotational temperature was found to be 3250 K.

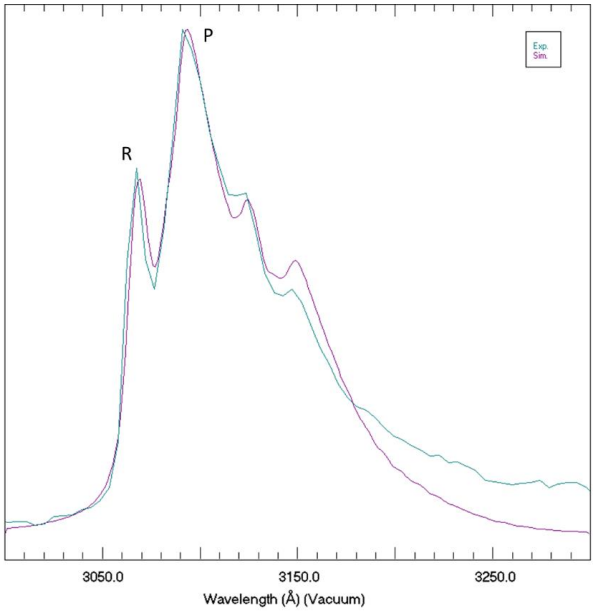

Figure 3.13: *Experimental and simulated spectra for the OH (A-X) band obtained using 'LIFBASE' software*

3.3.4.2 Plausible Reaction Mechanism

As stated in the literature, the flow rate and applied power mainly contribute to the conversion of CO_2, and it is safe to assume that the reaction mechanism follows a similar path when only flow rate and power varies [51]. Therefore, OES measurements from three different feed gas composition are considered to investigate the reaction mechanism, no H_2, 50% H_2 and 75% H_2. Figure 3.14 (a) shows the OES spectra for these 3 cases.

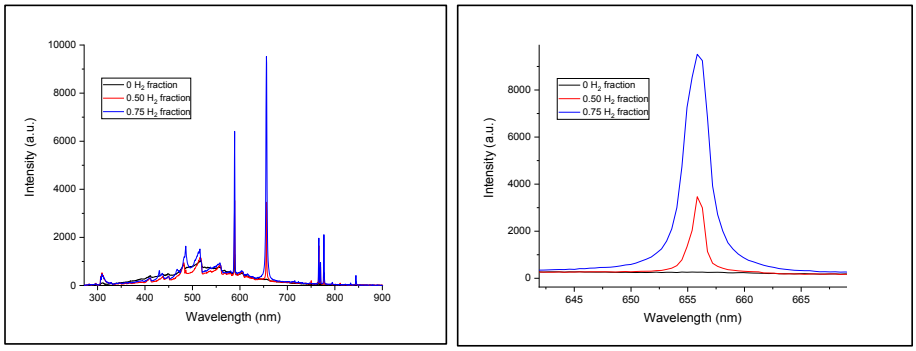

Figure 3.14: *(a) Optical emission spectra of the gliding arc plasma (b) zoomed-in region of the H_α emission*

Figure 3.14 (b) shows that the intensity of the H_α emission is highest when the H_2 content is highest. No H_α emission is observed in case of no H_2. The intensity of H_α emission corresponds to the population of atomic H. The broad protuberance in the region 300-700 nm was observed. This is attributed to the chemiluminescence phenomenon given by the reaction shown by equation 3.17. This protuberance is higher in case of pure CO_2 compared to the other two cases, where the CO recombination reaction towards CO_2 is slowed down. The electronic dissociation of CO_2 produces CO and atomic oxygen which emits atomic spectra observed at 777 and 844 nm. The OH (A-X) band is absent in case of no hydrogen but is present in the other two cases. In both of these cases the P and R peak ratio of OH band does not vary, indicating that both cases have similar rotational temperatures. The

significant reaction pathways of the gliding arc are listed in equation (3.10 to 3.17). Along with rotational and vibrational excitation from impact by electrons [52], CO_2 can be dissociated by electrons (equation 3.12). Similarly, H_2 is dissociated via electron impact (equation 3.13). OH radicals are formed by O reacting with H_2 and H reacting with CO_2 (equation 3.14 and 3.14). OH and CO combining together to form CO_2 is possible but undesired to drive RWGS reaction forward (equation 3.16). However, recombination to form water is desirable and drives the whole RWGS reaction forward.

$$CO_2 + e \rightarrow CO + e + O \quad (3.10)$$

$$H_2 + e \rightarrow H + H + e \quad (3.11)$$

$$H_2 + O \rightarrow OH + H \quad (3.12)$$

$$CO_2 + H \rightarrow OH + CO \quad (3.13)$$

$$OH + CO \rightarrow CO_2 + H \quad (3.14)$$

$$H_2 + OH \rightarrow H + H_2O \quad (3.15)$$

$$OH + OH \rightarrow H_2O + O \quad (3.16)$$

$$CO + O \rightarrow CO_2 + h\nu \quad (3.17)$$

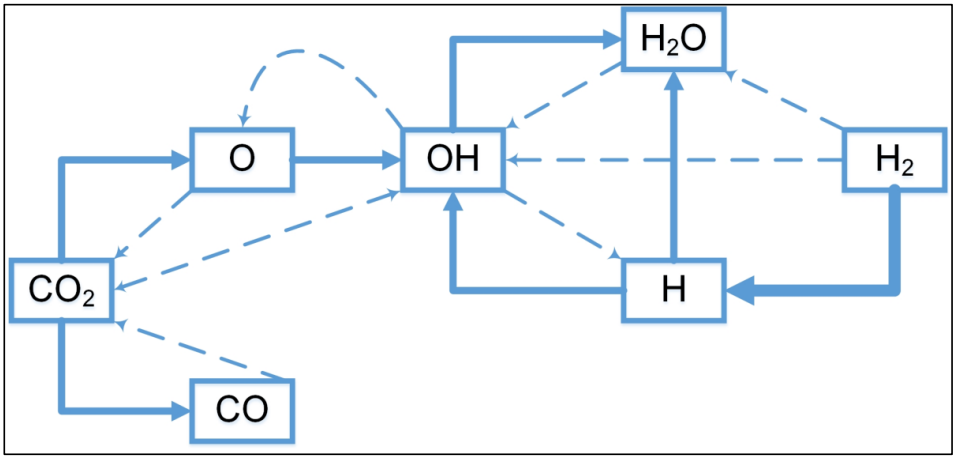

Figure 3.15: *Plausible reaction mechanism of the RWGS reaction in a gliding arc plasma reactor*

The plausible reaction mechanism is illustrated in Figure 3.15. Here the solid arrows denote the desired reaction mechanism of the RWGS reaction, while dashed arrows imply other reactions occurring simultaneously. Comparing CO_2 hydrogenation OES spectra (Appendix B) of a DBD reactor it can be observed that the chemiluminescence phenomenon has seen a severe declination in the gliding arc plasmas. Interestingly the OH (A-X) band which is predominantly detected in the gliding arc plasma was absent for the DBD reactors. Moreover, the CHO emissions observed in the DBD reactor spectra were absent in the gliding arc spectra. This suggests that the different path in the reaction mechanism is responsible for the better energy efficiency and yield of the gliding arc reactor.

3.4 Conclusions

The reverse water-gas shift reaction is carried out using an alternate current sinusoidal gliding arc plasma reactor at ambient conditions. The operating regime analysis of the gliding arc plasma elucidates technique to form a stable gliding arc plasma while carrying out the RWGS reaction. The effect of the composition of the feed gas mixture and the gas flow rate are evaluated based on overall CO_2 conversion, energy efficiency, CO productivity and energy required to produce CO. Optical emission spectroscopy is used to determine the active species in the plasma, which subsequently are used to justify the reaction performance and to deduct the plausible reaction mechanism. Electrical diagnostics revealed that with higher H_2 content in the feed gas increases, the gliding arc plasma requires more power to sustain. Likewise, a higher gas flow rate draws more power to sustain the gliding arc plasma. Increasing H_2 content in the feed gas mixture and having low feed gas flow rates benefits the overall CO_2 conversion Best performance in terms of the CO_2 conversion, 54% is obtained at 200 ml/min gas flow having 75% H_2. While from the energy point of view, the best performance is 11% energy efficiency which corresponds to 4.8 mol/kWh energy yield, achieved at 600 ml/min gas flow having 50-50% H_2 and CO_2 composition. When the feed gas composition is varied, an optimum value of CO productivity is observed at 50% H_2 in the feed gas mixture. The

reason for such optimal value is attributed to the combination of total power going to the discharge and available CO_2 to convert, giving most CO molecules/s. Overall highest productivity achieved in this study is 281 mmol/h. As mentioned in the literature [53,54], a 3-D configuration of the arc plasma potentially offers improved energy efficiencies, 2 more variants of gliding arc reactors were designed and fabricated.

Plasma parameters calculated using OES are used to decipher the reaction mechanism of the RWGS in a gliding arc reactor. The electron density calculated using H_α emission is in the range of 10^{16} cm^{-3}. The rotational temperature calculated using OH (A-X) band is 3250K. Both of these values represents a typical gliding arc discharge. The gliding arc discharge shows diminished chemiluminescence as compared to DBD discharge for the same reaction, which explains the high energy efficiency of gliding arc plasmas. From the optical analysis, it is established that the RWGS reaction in gliding arc plasma, the reaction mechanism proceeds via OH species formation, unlike DBD plasma. This outcome is important to propose a reaction mechanism for the RWGS reaction using a gliding arc reactor. This study confirms that industrially relevant RWGS reaction can be performed at ambient conditions while forming highly pure syngas by a gliding arc plasma process. The output gas composition from this gliding arc process is already acceptable for CAMERE and FT synthesis. Hence, a localised small scale methanol or FT plant can be designed in conjunction with a gliding arc process to provide syngas, if further energy efficiency can be achieved.

Reference

[1] Joo O S, Jung K D, Moon I, Rozovskii A Y, Lin G I, Han S H and Uhm S J 1999 Carbon dioxide hydrogenation to form methanol via a reverse-water-gas-shift reaction (the CAMERE process) *Ind. Eng. Chem. Res.* **38** 1808–12

[2] Centi G, Quadrelli E A and Perathoner S 2013 Catalysis for CO_2 conversion: a key technology for rapid introduction of renewable energy in the value chain of chemical industries *Energy Environ. Sci.* **6** 1711–31

[3] Pino L, Recupero V, Beninati S, Shukla A K, Hegde M S and Bera P 2002 Catalytic partial-oxidation of methane on a ceria-supported platinum catalyst for application in fuel cell electric vehicles *Appl. Catal. A Gen.* **225** 63–75

[4] Rostrupnielsen J R and Hansen J H B 1993 CO_2-Reforming of Methane over Transition Metals *J. Catal.* **144** 38–49

[5] Rath L K and Longanbach J R 1991 A perspective on syngas from coal *Energy Sources* **13** 443–59

[6] Speight J G 2014 *Heavy hydrocarbon gasification for synthetic fuel production* (Woodhead Publishing)

[7] Medrano-García J D, Ruiz-Femenia R and Caballero J A 2019 Optimal carbon dioxide and hydrogen utilization in carbon monoxide production *J. CO_2 Util.* **34** 215–30

[8] Wang W, Wang S, Ma X and Gong J 2011 Recent advances in catalytic hydrogenation of carbon dioxide *Chem. Soc. Rev.* **40** 3703–27

[9] Perathoner S and Centi G 2014 CO_2 recycling: A key strategy to introduce green energy in the chemical production chain *ChemSusChem* **7** 1274–82

[10] Centi G and Perathoner S 2009 Opportunities and prospects in the chemical recycling of carbon dioxide to fuels *Catal. Today* **148** 191–205

[11] Kaiser P, Unde R B, Kern C and Jess A 2013 Production of liquid hydrocarbons with CO_2 as carbon source based on reverse water-gas shift and fischer-tropsch synthesis *Chemie-Ingenieur-Technik* **85** 489–99

[12] D. Wang, H. A. Wright, B. C. Ortego, S. Trinh, R. Espinoza, US Patent 6992112-B2 (2006)

[13] Pastor-Pérez L, Baibars F, Le Sache E, Arellano-García H, Gu S and Reina T R 2017 CO_2 valorisation via Reverse Water-Gas Shift reaction using advanced Cs doped Fe-Cu/Al_2O_3 catalysts *J. CO_2 Util.* **21** 423–8

[14] Eliasson B, Kogelschatz U, Xue B and Zhou L 1998 Hydrogenation of carbon dioxide to methanol with a discharge-activated catalyst *Ind. Eng. Chem. Res.* **37** 3350–7

[15] Zeng Y and Tu X 2016 Plasma-Catalytic CO_2 Hydrogenation at Low Temperatures *IEEE Trans. Plasma Sci.* **44** 405–11

[16] Paulussen S, Verheyde B, Tu X, De Bie C, Martens T, Petrovic D, Bogaerts A and Sels B 2010 Conversion of carbon dioxide to value-added chemicals in atmospheric pressure dielectric barrier discharges *Plasma Sources Sci. Technol.* **19** 034015

[17] Bogaerts A, Kozák T, van Laer K and Snoeckx R 2015 Plasma-based conversion of CO_2: current status and future challenges *Faraday Discuss.* **183** 217-232

[18] Kelly S and Sullivan J A 2019 CO_2 Decomposition in CO_2 and CO_2/H_2 Spark- like Plasma Discharges at Atmospheric Pressure *ChemSusChem* **12** 3785–91

[19] de la Fuente J F, Moreno S H, Stankiewicz A I and Stefanidis G D 2016 Reduction of CO_2 with hydrogen in a non-equilibrium microwave plasma reactor *Int. J. Hydrogen Energy* **41** 21067–77

[20] Kano M, Satoh G and Iizuka S 2012 Reforming of Carbon Dioxide to Methane and Methanol by Electric Impulse Low-Pressure Discharge with Hydrogen *Plasma Chem. Plasma Process.* **32** 177–85

[21] Fridman A, Nester S, Kennedy L, Saveliev A and Mutaf-Yardimci O 1998 Gliding arc gas discharge *Prog. Energy Combust. Sci.* **25** 211–31

[22] Kusano Y 2009 Plasma surface modification at atmospheric pressure *Surf. Eng.* **25** 415–6

[23] Kuznetsova I, Kalashnikov N, Gutsol A, Fridman A and Kennedy L 2002 Effect of “ overshooting” in the transitional regimes of the low-current gliding arc discharge *J. Appl. Phys.* **92** 4231–7

[24] Bruggeman P J, Iza F and Brandenburg R 2017 Foundations of atmospheric pressure non-equilibrium plasmas *Plasma Sources Sci. Technol.* **26** 123002

[25] Fridman A, Chirokov A and Gutsol A 2005 topical review: Non-thermal atmospheric pressure discharges *J. Phys. D* **38** R1

[26] Zhu J, Ehn A, Gao J, Kong C, Aldén M, Salewski M, Leipold F, Kusano Y and Li Z 2017 Translational, rotational, vibrational and electron temperatures of a gliding arc discharge *Opt. Express* **25** 20243

[27] Lin L, Wu B, Yang C and Wu C 2006 Characteristics of gliding arc discharge plasma *Plasma Sci. Technol.* **8** 653–5
[28] Patil B S, Rovira Palau J, Hessel V, Lang J and Wang Q 2016 Plasma Nitrogen Oxides Synthesis in a Milli-Scale Gliding Arc Reactor: Investigating the Electrical and Process Parameters *Plasma Chem. Plasma Process.* **36** 241–57
[29] Stryczewska H D and Komarzyniec G K 2010 Properties of gliding arc (GA) reactors energized from AC/DC/AC power converters *Proc. - 2010 IEEE Reg. 8 Int. Conf. Comput. Technol. Electr. Electron. Eng. Sib.* 744–9
[30] Burlica R and Locke B R 2008 Pulsed plasma gliding-arc discharges with water spray *IEEE Trans. Ind. Appl.* **44** 482–9
[31] Burlica R, Shih K and Locke B R 2010 Formation of H_2 and H_2O_2 in a Water-Spray Gliding Arc Nonthermal Plasma Reactor **14** 6342–9
[32] Wang W, Patil B, Heijkers S, Hessel V and Bogaerts A 2017 Nitrogen Fixation by Gliding Arc Plasma: Better Insight by Chemical Kinetics Modelling *ChemSusChem* **10** 2110
[33] Korolev Y D, Frants O B, Geyman V G, Landl N V. and Kasyanov V S 2011 Low-current " gliding Arc" in an air flow *IEEE Trans. Plasma Sci.* **39** 3319–25
[34] Czernichowski A 1994 Gliding arc: Applications to engineering and environment control *Pure Appl. Chem.* **66** 1301–10
[35] Richard F, Cormier J M, Pellerin S and Chapelle J 1996 Physical study of a gliding arc discharge *J. Appl. Phys.* **79** 2245–50
[36] Czernichowski A, Nassar H, Ranaivosoloarimanana A, Fridman A A, Simek M, Musiol K, Pawelec E and Dittrichova L 1996 Spectral and electrical diagnostics of gliding arc *Acta Phys. Pol. A* **89** 595–603
[37] Griem H R 1974 Spectral Line Broadening by Plasmas *Pure Appl. Phys.* **39** 1-410
[38] Sun Z W, Zhu J J, Li Z S, Aldén M, Leipold F, Salewski M and Kusano Y 2013 Optical diagnostics of a gliding arc *Opt. Express* **21** 6028
[39] Nunnally T, Gutsol K, Rabinovich A, Fridman A, Gutsol A and Kemoun A 2011 Dissociation of CO_2 in a low current gliding arc plasmatron *J. Phys. D. Appl. Phys.* **44** 274009
[40] Snoeckx R and Bogaerts A 2017 Plasma technology – a novel solution for CO_2 conversion? *Chem. Soc. Rev.* **46** 5805–63
[41] Wang W, Mei D, Tu X and Bogaerts A 2017 Gliding arc plasma for CO_2 conversion: Better insights by a combined experimental and modelling approach *Chem. Eng. J.* **330** 11–25
[42] Kusano Y, Salewski M, Leipold F, Zhu J, Ehn A, Li Z and Aldén M 2014 Stability of alternating current gliding arcs *Eur. Phys. J. D* **68** 319
[43] Lieberman M A and Lichtenberg A J 2005 *Principles of Plasma Discharges and Materials Processing* **112** (John Wiley & Sons)
[44] El Sherbini A M, Hegazy H and El Sherbini T M 2006 Measurement of electron density utilizing the Hα-line from laser produced plasma in air *Spectrochim. Acta - Part B At. Spectrosc.* **61** 532–9
[45] Uman M A and Orville R E 2008 Electron density measurement in lightning from stark-broadening of Hα *J. Geophys. Res.* **69** 5151–4
[46] Yanguas-Gil A, Focke K, Benedikt J and Von Keudell A 2007 Optical and electrical characterization of an atmospheric pressure microplasma jet for Ar/ CH_4 and Ar/ C_2H_2 mixtures *J. Appl. Phys.* **101** 103307
[47] Laux C O, Spence T G, Kruger C H and Zare R N 2003 Optical diagnostics of atmospheric pressure air plasmas *Plasma Sources Sci. Technol.* **12** 125–38
[48] Luque J M, Calzada M D and Sáez M 2003 Experimental research into the influence of ion dynamics when measuring the electron density from the Stark broadening of the Hαand Hβlines *J. Phys. B At. Mol. Opt. Phys.* **36** 1573–84
[49] Gigosos M A, González M Á and Cardeñoso V 2003 Computer simulated Balmer-alpha, -beta and -gamma Stark line profiles for non-equilibrium plasmas diagnostics *Spectrochim. Acta Part B At. Spectrosc.* **58** 1489–504
[50] Gicquel A, Hassouni K, Breton Y, Chenevier M and Cubertafon J C 1996 Gas temperature measurements by laser spectroscopic techniques and by optical emission spectroscopy *Diam. Relat. Mater.* **5** 366–72
[51] Ozkan A, Dufour T, Silva T, Britun N, Snyders R, Bogaerts A and Reniers F 2016 The influence of power and frequency on the filamentary behavior of a flowing DBD – Application to the splitting of CO_2 *Plasma Sources Sci. Technol.* **25** 025013

[52] Kozàk T and Bogaerts A 2014 Splitting of CO_2 by vibrational excitation in non-equilibrium plasmas: A reaction kinetics model *Plasma Sources Sci. Technol.* **23** 045004

[53] Ramakers M, Medrano J A, Trenchev G, Gallucci F and Bogaerts A 2017 Revealing the arc dynamics in a gliding arc plasmatron: a better insight to improve CO_2 conversion *Plasma Sources Sci. Technol.* **26** 125002

[54] Kalra C S, Cho Y I, Gutsol A, Fridman A and Rufael T S 2005 Gliding arc in tornado using a reverse vortex flow *Rev. Sci. Instrum.* **76** 025110

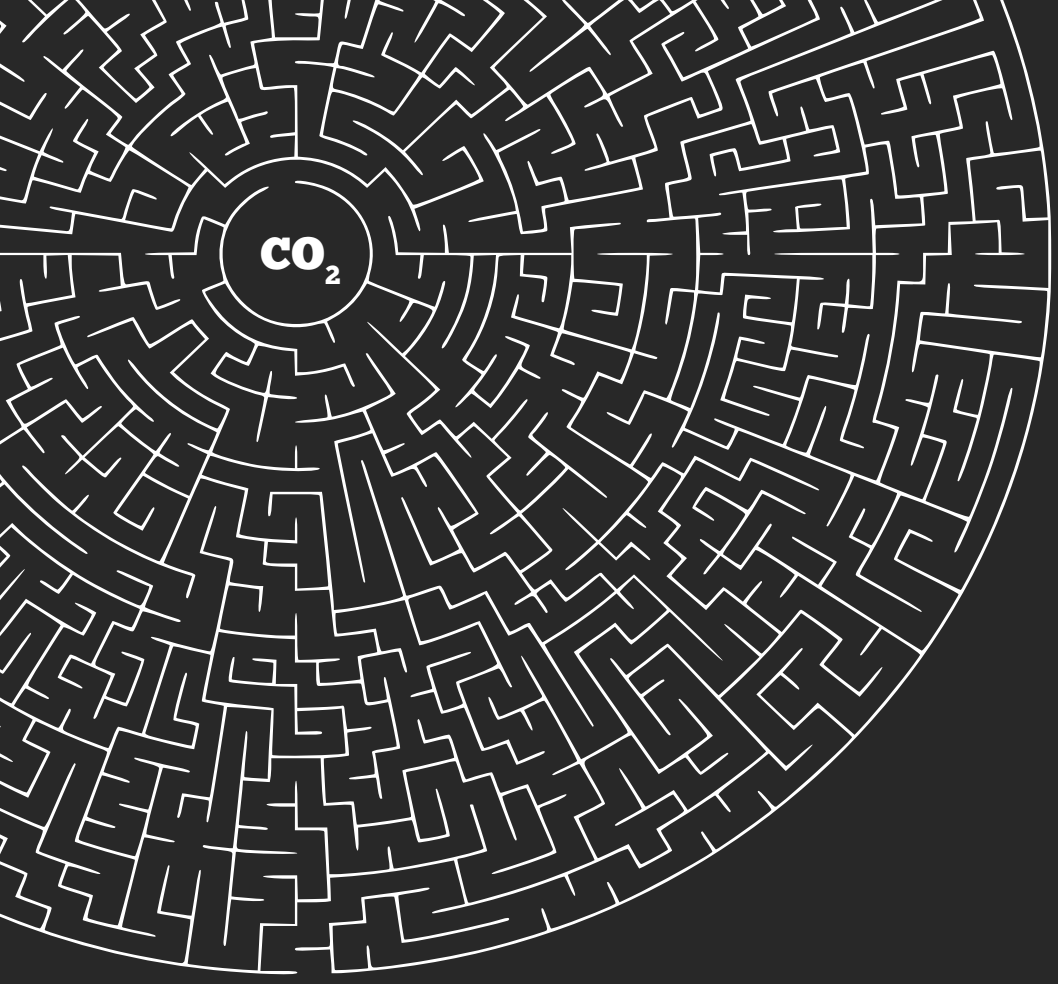
CO_2

Chapter 4

CO_2 methanation reaction using an atmospheric pressure plasma with Rh/γ-Al_2O_3 catalyst

This chapter is adapted from

CO_2 methanation reaction using an atmospheric pressure plasma with Rh/γ-Al_2O_3 catalyst, Chaudhary, R., van Rooij, G., Li, S., Hessel, V., in preparation.

Abstract.

There is an increasing quantity of research that recognises the importance of Power-to-Gas technology to store surplus renewable energy into methane gas. If P2G is realised with recycled CO_2 as a carbon source, then it could provide a solution to the CO_2 mitigation problem. This chapter focuses on the direct CO_2 methanation via atmospheric pressure, through the pathway of the non-thermal plasma-catalytic hybrid reaction by using Rh/γ-Al_2O_3 catalyst. A dielectric barrier discharge reactor was used for this investigation. The effect of different support materials in plasma was investigated, which shows improved CO_2 conversion compared to an empty reactor with plasma discharge. Without the metal catalyst, the support material shows high selectivity towards CO, which was inverted by the implementation of Rh/γ-Al_2O_3 catalyst in the plasma discharge. The plasma reaction with the Rh/γ-Al_2O_3 catalyst increases the CH_4 selectivity to 97%. Lowering the residence time and applied power resulted in enhanced energy efficiency. The burst mode was employed to further improve the energy efficiency of the reaction, with the best value of 2.4 mol/kWh for the formation of CH_4. The results of Rh/γ-Al_2O_3 catalyst plasma reaction are used to predict a reaction mechanism for plasma-catalytic direct CO_2 methanation.

4.1 Introduction

The power to gas (P2G) process is highly regarded as a potential technique to provide a sustainable solution to renewable energy storage problems as well as to CO_2 mitigation [1]. The prospect of large-scale implementation of this process is compelling for the scientific community to explore since it has the advantage of using already existing natural gas infrastructure for transport and distribution of methane [2–7]. CO_2 methanation (eq. 4.1) serves as a backbone of the P2G process for the production of synthetic natural gas, and non-thermal plasma technologies are considered as a potential approach to implementing the CO_2 methanation [8–11]. Figure 4.1 presents an overview of the plasma integrated P2G process. This approach uses the surplus energy for the production of hydrogen via water electrolysis process as well as for the process of conversion of the CO_2 to methane via the non-thermal plasma route.

$$CO_2 + 4H_2 \leftrightarrow CH_4 + 2H_2O \quad \Delta H_{25°C} = -165\ \text{kJ/mol} \tag{4.1}$$

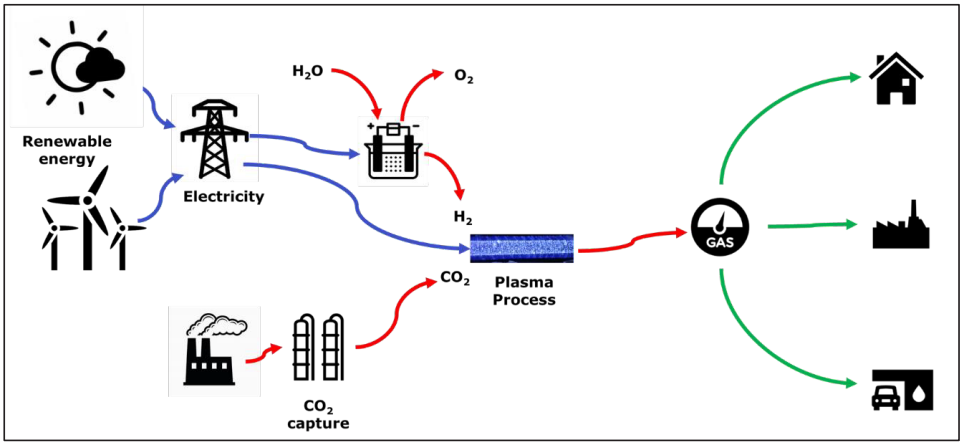

Figure 4.1: *Schematic representation of the Power-to-Gas process comprising of the plasma-assisted CO_2 methanation process*

The non-thermal plasma medium allows collisions of highly energetic electrons with other heavy species in the plasma which assists ionization and dissociation of even the thermodynamically stable molecules, such as CO_2, via electronic, vibrational, or rotational excitation at ambient conditions [12–19]. This principle is being widely explored and implemented to various fields from the purification of exhaust gases to the synthesis of chemicals [20,21]. The high concentration of energetic and chemically active species offers alternate pathways which promote thermodynamically unfavourable reactions even at low temperature [22]. Therefore, CO_2 excitation via electrical energy in a plasma reactor generates active radicals, excited molecules, atoms, and ions, which are even at low temperatures energetic enough to initiate chemical reactions of CO_2 and H_2 to achieve methanation. Furthermore, a plasma reaction operated along with a catalyst could further help in achieving a high selective yield of the desired product at mild reaction conditions via the synergistic impact of plasma and catalytic combination [23–26]. Moreover, the plasma reaction route offers additional advantages, viz., rapid startup, simpler assembly and operations at atmospheric pressure, which could reflect positively on the economics of the process.

The plasma-catalytic synergy for the CO_2 methanation is well established as known from a few prior studies with a DBD reactor. Fan et al. obtained about 80% CH_4 yield in an atmospheric pressure DBD packed with Ni/$MgAl_2O_4$ catalysts; however, external heating was needed to maintain the temperature at 350 °C [27]. The ratio of H_2: CO_2 was 4, and the whole feed gas mixture was diluted by 20% with nitrogen. A study by Lee et al. reported to achieve 95% CH_4 selectivity with 23% of the CO_2 conversion with the ratio of H_2 to CO_2 as 7 [28]. A few recent studies with Ni catalyst on a modified ceria-zirconia support showed the selectivity of CH_4 close to 100% [29,30]. Group VIII metal catalysts on various supports have been investigated for the direct CO_2 methanation [5,31–35]. So far, Ni, Ru and Rh have been stated as the most effective metals for this reaction, while Ru and Rh have been reported as the most selective towards methane [36]. Although Ni is very widely accepted the catalyst for the CO_2 methanation, it tends to get deactivated at low temperatures

due to the surface saturation of the metal particles with carbon monoxide via formation of nickel subcarbonyls [37]. The plasma-assisted CO_2 methanation is carried out at low temperatures, hence the application of the Ni-based catalyst is not considered in this study. Rhodium has been demonstrated as one of the most stable and active catalysts, even at low-temperature reactions for the CO_2 methanation. Moreover, Rh has been shown to be one of the most active metal for the direct CO_2 hydrogenation [36]. Rh/γ-Al_2O_3 was used as a probe catalyst to infer plausible reaction mechanism of CO_2 methanation. The reaction mechanism analysis is primary in nature as understanding of a hybrid plasma-catalytic system is underdeveloped to the current date. The interdependence of the plasma properties on the packing material and surface behaviour of the catalysts on the surrounding plasma phase and simultaneous surface and plasma phase reactions increases the difficulties in prediction of the reaction pathway.

A green reaction route for the CH_4 synthesis from CO_2 is proposed to be enabled and facilitated by non-equilibrium cold plasma using Rh/γ-Al_2O_3 as a catalyst. Therefore, in this chapter, we will examine the way to steer the selectivity in plasma-catalytic reaction in order to achieve better performance of CO_2 methanation while lowering the energy consumption. This chapter also discusses a plausible reaction mechanism for plasma-catalytic hybrid reaction route.

4.2 Methods and Materials

4.2.1 Experimental Setup

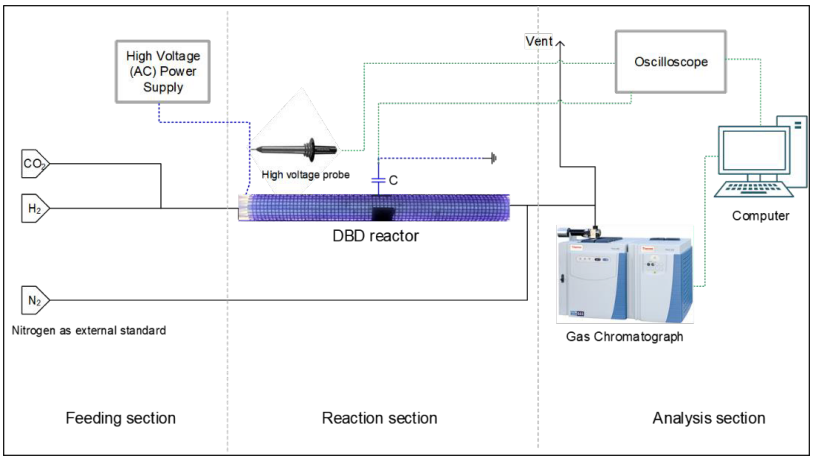

Figure 4.2: *Schematics of plasma-assisted CO_2 methanation experimental setup*

The schematic representation of the experimental setup is shown in Figure 4.2. To perform plasma-assisted catalytic methanation of CO_2, a cylindrical quartz reactor is used, where the quartz serves the dual purpose of reactor wall and a dielectric barrier that is required for the generation of the plasma discharge. The outer diameter of the quartz reactor is 13 mm, and the inner diameter is 10 mm, making the dielectric barrier thickness to be 1.5 mm. The discharge zone in the reactor is 100 mm long, while the discharge gap is 1.5 mm by using an inner electrode of 7 mm. This configuration provides 16 ml of reactor volume. The empty volume surrounding the electrode was filled with the designated packing materials. Quartz wool was put at the end of the filled tube to fixate the catalyst bed. This reactor was implemented into a Carbolite Gero oven and operated at atmospheric pressure, and the temperature was maintained at 100 °C to prevent condensation of water inside the reactor. A conductive silver coating on the outside of the quartz cylinder serves as a ground electrode. Furthermore, to prevent the condensation of the liquid products inside the reactor, an oven is used for heating the DBD reactor. An AC high voltage

power supply (AFS G15S-150K) is used to generate plasma in the DBD reactor. All electrical signals are recorded by a 4 channel oscilloscope (Picoscope® 3405D). The applied voltage (U) across the DBD reactor is measured with a 1:1000 high voltage probe (Tektronics P6015A). An external capacitor (100nF) is connected between the ground electrode and the grounding point, and the voltage across this capacitor is measured using a 1:10 voltage probe. The voltage measured by this probe gives information regarding the generated charges (Q) in the plasma. Plotting Q as a function of the applied voltage (U) gives a Q-U Lissajous plot which is further used to calculate the power consumed by the DBD reactor. The power is calculated by multiplying the area obtained by Lissajous plot with the operating frequency (equation 4.2), where P (W) is the power consumption by the DBD, A_{Lissa} (J/cycle) is area measured by Lissajous plot and f is the operating frequency (kHz).

$$P = A_{Lissa}\, x\, f \tag{4.2}$$

The reactant gases, hydrogen and carbon dioxide (Linde Gases) were supplied to the reactor via mass flow controllers (Bronkhorst). The product gas containing mainly CO, CH_4, unreacted CO_2/H_2 and small amounts of CH_3OH, C_2H_6, and some traces of higher hydrocarbons, was analysed by an online gas chromatograph (Thermo Scientific) consisting of two thermal conductivity detectors (TCD) and a flame ionization detector (FID). For each measurement, the results are reported with 95% confidence interval calculated from three repetitions of an experiment. Performance of the reaction is characterized by the following set of parameters.

The conversion, X, of CO_2 is defined as:

$$X\ (\%) = \frac{CO_{2,in} - CO_{2,out}}{CO_{2,in}} x100 \tag{4.3}$$

The selectivity, S_i, where i can be CO or CH_4 is defined as:

$$S_i\ (\%) = \frac{i_{\text{produced}}}{CO_{2,in} - CO_{2,out}} x100 \tag{4.4}$$

The yield, Y_i, where i can be CO or CH_4 is defined as:

$$Y_i\ (\%) = X\ x\ S_i \tag{4.5}$$

The energy yield for product formation, E_i, where i can be CO or CH_4 is defined as:

$$E_i(mmol/kWh) = \frac{Molar\ flowrate\ of\ CO(\frac{mmol}{h})}{Power\ (kW)} x100 \tag{4.6}$$

The Specific Energy Input (SEI) is defined as:

$$SEI\ \left(\frac{J}{ml}\right) = \frac{Power\ (W)}{Flow\ rate(ml/min)x(\frac{1}{60})} \tag{4.7}$$

The plasma-catalytic reactions have demonstrated synergy in performance between plasma and catalyst. The synergy between plasma and catalyst can be interpreted as the percentage change in a performance parameter (consider yield of a product) when plasma and catalyst are employed together, with the total performance from their individual application. This synergistic effect (SE_i) [38] on the yield can be quantified according to Equation 4.8, where 'i' can be CO or CH_4. If CO_2 conversion is used in place of yield, then synergy between plasma and catalyst in terms of CO_2 conversion will be obtained.

$$SE_i\ (\%) = \frac{Y_{i,p+c} - (Y_{i,p} + Y_{i,c})}{(Y_{i,p} + Y_{i,c})} x100 \tag{4.8}$$

The reactor used in this study was operated at atmospheric pressure, and the reactor wall temperature was maintained at 100 °C to avoid any condensation in the reactor and pipelines via an external oven heating. The temperature of the outer wall of the reactor was monitored by an infrared thermal imaging camera (FLIR One Pro), and the temperature of discharge zone (from the exterior) was found to be within 100 to 160 °C. The highest value, a bit higher than 180 °C was observed at the edge of the discharge zone (Appendix A3). The total gas flow rate was varied from 40 to 200 ml/min. The 20 and 30 kHz frequencies of the high voltage power supply were

set according to the desired process conditions. The different values of voltage across the reactor tried were 12 and 15 kV_{p-p}. For the burst mode operation, the time for the voltage applied (T_{on}), and voltage switched off (T_{off}) was kept constant at 1 ms each. In the chapter, plasma discharge without burst mode is referred to as AC mode operation. Assuming 40% voidage in the packed bed plasma reactions, the empty reactor experiments were carried out at two different flow rates, one representing the same residence time of the reactant and another having same feed gas flow rate as that of packed bed conditions.

4.2.2 Catalyst Preparation and Characterization

The support materials used in this study were SiO_2, $PbTiO_3$, $BaZrO_3$, α-Al_2O_3, and γ-Al_2O_3. Among them α-Al_2O_3 and γ-Al_2O_3 pellets were purchased from Sigma Aldrich. SiO_2 and $PbTiO_3$ were synthesized and procured from Inorganic Materials & Catalysis research group, Eindhoven University of Technology. $BaZrO_3$ was synthesized via coprecipitation of $BaCl_2.2H_2O$ (Sigma Aldrich) and $ZrOCl_2.8H_2O$ (Alfa Aesar) by the methods reported in the literature [39]. The pellets of 630–850 μm size were prepared for packing in the plasma discharge. The 5%wt Rh/γ-Al_2O_3 catalyst was prepared by wet impregnation method using a rhodium precursor (Rhodium(III) chloride hydrate, Alfa Aesar) on the γ-Al_2O_3 support pellets with the same size. The γ-Al_2O_3 support was dipped in the precursor solution prepared to contain desired (5 %wt) amount of rhodium and then evaporated naturally with constant shaking using an Orbit Environ-Shaker. The catalyst was dried at 120 °C for 12 h and calcined in an oven at 450 °C for 2 h under static air. The prepared catalyst was reduced in hydrogen flow before using in a plasma reaction. The temperature for reduction of the catalyst was obtained by H_2 temperature-programmed reduction (TPR) analysis. For the TPR, the temperature was increased from 20 to 850 °C in 10% H_2/Ar with a flow rate of 25 mL min^{-1} and a temperature ramp of 10°C min^{-1} using the Micromeritics® Autochem II 2920 Chemi-sorption Analyzer.

In order to determine the specific surface area of the support materials and the catalysts, standard multipoint Brunauer-Emmett-Teller (BET) analysis was performed using TriStar 3000 Micromeritics® analyser. On the same equipment, Barrett Joyner Halenda (BJH) analysis yielded pore size distributions and pore volumes. Prior to the measurements, the samples were dried in the Nitrogen gas environment at 120 °C for 6h. The analyser employs multilayer nitrogen adsorption measured as a function of relative pressure. The nitrogen adsorption-desorption isotherms were collected at -196 °C, and the specific surface area was calculated by applying the BET equation.

The scanning electron microscope (SEM) was used to evaluate the topography of the catalytic surface. This was done using a Quanta™ 3D FEG with an electron beam resolution of 1.2 nm at 30 kV (SE) and an accelerating voltage of 200V–30 kV. SEM-EDX provides the information about the components present on the catalyst. The SEM, SEM-EDX data can be found in Appendix B1.

4.3 Results and Discussion

4.3.1 Effect of Support Materials on the Reaction Performance

The plasma conversion of CO_2 and H_2 was carried out with different support materials packed in the plasma zone, to investigate the effect of the support materials on the reaction performance. The feed gas ratio and flow rate were kept constant in all the experiments. The ratio of H_2:CO_2 used was 3:1 and the feed gas flow rate for 40 ml/min. For comparison of the process performance with the empty reactor (no support packing), the experiments were carried out at two conditions, the one with the same flow rate and the with same residence time. Considering average void fraction for the given geometry as 0.4 [40], the flow rate for the case of same residence time was 9.6 s, which corresponds to 100 ml/min of flow rate for the empty reactor. The pellet size of the support material was 630-850 µm (Appendix B2). The dielectric properties of the support materials are given in Table 4.1. Both

forms of the alumina support were tested although they have the same dielectric constant; they differ significantly in their surface area.

Table 4.1: *Dielectric properties of the support materials*

Support material	Relative dielectric constant
SiO_2	3.9
γ-Al_2O_3	9
α-Al_2O_3	9
$BaZrO_3$	40
$PbTiO_3$	100-200

The different dielectric properties of each support material affect the plasma power dissipation, as operating frequency and voltage are maintained constant in all the conditions. Combining plasma and packing material exhibits lower plasma power than that of an empty reactor. The electrical characteristics of the plasma discharge get modified when the plasma zone is packed with support materials. The variation in the discharge characteristics occurs from the filamentary discharge in the empty reactor to the combination of filamentary and surface discharge with the packing material. This allows to generate filaments within the pellet-pellet and the pellet-quartz wall gaps, and surface discharge generated over the surface of pellets near the contact points between the pellets [41–43]. The change in discharge characteristics may affect electron energy distribution and subsequently, the reaction performance [44,45]. The overall capacitance of the reactor is determined by the collective contribution of the capacitance of the dielectric barrier, gases flowing through the reactor and the packing material [46,47]. Therefore, having a packing material with higher dielectric constant results in a higher electric field within the voids where the reaction gas is flowing.

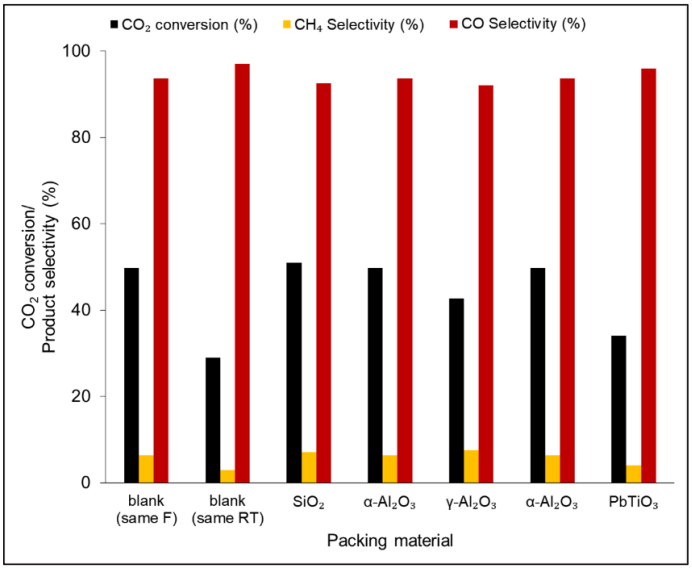

(a)

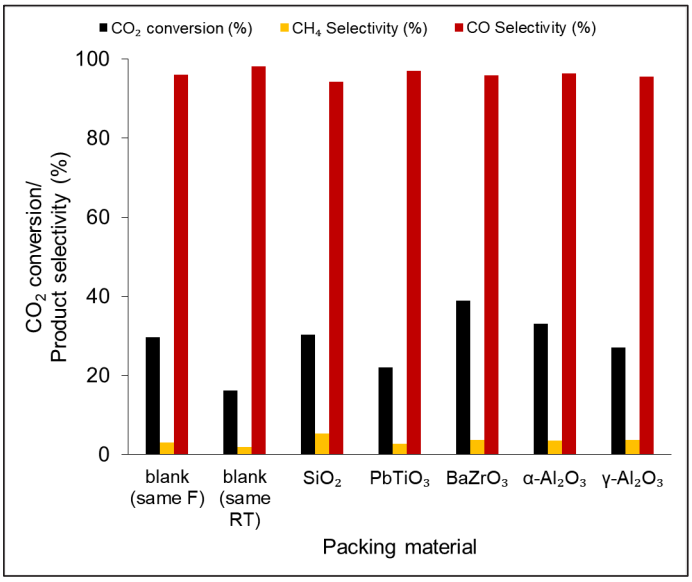

(b)

Figure 4.3: *Effect of the support material on the CO_2 hydrogenation in terms of conversion and CO/CH_4 selectivity, 40 ml/min, 3:1 ratio of H_2 and CO_2, 30 kHz, 15 kV_{p-p} (a) normal mode, (b) burst mode*

Figure 4.3 (a) presents an overview of the CO_2 hydrogenation reaction performance with different support materials. In general, having a packing material demonstrates a higher conversion than an empty reactor while keeping the residence time constant. Therefore, when the feed gases are exposed to the plasma for the same amount of time the activity of CO_2 reduction is higher in the presence of packing materials. Here, SiO_2 has the highest CO_2 conversion with the value of 51% closely followed by $BaZrO_3$ and α-Al_2O_3 with 49 % CO_2 conversion each, whereas γ-Al_2O_3 gives 43% CO_2 conversion. $PbTiO_3$ displays the least activity towards CO_2 conversion among this group of packing materials. However, $PbTiO_3$ packing has revealed maximum selectivity towards CO (95%) than remaining support materials. The CH_4 selectivity is generally less in all the cases. Amongst them, γ-Al_2O_3 is most selective towards CH_4 with a value of 7.6%. The trend of selectivities of CO and CH_4 has not changed even with the application of supporting material in the plasma zone. Therefore, without metal catalyst doping, the CO_2 hydrogenation in plasma undergoes mainly reverse water-gas shift reaction than methanation reaction. Nonetheless, an improvement of approximately 200% in the CO_2 conversion is obtained by the implementation of packing materials in the plasma discharge when the residence time of the reactants is kept constant.

The CO_2 reaction evaluation is also performed in a burst mode plasma operation (Figure 4.3 (b)). Chapter 1 has established that the burst mode plasma operation demonstrates a better energy performance of the plasma reaction than continuous AC mode plasma operation. In burst mode, $BaZrO_3$ yields significantly higher CO_2 conversion (39%) than other packing materials and the blank reactor. The CO_2 conversions of SiO_2, $PbTiO_3$, α-Al_2O_3 and γ-Al_2O_3 are found to be 30, 22, 33 and 27% respectively. Burst mode plasma is observed to be even more selective towards CO than that of AC mode reaction. It must be highlighted that the applied power in burst mode plasma is 50% less than that of the AC operated mode plasma; however, the CO_2 conversion is considerably higher than 50%. For instance, in the case of $BaZrO_3$, the CO_2 conversion in burst mode operation is 80% of AC mode operation. Hence burst mode plasma produces better energy performance than continuous AC

mode plasma processes. The improvement in energy performance can be realized through Figure 4.4, where CO_2 conversion is plotted against specific energy input (SEI), where SEI is calculated through the power dissipated in the plasma reactor.

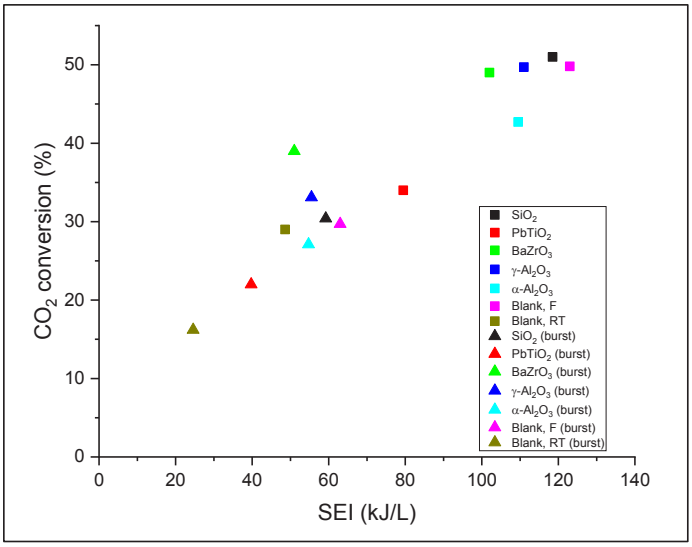

Figure 4.4: *CO_2 conversion as a function of SEI, 3:1 ratio of H_2 and CO_2, 40 ml/min, 30 kHz, 15 kV_{p-p}*

4.3.2 Performance Evaluation of the Rh/ γ-Al_2O_3 Catalyst

Chapter 2 showed that the presence of H_2 favours the CO_2 dissociation, but in the absence of a catalyst mainly reverse water-gas shift reaction prevails. Moreover, combining a support material with the plasma discharge improves CO_2 conversion and energy performance of the CO_2 hydrogenation reaction; however, it fails to steer the reaction away from reverse water-gas shift and towards CO_2 methanations. Therefore, to transpose the selectivities of CH_4 and CO during plasma-assisted CO_2 hydrogenation reactions, a Rh/γ-Al_2O_3 catalyst was employed. The initial experiment was carried out to investigate the thermal activity of the catalyst at 100 °C, and it was found that the catalyst shows almost no activity. Furthermore, to assess the effect of the Rh loading on the γ-Al_2O_3 catalyst, plasma-catalytic reactions with Rh/ γ-Al_2O_3 catalyst were carried out at the same reaction conditions

as given when using only a γ-Al_2O_3 packing. The voltage and operating frequency were kept constant at 15 kV_{p-p} and 30 kHz, while the feed gas flow rate was maintained at 40 ml/min with 3:1 H_2 to CO_2 ratio. The results, as shown in Figure 4.5 confirm complete inversion of the selectivities of CO and CH_4 when the Rh/γ-Al_2O_3 catalyst is packed in the discharge zone, having values of 2 and 96% respectively. Analysis of the product steam showed that the remaining 2% product contains mainly C_2H_6 (>1%), methanol (<0.01%) and a few higher hydrocarbons (in traces). The conversion of CO_2 and therefore the yield of CH_4 are also improved from 42 to 68% and from 3 to 65%, respectively. The burst mode reaction for the Rh/γ-Al_2O_3 catalyst demonstrates significant enhancement in the CO_2 conversion, where 63% conversion is obtained in burst mode. Hence with almost 50% of SEI, 93% of conversion compared to the reaction without burst mode, is achieved via the burst mode operation while having 95 % CH_4 selectivity. The detailed analysis of the energy performance of the plasma reactions is discussed in the subsequent section.

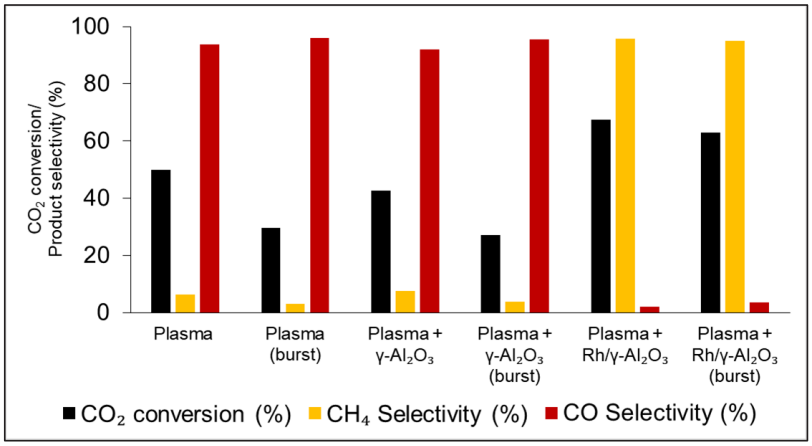

Figure 4.5: *Effect of the Rh/γ-Al_2O_3 catalyst on the CO_2 conversion and product selectivities; 3:1 ratio of H_2 and CO_2, 40 ml/min, 30 kHz, 15 kV_{p-p}*

Since no CO_2 activity is observed in the only thermal reaction using Rh/γ-Al_2O_3 catalyst, the yield of CH_4 is found to be zero. From Figure 4.5, the yield of CH_4 for plasma only reaction and plasma + Rh/γ-Al_2O_3 catalyst reaction can be used to calculate the synergistic capability using equation 4.8. The plasma catalytic reaction shows the synergistic capability of CO_2 conversion as 35% for AC mode plasma and 112% for burst mode plasma. The synergy between plasma and Rh/γ-Al_2O_3 catalyst in terms of CH_4 yield is monumental since a small yield of CH_4 is observed for plasma only reaction having 1900 and 6600% value for the AC mode and the burst mode operations, respectively.

The Rh/γ-Al_2O_3 demonstrates to be a suitable catalyst for the direct CO_2 methanation using a plasma discharge; however, the process parameters used above do not reflect well in terms of energy yield. The specific energy input for this condition is quite high (106 kJ/L) resulting in a low output of CH_4 with respect to energy yield, 0.23 and 0.41 moles/kWh for the AC mode and the burst mode, respectively. However, examining the burst mode performance, it can be inferred that even lowering the SEI did not inhibit the CO_2 methanation activity and simultaneously improved the energy efficiency by lowering the energy requirements for the formation of CH_4. From Chapter 2, it is already established that the energy performance of the plasma reaction improves via high flow rate and low operating frequency. Hence we carried out experiments with a total flow rate of 200 ml/min, with a 20kHz operating frequency and applied a voltage of 12 kV_{p-p}, in both the AC and burst mode plasma. The results are presented in Figure 4.6.

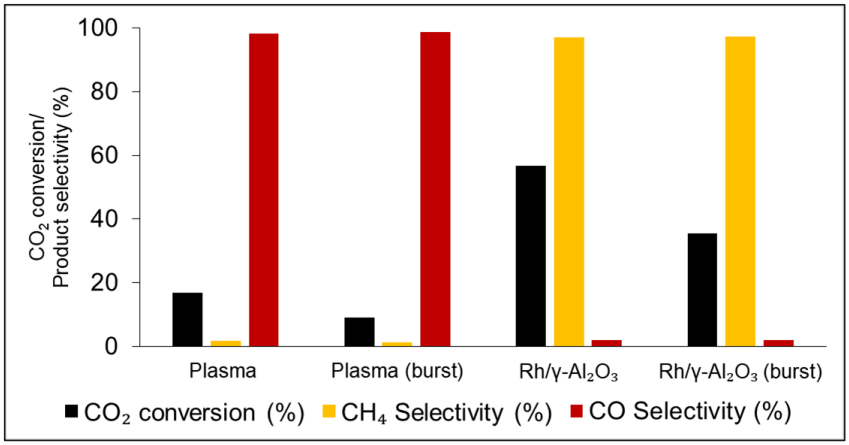

Figure 4.6: *Effect of the Rh/γ-Al_2O_3 catalyst on the CO_2 conversion and product selectivities; 3:1 ratio of H_2 and CO_2, 200 ml/min, 20 kHz, 12 kV_{p-p}*

Lowering the residence time to 20% and the applied power to almost 50% displays the effect on the CO_2 conversion as it decreases from 68 to 56% and 63 to 36% for the AC and burst mode operations, respectively. On the contrary, the CH_4 selectivities increases to 97 % in both plasma operating modes, which gives a CH_4 yield as 55 and 35 % consequently. With this combination of process and electrical parameters, a substantial enhancement is observed in the energy efficiency for the CH_4 molecules produced. In the AC mode operation, 2.05 moles of CH_4 gas are produced per kWh consumed. The burst mode operation requires the lowest energy to produce a unit quantity of CH_4, resulting in the highest energy efficiency value of 2.4 moles/kWh (Figure 4.7). The synergistic capability of the CO_2 conversion and CH_4 yield are found to be very high, especially seen that without plasma no reaction occurred and that in the empty reactor with plasma reaction performance was very low. According to Table 4.2, the AC mode plasma operation at lower residence time case shows the highest productivity of CH_4.

Table 4.2: *Effect of the residence time and type of plasma mode on the CH_4 productivity and energy yield*

Flow rate (ml/min)	Plasma mode	Operating frequency (kHz)	Applied voltage (kV_{p-p})	SEI (kJ/L)	CH_4 productivity (mmol/h)	Energy yield (mol/kWh)
40	AC	30	15	106	16.1	0.2
200	AC	20	12	10.5	14.9	0.4
40	Burst	30	15	54	68.7	2.1
200	Burst	20	12	5.2	43.2	2.4

Figure 4.7 (a) and (b) illustrate that the catalytic activity does not change with time, over a period of 3 hours, and the effluent composition does not vary significantly. The first data-point corresponds to the instance (t=0) when the plasma discharge is switched on in the reactor. Here, only a small CO_2 conversion with total selectivity towards CO is observed. It should be noted that the results are displayed with a time resolution of 17 minutes since the gas chromatograph takes about 15 minutes for each run with about 2 minutes of preparation time in between.

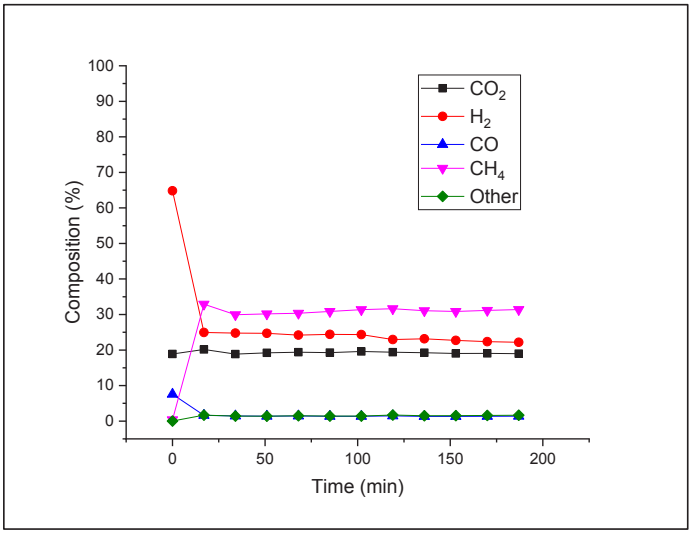

(a)

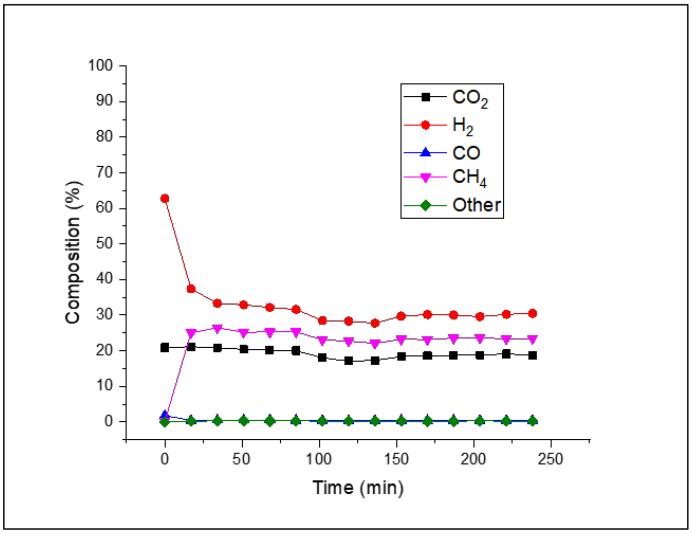

(b)

Figure 4.7: *Effect of the catalytic activity of the Rh/γ-Al_2O_3 catalyst with respect to time on the outlet product composition (dry basis) in case of (a) 3:1 ratio of H_2 and CO_2, 40 ml/min, 30 kHz, 15 kV_{p-p} (b) 3:1 ratio of H_2 and CO_2, 200 ml/min, 20 kHz, 12 kV_{p-p}*

The hybrid plasma-catalyst process shows significant improvement in the CO_2 methanation reaction. The thermal reaction at the same temperature did not show any activity of the CO_2 conversion. Whereas reactions with only plasma and plasma with support material packing were not selective towards methane. Packing the Rh/γ-Al_2O_3 catalyst in the plasma discharge overwhelmingly enhanced the overall CH_4 yield. This indicates the synergistic effect of the plasma-catalytic system where plasma seems to influence the surface reactions. A study by De Bie et al. studying the reactions occurring in the plasma phase (Figure 4.8) system without catalyst reveals that in presence of H_2, CO_2 dissociation to CO is very fast and dominating. Several intermediate species are formed, but the absence of surface reactions prevents other hydrocarbons formation, and product gas mainly contains CO [10]. The presence of a catalytic surface offers an alternate reaction route leading to lower CO and significantly higher CH_4 output. In a plasma-catalytic system, the plasma reactive species generated in the plasma phase can associate with the

catalytic surface in contact even at mild reaction conditions. Pre-activation through plasma may decrease the energy required for adsorption of different species on the catalyst surface, making the first step of adsorption very fast [48,49], which can lead to subsequent reactions to achieve the methanation reaction.

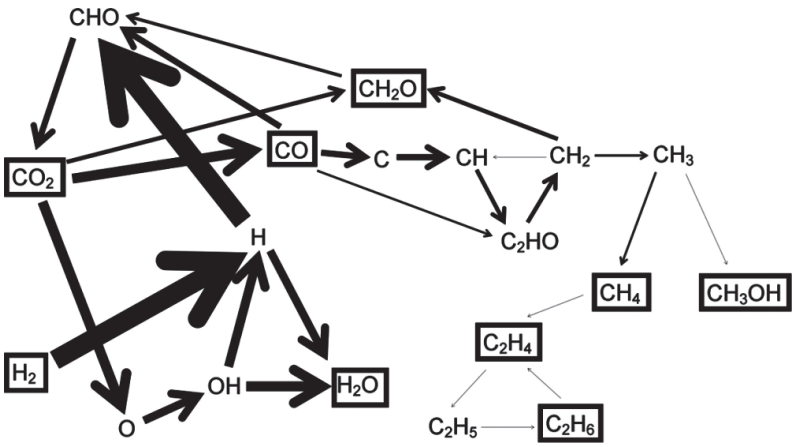

Figure 4.8: *Dominant reaction pathways for the plasma-based conversion (without catalysts) of CO_2 and H_2 into various products, in a 50/50 CO_2/H_2 gas mixture. The thickness of the arrow lines is proportional to the rates of the net reactions. The stable molecules are indicated with black rectangles, reprinted with permission from [10]. Copyright American Chemical Society, 2016.*

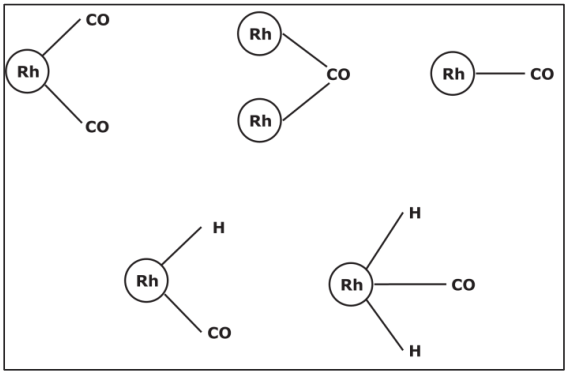

Figure 4.9: *CO adsorption on Rh surface with and without H_2 [50]*

Assisted by plasma, the surface adsorption of rhodium has demonstrated significant affinity to adsorb CO on its surface along with the hydrogen, even at low temperatures [50–52]. Prior studies with in-situ IR revealed that the CO adsorption on the rhodium surface exhibits the geminal dicarbonyl ($Rh(CO)_2$) structure, bridged structure, and the linearly bonded structure [53]. Whereas, hydrogen adsorption displays atomic attachment on the rhodium surface [54], in a system comprising of a mixture of CO and H_2 gases the structure of the adsorbed species on the rhodium surface differs from that of the pure component system. The adsorbed atomic hydrogen and CO species are reported to coexist on the rhodium surface [50] as illustrated in Figure 4.9. In the CO_2 methanation reaction mechanism, it is reported that initially CO_2 undergoes dissociative adsorption on Rh surface generating adsorbed CO species [53]. The CO_2 activation and dissociation to CO with the aid of plasma discharge would accelerate CO adsorption on the Rh surface. Therefore, it can be considered that the Rh/Al_2O_3 catalyst while performing the direct CO_2 methanation in a plasma medium, would resemble the CO and H_2 co-adsorption.

In contact with the plasma, the CO surface adsorption can take place via the CO_2 dissociation in either plasma or on the surface itself (Equation 4.9–4.11). Which leads to the formation of C_s and $CH_{x,s}$ species on the Rh surface via subsequent reactions (Equation 4.12–4.18). Simultaneously, water formation can take place via reactions mentioned in Equation 4.17 and 4.18 to consume and balance the O containing species being formed on the surface or in plasma. The stepwise addition of H to these C_s and $CH_{x,s}$ species leads to methane formation (Equation 4.19–4.22). Having dissociative adsorbed H on the Rh catalytic site and plasma-activated H species in gas accelerates methane formation steps. The reaction between surface species and plasma gas-phase species could follow both The Langmuir-Hinshelwood-Hougen-Watson (LHHW) mechanism where adjacent surface species react together and/or Eley- Rideal (E-R) mechanism where a surface species reacts with a gas-phase species. The fast consumption of the C_s and $CH_{x,s}$ species consumes surface adsorbed CO quickly, which results in shifting the CO_s

consumption reactions forward. This could explain the overall higher CH_4 and low CO selectivities. From the experimental results, it was observed that lowering the value of SEI by 10 times resulted in the 17% decrease in the yield of CH_4. This also explains the role of plasma to be most influential in the initial steps which lead to CO adsorption on the catalyst surface. Hence the majority of the energy applied through plasma supports the desired reaction pathway, and plasma energy is not lost for other undesired reaction pathways (from Figure 4.8). This hypothesis is also supported by tremendous improvement in energy efficiency.

It is reported in the literature that during the methanation of CO_2 at low-temperature range (up to 200 °C), the formate species forms on the support, however, they do not participate in the desired methanation reaction mechanism [55]. Hence the surface reaction through the formate species is not significant compared to the methyl group pathway and is not considered in the plausible surface reactions of CO_2 methanation.

$$CO_2 + e \rightarrow CO + O + e \quad (4.9)$$

$$CO_{2,s} \rightarrow CO_s + O_s \quad (4.10)$$

$$CO \rightarrow CO_s \quad (4.11)$$

$$CO_s \rightarrow C_s + O_s \quad (4.12)$$

$$CO_s + H_2 \rightarrow CH_s + OH_s \quad (4.13)$$

$$CO_s + H_s \rightarrow CH_s + O_s \quad (4.14)$$

$$CO_s + H_s \rightarrow CHO_s \quad (4.15)$$

$$CHO_s + H_s \rightarrow CH_s \quad (4.16)$$

$$O_s + H_s \rightarrow OH_s \quad (4.17)$$

$$OH_s + H_s \rightarrow H_2O \quad (4.18)$$

$$C_s + H_s \rightarrow CH_s \quad (4.19)$$

$$CH_s + H_s \rightarrow CH_{2s} \quad (4.20)$$

$$CH_{2s} + H_s \rightarrow CH_{3s} \quad (4.21)$$

$$CH_{3s} + H_s \rightarrow CH_4 \quad (4.22)$$

4.4 Conclusions

In this investigation, the aim was to assess the effect of the Rh/γ-Al_2O_3 catalyst on the plasma-assisted direct CO_2 methanation. Improved CO_2 methanation was obtained by Rh/γ-Al_2O_3 catalyst with the assistance of plasma at ambient pressure producing CH_4 with very high selectivity. The experimental study of the methanation of CO_2 over the Rh/γ-Al_2O_3 catalyst in plasma discharge reveals a strong synergy among plasma and catalyst. Without the Rh catalyst, loading only support materials (SiO_2, $PbTiO_3$, $BaZrO_3$, α-Al_2O_3 and γ-Al_2O_3) were tested. CO was found to be the main product with a selectivity of >95, mainly due to lack of surface reaction within hydrogen and CO_2 species. The reactions without any packing in the active plasma discharge show less CO_2 conversion than for the preceding case and similar product selectivities. The thermal reaction at the same conditions did not show any kind of activity. The use of the Rh/γ-Al_2O_3 as a hybrid plasma-catalytic system has been proven beneficial to steer the selectivity of products to achieve a high degree of the methanation reaction. A maximum yield of 65% is obtained in this study with the selectivity of CH_4 as 96%. Lowering the SEI via low applied plasma power and high feed gas flow rates decreases the CO_2 conversion by a modest fraction and further improved CH_4 selectivity, to 97%. However, the energy efficiency improves by 10 fold, 2.1 mol/kWh of CH_4 being produced compared to 0.2 mol/kWh.

To our best knowledge, this is the first study in literature for implementation of the burst mode on a plasma-catalytic CO_2 methanation reaction. The investigation with the burst mode provides the highest energy efficiency with 2.4 moles of CH_4 being produced per spent kWh of energy. Specific properties of Rh were used to justify the reaction mechanism of the plasma-catalytic hybrid CO_2 methanation. Using a plasma in conjunction with a catalyst allows the CO_2 to get activated and additionally accelerates the overall reaction to occur at the atmospheric pressure and lower temperatures. This research shows that the amount of energy consumption for CH_4 production can be substantially lowered and a high selectivity of CH_4 up to 97% can be achieved. Further research is required to accomplish at least 50% reduction in the current energy consumption in order to materialize an economic small-scale plant operation for direct CO_2 methanation via the plasma route.

References

[1] Goede A, Bongers W, Graswinckel M, Langereis E and Sanden R Van De 2014 The potential of CO_2 - neutral fuels *Power2Gas: From theory to practice*

[2] Mebrahtu C, Krebs F, Abate S, Perathoner S, Centi G and Palkovits R 2019 *CO_2 Methanation: Principles and Challenges* 178 (Elsevier)

[3] Koytsoumpa E I, Bergins C and Kakaras E 2018 The CO_2 economy: Review of CO_2 capture and reuse technologies *J. Supercrit. Fluids* **132** 3–16

[4] Goede A and van de Sanden R 2016 CO_2 -Neutral Fuels *Europhys. News* **47** 22–6

[5] Burkhardt M and Busch G 2013 Methanation of hydrogen and carbon dioxide *Appl. Energy* **111** 74–9

[6] Bailera M, Lisbona P, Romeo L M and Espatolero S 2017 Power to Gas projects review: Lab, pilot and demo plants for storing renewable energy and CO_2 *Renew. Sustain. Energy Rev.* **69** 292–312

[7] Buchholz O S, Van Der Ham A G J, Veneman R, Brilman D W F and Kersten S R A 2014 Power-to-Gas: Storing surplus electrical energy a design study *Energy Procedia* **63** 7993–8009

[8] Liu C J, Xia Q, Zhang Y P, Li Y, Zou J J, Xu G H, Eliasson B and Xue B 2000 Converting of carbon dioxide into more valuable chemicals using catalytic plasmas *ACS Div. Fuel Chem. Prepr.* **45** 694–7

[9] Bill A, Eliasson B, Kogelschatz U and Zhou L 1998 Comparison of CO_2 hydrogenation in a catalytic reactor and in a dielectric-barrier discharge *Adv. Chem. Conversions* **114** 541–4

[10] De Bie C, van Dijk J and Bogaerts A 2016 CO_2 Hydrogenation in a Dielectric Barrier Discharge Plasma Revealed *J. Phys. Chem. C* **120** 25210–24

[11] Bogaerts A, Berthelot A, Heijkers S, Kolev S, Snoeckx R, Sun S, Trenchev G, Van Laer K and Wang W 2017 CO_2 conversion by plasma technology: Insights from modeling the plasma chemistry and plasma reactor design *Plasma Sources Sci. Technol.* **26** 063001

[12] Whitehead J C Plasma – catalysis : the known knowns , the known unknowns and the unknown unknowns *J. Phys. D. Appl. Phys.* **49** 243001

[13] Wang W, Mei D, Tu X and Bogaerts A 2017 Gliding arc plasma for CO_2 conversion: Better insights by a combined experimental and modelling approach *Chem. Eng. J.* **330** 11–25

[14] Ashford B and Tu X 2017 Non-thermal plasma technology for the conversion of CO_2 *Curr. Opin. Green Sustain. Chem.* **3** 45–9

[15] Chen G, Georgieva V, Godfroid T, Snyders R and Delplancke-Ogletree M P 2016 Plasma assisted catalytic decomposition of CO_2 *Appl. Catal. B Environ.* **190** 115–24

[16] Brehmer F, Welzel S, Van De Sanden M C M and Engeln R 2014 CO and byproduct formation during CO_2 reduction in dielectric barrier discharges *J. Appl. Phys.* **116** 123303

[17] Bongers W, Bouwmeester H, Wolf B, Peeters F, Welzel S, van den Bekerom D, den Harder N, Goede A, Graswinckel M, Groen P W, Kopecki J, Leins M, van Rooij G, Schulz A, Walker M and van de Sanden R 2017 Plasma-driven dissociation of CO_2 for fuel synthesis *Plasma Process. Polym.* **14** 1600126

[18] Ma X, Li S, Ronda-Lloret M, Chaudhary R, Lin L, van Rooij G, Gallucci F, Rothenberg G, Raveendran Shiju N and Hessel V 2019 Plasma Assisted Catalytic Conversion of CO_2 and H_2O Over Ni/Al_2O_3 in a DBD Reactor *Plasma Chem. Plasma Process.* **39** 109–24

[19] Bruggeman P J, Iza F and Brandenburg R 2017 Foundations of atmospheric pressure non-equilibrium plasmas *Plasma Sources Sci. Technol.* **26** 123002

[20] Whitehead J C 2010 Plasma catalysis: A solution for environmental problems *Pure Appl. Chem.* **82** 1329–36

[21] Tatarova E, Bundaleska N, Sarrette J P and Ferreira C M 2014 Plasmas for environmental issues: From hydrogen production to 2D materials assembly *Plasma Sources Sci. Technol.* **23** 063002

[22] Malik M a and Jiang X Z 1999 The CO_2 Reforming of Natural Gas in a Pulsed Corona Discharge Reactor *Plasma Chem. Plasma Proc.* **19** 505–12

[23] Tu X and Whitehead J C 2012 Plasma-catalytic dry reforming of methane in an atmospheric dielectric barrier discharge: Understanding the synergistic effect at low temperature *Appl. Catal. B Environ.* **125** 439–48

[24] Bian L, Zhang L, Xia R and Li Z 2015 Enhanced low-temperature CO_2 methanation activity on plasma-prepared Ni-based catalyst *J. Nat. Gas Sci. Eng.* **27** 1189–94

[25] Tanaka S, Uyama H and Matsumoto O 1994 Synergistic effects of catalysts and plasmas on the

synthesis of ammonia and hydrazine *Plasma Chem. Plasma Process.* **14** 491–504
[26] Wang Q, Cheng Y and Jin Y 2009 Dry reforming of methane in an atmospheric pressure plasma fluidized bed with Ni/γ-Al_2O_3 catalyst *Catal. Today* **148** 275–82
[27] Fan Z, Sun K, Rui N, Zhao B and Liu C J 2015 Improved activity of Ni/$MgAl_2O_4$ for CO_2 methanation by the plasma decomposition *J. Energy Chem.* **24** 655–9
[28] Lee C J, Lee D H and Kim T 2017 Enhancement of methanation of carbon dioxide using dielectric barrier discharge on a ruthenium catalyst at atmospheric conditions *Catal. Today* **293–294** 97–104
[29] Nizio M, Albarazi A, Cavadias S, Amouroux J, Galvez M E and Da Costa P 2016 Hybrid plasma-catalytic methanation of CO_2 at low temperature over ceria zirconia supported Ni catalysts *Int. J. Hydrogen Energy* **41** 11584–92
[30] Nizio M, Benrabbah R, Krzak M, Debek R, Motak M, Cavadias S, Gálvez M E and Da Costa P 2016 Low temperature hybrid plasma-catalytic methanation over Ni-Ce-Zr hydrotalcite-derived catalysts *Catal. Commun.* **83** 14–7
[31] Stangeland K, Kalai D, Li H and Yu Z 2017 CO_2 Methanation: The Effect of Catalysts and Reaction Conditions *Energy Procedia* **105** 2022–7
[32] Martin N M, Velin P, Skoglundh M, Bauer M and Carlsson P A 2017 Catalytic hydrogenation of CO_2 to methane over supported Pd, Rh and Ni catalysts *Catal. Sci. Technol.* **7** 1086–94
[33] Wang W and Gong J 2011 Methanation of carbon dioxide: An overview *Front. Chem. Eng. China* **5** 2–10
[34] Weatherbee G D and Bartholomew C H 1982 Hydrogenation of CO_2 on group VIII metals. II. Kinetics and mechanism of CO_2 hydrogenation on nickel *J. Catal.* **77** 460–72
[35] Edwards J H and Maitra A M 1995 The chemistry of methane reforming with carbon dioxide and its current and potential applications *Fuel Process. Technol.* **42** 269–89
[36] Kuznecova I and Gusca J 2017 Property based ranking of CO and CO_2 methanation catalysts *Energy Procedia* **128** 255–60
[37] Agnelli M, Kolb M and Mirodatos C 1994 CO Hydrogenation on a Nickel Catalyst .: 1. Kinetics and Modeling of a Low-Temperature Sintering Process *J. Catal.* **148** 9–21
[38] Zeng Y and Tu X 2017 Plasma-catalytic hydrogenation of CO_2 for the cogeneration of CO and CH_4 in a dielectric barrier discharge reactor: Effect of argon addition *J. Phys. D. Appl. Phys.* **50** 184004
[39] Boschini F, Rulmont A, Cloots R and Vertruyen B 2009 Rapid synthesis of submicron crystalline barium zirconate $BaZrO_3$ by precipitation in aqueous basic solution below 100 °C *J. Eur. Ceram. Soc.* **29** 1457–62
[40] Benyahia F and O'Neill K E 2005 Enhanced voidage correlations for packed beds of various particle shapes and sizes *Part. Sci. Technol.* **23** 169–77
[41] Wang W, Kim H H, Van Laer K and Bogaerts A 2018 Streamer propagation in a packed bed plasma reactor for plasma catalysis applications *Chem. Eng. J.* **334** 2467–79
[42] Mei D, Zhu X, He Y-L, Yan J D and Tu X 2015 Plasma-assisted conversion of CO_2 in a dielectric barrier discharge reactor: understanding the effect of packing materials *Plasma Sources Sci. Technol.* **24** 15011–21
[43] Van Laer K and Bogaerts A 2017 How bead size and dielectric constant affect the plasma behaviour in a packed bed plasma reactor: A modelling study *Plasma Sources Sci. Technol.* **26** 085007
[44] Wang W, Kim H H, Van Laer K and Bogaerts A 2018 Streamer propagation in a packed bed plasma reactor for plasma catalysis applications *Chem. Eng. J.* **334** 2467–79
[45] Butterworth T, Elder R and Allen R 2016 Effects of particle size on CO_2 reduction and discharge characteristics in a packed bed plasma reactor *Chem. Eng. J.* **293** 55–67
[46] Peeters F J J and Van De Sanden M C M 2015 The influence of partial surface discharging on the electrical characterization of DBDs *Plasma Sources Sci. Technol.* **24** 015016
[47] Ozkan A, Dufour T, Bogaerts A and Reniers F 2016 How do the barrier thickness and dielectric material influence the filamentary mode and CO_2 conversion in a flowing DBD? *Plasma Sources Sci. Technol.* **25** 045016
[48] Parastaev A, Hoeben W F L M, van Heesch B E J M, Kosinov N and Hensen E J M 2018 Temperature-programmed plasma surface reaction: An approach to determine plasma-catalytic performance *Appl. Catal. B Environ.* **239** 168–77
[49] Van Durme J, Dewulf J, Leys C and Van Langenhove H 2008 Combining non-thermal plasma with heterogeneous catalysis in waste gas treatment: A review *Appl. Catal. B Environ.* **78** 324–33

[50] Solymosi F, Erdöhelyi A and Bánsági T 1981 Infrared study of the surface interaction between H_2 and CO_2 over rhodium on various supports *J. Chem. Soc. Faraday Trans. 1 Phys. Chem. Condens. Phases* **77** 2645–57

[51] Oliveira R L, Bitencourt I G and Passos F B 2013 Partial oxidation of methane to syngas on Rh/Al_2O_3 and $Rh/Ce\text{-}ZrO_2$ catalysts *J. Braz. Chem. Soc.* **24** 68–75

[52] Basile F, Bersani I, Del Gallo P, Fiorilli S, Fornasari G, Gary D, Mortera R, Onida B and Vaccari A 2011 In Situ IR Characterization of CO Interacting with Rh Nanoparticles Obtained by Calcination and Reduction of Hydrotalcite-Type Precursors *Int. J. Spectrosc.* **2011** 1–8

[53] Beuls A, Swalus C, Jacquemin M, Heyen G, Karelovic A and Ruiz P 2012 Methanation of CO_2: Further insight into the mechanism over $Rh/\gamma\text{-}Al_2O_3$ catalyst *Appl. Catal. B Environ.* **113–114** 2–10

[54] Drault F, Comminges C, Can F, Pirault-Roy L, Epron F and Le Valant A 2018 Palladium, iridium, and rhodium supported catalysts: Predictive H_2 chemisorption by statistical cuboctahedron clusters model *Materials* **11** 819

[55] Karelovic A and Ruiz P 2012 CO_2 hydrogenation at low temperature over $Rh/\gamma\text{-}Al_2O_3$ catalysts: Effect of the metal particle size on catalytic performances and reaction mechanism *Appl. Catal. B Environ.* **113–114** 237–49

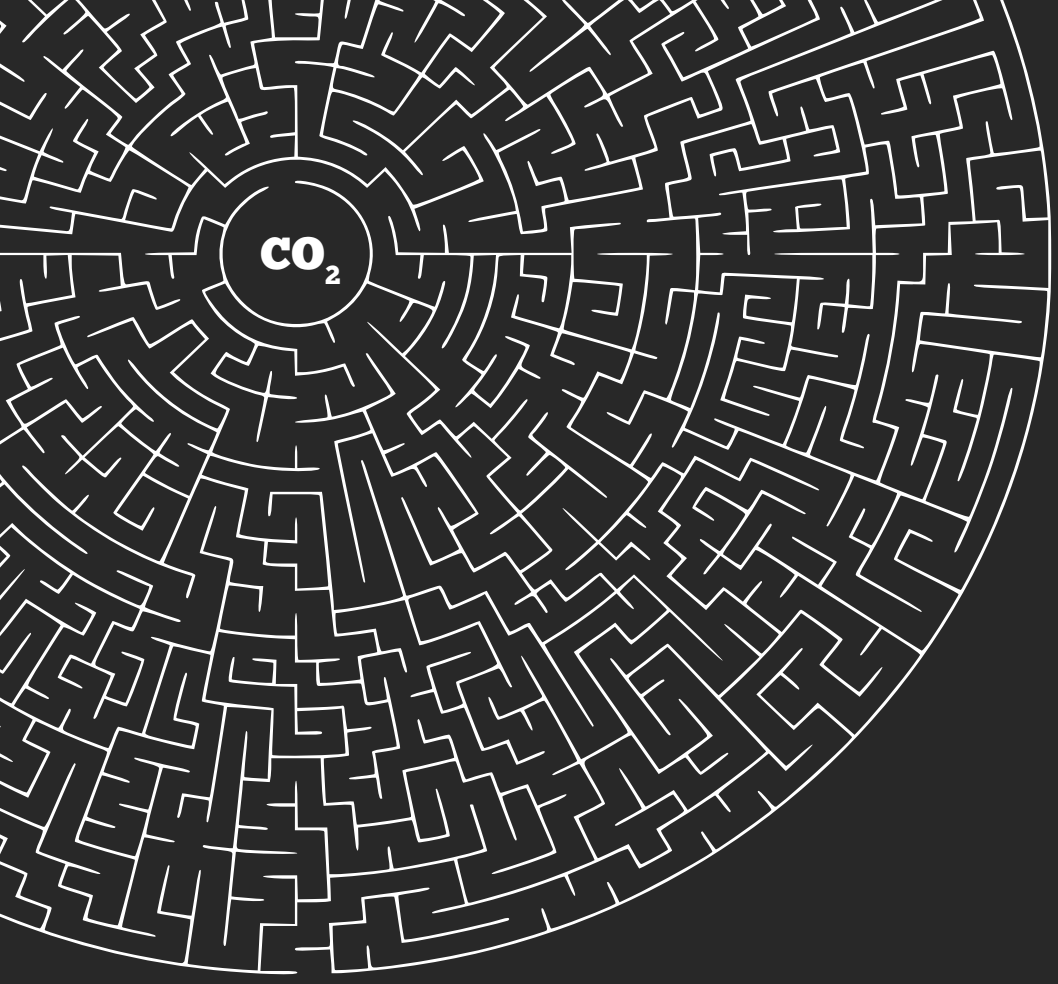
CO_2

Chapter 5

Prospects of ambient condition plasma-assisted direct CO_2 hydrogenation to methanol

Adapted from:

Prospects of ambient condition plasma-assisted direct CO_2 hydrogenation to methanol, Chaudhary, R., van Rooij, G., Li, S., Hessel, V., in preparation.

Abstract.

Direct CO_2 hydrogenation to methanol is identified as a significant route to convert vast CO_2 resource into chemicals and fuels. The use of non-thermal plasma process can assist this reaction to take place at ambient operating conditions. This chapter provides an initial analysis and evaluation of the current, and prospective feasibility of methanol synthesis reaction carried out with a water-electrode dielectric barrier discharge (DBD) operated at ambient pressure and temperature. A water-electrode DBD reactor was designed and fabricated to minimise the heating of a DBD reactor, the low-temperature profile of this reactor was observed to promote the oxygenated hydrocarbons formation over CO or CH_4 even without using a catalyst in the plasma discharge. The use of Pd-Au/γ-Al_2O_3 in the plasma discharge showed substantial improvement in the selectivity towards oxygenated hydrocarbons products through the synergistic effect. These oxygenates were identified as methanol and formaldehyde, which are different from the previous study where methanol and ethanol were produced together. The maximum conversion of CO_2 observed was 49%, while the maximum selectivity of liquid product was 47%. The research output highlights the significance of the appropriate selection of a plasma reactor configuration to achieve methanol formation from CO_2 via plasma operated at ambient conditions. The water-electrode DBD reactor is found to be an essential factor to steer the selectivity of plasma-assisted CO_2 hydrogenation reaction towards oxygenate hydrocarbons.

5.1 Introduction

The largest global concerns of the last few decades are climate change, and its most significant contributor is the emission of CO_2 [1]. Converting CO_2 to a feedstock for the manufacture of chemicals and fuels has been suggested to be one of the best ways of storing surplus renewable energy as well as CO_2 recycle. Liquid chemicals such as methanol and formaldehyde can be used for this purpose. Methanol has a high volumetric energy density, and it is easier to handle and transport. It used widely for the synthesis of numerous chemicals, and it is found beneficial for various direct applications in domestic and industrial scale [2,3]. A large fraction (30%) of methanol consumed in the chemical industry is for the synthesis of the formaldehyde, which itself is one of the most essential feedstock chemical industry [4]. It is estimated that the global methanol demand is going to increase by more than 200% in the span of 10 years, from 60 million MT in 2012 to approximately 137 million MT in 2022 [5]. Presently, the centralised large-scale production of methanol via syngas, obtained from steam reforming of the natural gas, occupies the majority of share in the market [6]. Conventional catalytic methanol synthesis from syngas is a high temperature, high-pressure, exothermic, and equilibrium limited reaction. To realise small-scale production of methanol directly from CO_2, two main problems need to be overcome, which are the removal of the large excess heat of reaction, and elimination of thermodynamic [7,8].

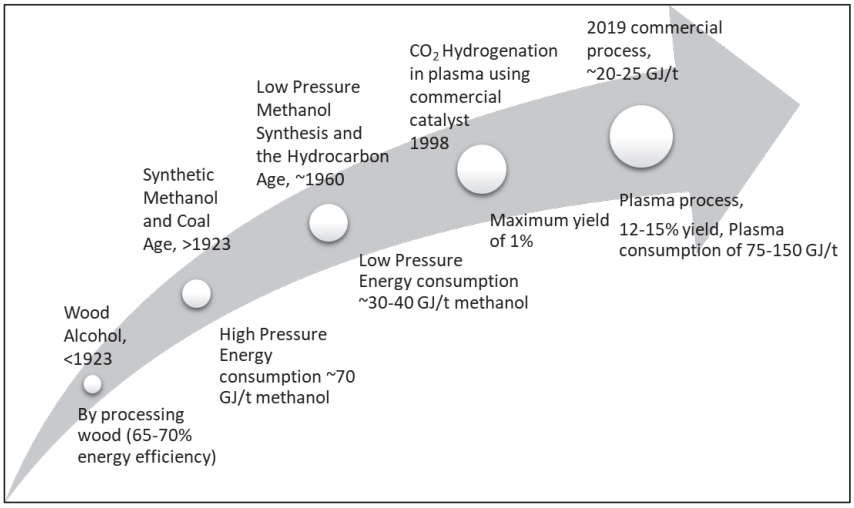

Figure 5.1: *Developments in methanol production technology through the years*

$$CO_2 + 3H_2 \rightleftarrows CH_3OH + H_2O \ (\Delta H_{25^\circ C} = -49.5 \text{ kJ/mol}) \quad (5.1)$$

The above reaction (eq. 5.1) is facilitated at high pressure and low temperature as it is highly exothermic and results in a reduction in the number of molecules. Moreover, CO_2 is a highly oxidized, thermodynamically stable compound having low activity. Hence in order to perform direct hydrogenation of CO_2 to methanol, it is necessary to overcome a thermodynamic barrier at ambient conditions. The CO_2 activation for subsequent methanol synthesis can be achieved via non-thermal plasma, where high energetic electrons, excited atoms and molecules, charged particles assist activation of CO_2 at ambient conditions [9,10]. The direct CO_2 hydrogenation to synthesise methanol eliminates an extra process step for the syngas synthesis, and hence it is found suitable to realise small-scale methanol production. The use of non-thermal plasma for the synthesis of methanol from the recycled CO_2 is a great way to introduce the surplus renewable energy into the CO_2 neutral cycle [11–16]. There is evidence of a synergistic catalytic effect between the non-equilibrium cold plasma and suitable catalyst to synthesise the methanol directly from CO_2 and H_2 under low temperature and atmospheric pressure [17,18]. The development of methanol production technologies through the years as

summarised in Figure 5.1, show that plasma technology has a long way to go to compete with conventional catalysts.

Klier et al. reported that methanol production with Cu/ZnO catalyst was promoted at low CO_2 concentration in $CO/CO_2/H_2$ mixtures, and it was inhibited in CO_2-rich atmospheres [19]. However, a study by Sahibzada et al. contradicted it and explained that the CO_2 did not inhibit methanol synthesis; instead, the progressive inhibition in CO_2-rich atmosphere was due to the increasing product water concentration reaction; while using a Pd promoted Cu/ZnO catalyst [20]. Using isotope-labelled $^{14}CO_2$, Chinchen et al. indicated that during the methanol synthesis, from $CO/CO_2/H_2$ with the Cu/ZnO catalyst, most of the methanol was produced from CO_2 reaction [21]. Later, it was shown that the direct methanol synthesis from CO_2 can be improved by a catalyst containing Pd, since H_2 spill-over from Pd counteracted the inhibition by water formation [22–26]. The reaction mechanism of direct catalytic CO_2 hydrogenation to methanol is well established in the literature. It suggests that the rate-determining steps are the formation of formate intermediates from CO_2, and the hydrogenation of a formate intermediate [27,28].

The main issue with the conventional approaches, like in the studies mentioned above, is the high temperature and high pressure needed in order to reach high conversions and selectivity. This high-temperature requirement causes energy yield to be less. Another drawback is the deposition of carbon on the catalyst at these higher temperatures, rendering it saturated. It would be more desirable to perform the reaction at a lower temperature (ideally room temperature) and atmospheric pressure. The hydrogenation by the use of the non-thermal plasma-driven catalysis could achieve this. In the past few years, research has been done involving different types of plasma reactors and catalysts. In the study of Eliasson et al. in a packed-bed dielectric barrier discharge (DBD), a maximum yield by the plasma-catalyst hybrid reaction was obtained as 2.2%. While an investigation by Kano et al. at low-pressure in a DBD reactor (1-10 Torr), without any catalyst reported increased CO_2 conversion (20–30%), but a low selectivity for the methanol (4%) on the expense of increased methane selectivity. The investigation by Kawasaki et al.

using a specially fabricated water-sealed DBD reactor showed the synthesis of performic acid from CO_2 and H_2O system, signifying the structural configuration of plasma reactor to target a particular product selectivity [29]. A recent study performed by Wang et al. researched the conversion of CO_2 to methanol in different kinds of plasma reactors. The best result using a water electrode DBD and a Cu/γ-Al_2O_3 catalyst showed the maximum methanol yield of 11.3% with a selectivity of 53.7%. These results are obtained when the Cu/γ-Al_2O_3 catalyst was placed directly in the plasma-discharge, the highest methanol yield and selectivity reported in the plasma CO_2 hydrogenation process was observed. However, this is much lower than conventional methods can achieve. Hence, further research is necessary to be able to implement plasma reactors in the industry.

In this chapter, the plasma-assisted catalytic hydrogenation of CO_2 to yield methanol is being investigated by using a water electrode Dielectric barrier Discharge (DBD) reactor. A new reactor design which uses water as the ground electrode and as a coolant to remove excess heat is designed and fabricated to investigate this reaction. The catalyst used for his reaction is Pd-Au supported on γ-Al_2O_3. This synergy between catalyst and plasma benefits the reaction additional with the milder reaction conditions of pressure and temperature, as favoured by the thermodynamics of the reaction. The effect of burst mode application is investigated. The preliminary findings of this process are reported and discussed. Although this synergy increases the complexity of understanding the reaction kinetics/mechanism, it can be used to affect the methanol yield positively.

5.2 Materials and Methods

The key reason for using the plasma for the direct methanol synthesis from CO_2 is to activate CO_2 at an atmospheric temperature as it is favoured thermodynamically for this reaction. However, in a typical DBD reactor, the temperature usually escalates quickly up to 150–180 °C, and also the temperature is non-uniform in the reactor volume. Hence, to control the temperature and keep it uniform, a water jacket was outside the reactor was fabricated. The water in this jacket serves the

dual purpose of acting as a ground electrode and a coolant for the DBD reactor. Initial experiments showed the DBD operations to be steady at ambient conditions with the DBD wall temperature at 50–60 °C. A cylindrical quartz reactor with a quartz jacket around the discharge zone was used to carry out the plasma-assisted catalytic experiments of CO_2 hydrogenation. The characteristic dimensions of the reactor were kept the same to the previously used DBD reactor with the outer diameter as 13 mm and the inner diameter as 10 mm. This makes the dielectric barrier thickness to be 1.5 mm. The 100 mm discharge zone was also identical with the DBD reactor used for methanation in chapter 4. A discharge gap of 1.5 mm was employed with a 7 mm diameter stainless steel axial inner electrode. Water was circulated through the quartz jacket outside the quartz DBD reactor. The water in this jacket serves the dual purpose of acting as a ground electrode and a coolant for the DBD reactor (Figure 5.2).

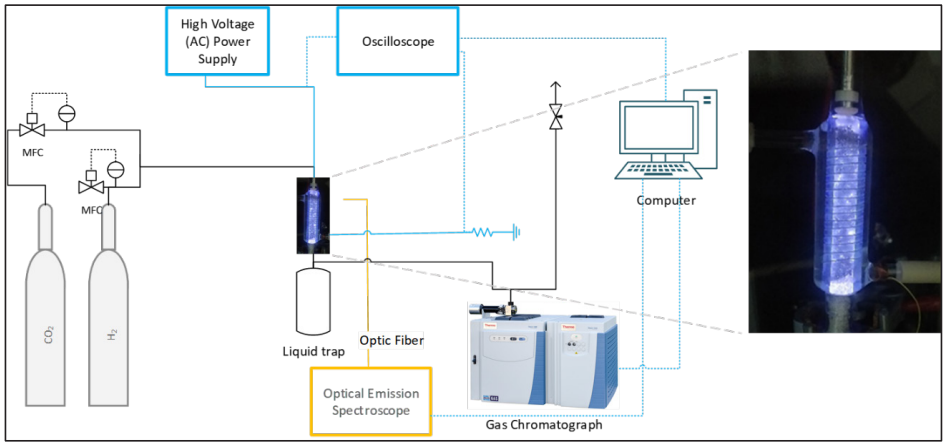

Figure 5.2: *Schematic representation of the experimental setup of the water-electrode DBD reactor*

An AC high voltage power supply (AFS G15S-150K) was used to supply the power to the DBD reactor. The voltage across the reactor and operating frequency were maintained at 15 kV_{p-p} and 30 kHz, the same conditions from chapter 4. Picoscope® 3405D, a 4 channel oscilloscope was used to record the electrical signals. An

external capacitor (100 nF) is connected between the ground electrode and the grounding point, and the voltage across this capacitor corresponds to the generated charges (Q) in the plasma. The applied voltage (U) across the DBD reactor is recorded with a 1:1000 high voltage probe (Tektronics P6015A) and the voltage across the external capacitor is recorded using a 1:10 voltage probe. The same method for power calculation used in chapter 2 and 4 was applied, by plotting Q-U Lissajous plot. The area (A_{Lissa}) of Q-U plot gives energy dissipated in the DBD reactor per cycle of the applied voltage. Hence multiplying this value with applied frequency (f) gives the power (P) consumption of the DBD reactor, which is illustrated by the equation 5.2.

$$P = A_{Lissa}\ x\ f \tag{5.2}$$

The assembly of the DBD reactor was vertical with inlet at the top. The inlet reactant gases, hydrogen and carbon dioxide (Linde Gases) were supplied to the reactor via mass flow controllers from Bronkhorst. The flow rate of the feed gas mixture used in this study was 40 ml/min. The outlet stream coming from the bottom of the reactor was bubbled through water kept in an ice bath to condense and collect the liquid product. The plasma reaction was continued for 3 to 6 hours, after that the liquid products were collected from the bottom and analysed using a gas chromatograph. The gas chromatograph was equipped with a methaniser at flame ionisation detector (FID) to analyse formaldehyde. A nitrogen gas fed at a fixed flow rate was mixed with the gaseous products containing CO, CH_4, unreacted CO_2/H_2 and some traces of C_2H_6 after the liquid trap. Here nitrogen serves as an external standard for the analysis. This gas mixture was analysed by an online gas chromatograph (Thermo Scientific) consisting of two thermal conductivity detectors (TCD) and a flame ionisation detector (FID). However, it was observed that the liquid collection via cooing does not condense all the liquid products, and some amount of desired liquid product are continuously lost through flowing gas-phase products. Hence separately measured liquid products are used only for the identification of the chemicals, and the calculation of total liquid product is done based on measured gas products to satisfy the mass balance.

The conversion, X, of CO_2 is defined as:

$$X\ (\%) = \frac{CO_{2,\text{in}} - CO_{2,\text{out}}}{CO_{2,\text{in}}} x100 \tag{5.3}$$

The selectivity of gas products, S_i, where i can be CO, CH_4 or higher hydrocarbons is defined as:

$$S_i\ (\%) = \frac{i_{\text{produced}}}{CO_{2,\text{in}} - CO_{2,\text{out}}} x100 \tag{5.4}$$

Collectively, $\Sigma\ S_i$ gives total selectivity of gas products, i.e. S_G

The selectivity of liquid products, S_L, is defined as:

$$S_L\ (\%) =\ 100 - S_G \tag{5.5}$$

The energy yield of product formation, E_i, where i can be CO, CH_4 or CH_3OH is defined as:

$$E_i(mmol/kWh) = \frac{Molar\ flowrate\ of\ CO(\frac{mmol}{h})}{Power\ (kW)} x100 \tag{5.6}$$

The Specific Energy Input (SEI) is defined as:

$$SEI\ \left(\frac{J}{ml}\right) = \frac{Power\ (W)}{Flow\ rate(ml/min)x(\frac{1}{60})} \tag{5.7}$$

The reactor used in this study was operated at atmospheric pressure. Unlike a typical DBD reactor where the reactor wall temperature usually escalates up to 150–180 °C, this water electrode DBD remained cooler as observed by an infrared thermal imaging camera (FLIR One Pro). To measure the typical operating temperature in this reactor, infrared thermal imaging was done longitudinally through the downstream outlet of the reactor. For such measurement, the reactor filled with catalyst bed was operated in flowing Argon gas instead of the reaction mixture to

satisfy the safety concerns. From Figure 5.3, we can see that the temperature of the catalyst bed in the plasma zone reaches up to 44 °C.

The support material and catalyst used in this study was γ-Al_2O_3 and Pd-Au/γ-Al_2O_3. The γ-Al_2O_3 pellets were purchased from Sigma Aldrich and crushed to desired sized pellets (630-850 µm). The prepared γ-Al_2O_3 pellets were used directly for packing in plasma discharge and to synthesise the supported catalyst. A 2.5-2.5 %wt Pd-Au/γ-Al_2O_3 catalyst was prepared by wet impregnation method using a Pd and Au precursors (Palladium (II) Chloride and Gold (III) Chloride solution, Sigma-Aldrich). The prepared catalyst was characterised using H_2 temperature-programmed reduction (TPR) analysis, Brunauer-Emmett-Teller (BET) analysis and the scanning electron microscope (SEM).

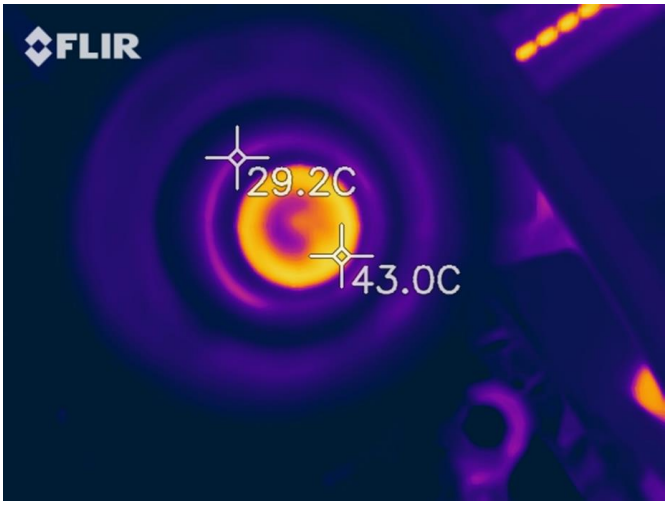

Figure 5.3: *Thermal image of the cross-section of a water-electrode DBD reactor operated in Ar plasma*

5.3 Results and Discussion

5.3.1 Effect of Type of DBD Reactor

Experiments investigating the plasma-assisted direct CO_2 hydrogenation to methanol, with and without catalysts, carried out using water-electrode DBD reactor are presented. Those were gained in the last stage of the PhD research and related project, could not be completed in their full dimension, and open possibilities for future research.

The use of the water-electrode reactor showed an improved heat removal from the plasma reactor as compared to the DBD with a silver-coated ground electrode (in Chapters 2 and 4), as confirmed by the thermal imaging. GC analysis confirmed that the methanol is formed along with formaldehyde and some traces of impurities. Even with a cold liquid trap to condense the liquid products, some amount of water, methanol and formaldehyde may have escaped with the gas outlet. Improvement with collecting liquid products is required to have a comprehensive quantification of products. The reported selectivities of liquid products were calculated from the total selectivity of the measured gas products.

Employing a water-electrode DBD reactor without even a catalyst or any packing material showed a substantial increase in the methanol selectivity. Figure 5.4 illustrates the differences in the performance of the CO_2 hydrogenation reaction in a DBD and water-electrode DBD reactor. The overall CO_2 conversion is lower in case of the water-electrode DBD reactor when the plasma discharge was not packed with any packing material. However, the liquid products selectivity (mainly methanol) is observed to improve significantly, from almost 0 to 9%, with an expense of CO selectivity. Use of γ-Al_2O_3 in the discharge zone improved the CO_2 conversion slightly and methanol selectivity considerably (from 0 to 10%). A slight effect on the CH_4 selectivity was observed. Hence it is inferred that the importance of the selection of the plasma reactor configuration is a crucial factor to synthesise methanol directly from CO_2 at near ambient conditions with plasma. The choice of a plasma reactor

and its configuration is also essential to steer the selectivity towards desired products along with a suitable catalyst packing. From preceding chapters, we learnt that the DBD reactor without any metal catalyst material in the plasma discharge undergoes the RWGS reaction giving a highly selective CO. However the formation of methanol or other oxygenated hydrocarbons was negligible in that process. Using a metal catalyst completely inverted the selectivities of CO and CH_4, yet the output towards the methanol was insignificant. Doping Ag with Rh catalyst in the same DBD setup (Appendix B3) showed a marginal improvement in the methanol and other hydrocarbons, but selectivity for methanol was still <0.6%. Apart from the catalyst property heat accumulation was one of the main reason for the low methanol productivity, as it is thermodynamically limited at higher temperatures [30], which is addressed by the use of water-electrode in DBD reactor.

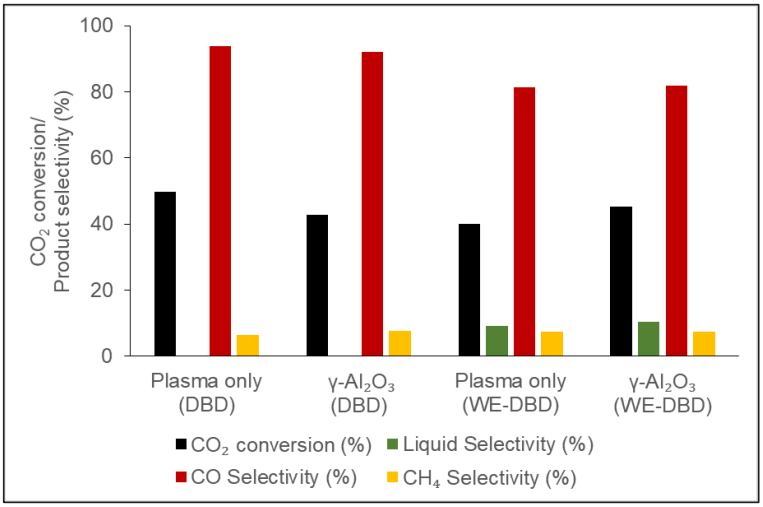

Figure 5.4: *Effect of the type of plasma DBD reactor on the CO_2 conversion and product selectivities including liquid products; 3:1 ratio of H_2 and CO_2, 40 ml/min, 30 kHz, 15 kV_{p-p}, 100 ± 5 W*

5.3.2 Effect of Pd-Au/γ-Al_2O_3 Catalyst

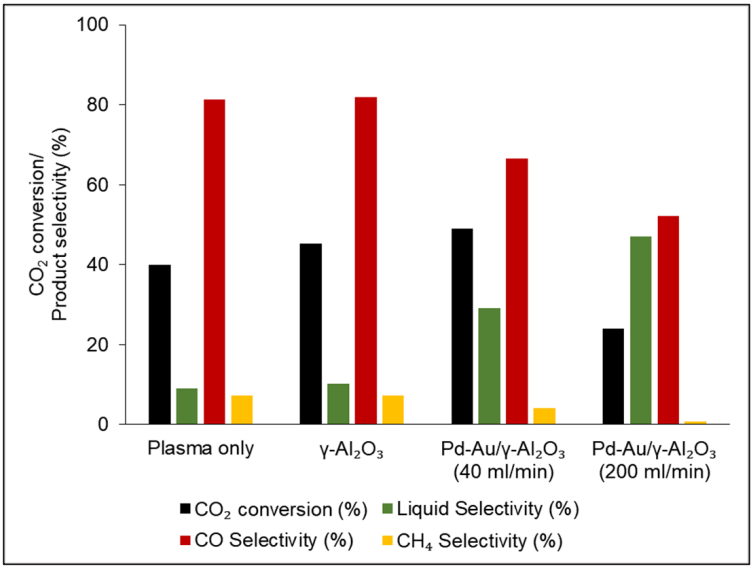

Figure 5.5: *Effect of the Pd-Au/γ-Al_2O_3 catalyst on the CO_2 conversion and product selectivities including liquid products; 3:1 ratio of H_2 and CO_2, 40 ml/min, 30 kHz, 15 kV_{p-p}, 100 ± 5 W*

Figure 5.5 compares the results obtained from the Pd-Au/γ-Al_2O_3 catalyst reaction carried out in a water-electrode DBD reactor. The reaction with an empty reactor showed 40% CO_2 conversion with 9% liquid product selectivity. Since the catalytic experiments without plasma did not show any CO_2 conversion at the same reaction conditions; it can be inferred that the application plasma discharge is necessary to achieve CO_2 conversion to methanol. By virtue of the Pd-Au/γ-Al_2O_3 catalyst, a small increase in CO_2 conversion was achieved compared to the plasma reaction without the catalyst. A three-fold enhancement in the liquid product selectivity was observed at the expense of CO and CH_4 selectivities when the feed gas flow rate was kept constant for the Pd-Au/γ-Al_2O_3 experiment compared to the empty reactor and γ-Al_2O_3 packed reactor. This is an indication for synergy between the plasma and the catalyst. When the feed gas flow rate was increased from 40 to 200 ml/min to

reduce the residence time, a 61% improvement in the methanol selectivity was observed. This provides the highest selectivity towards liquid products found in this study (47%). However, the CO_2 conversion was decreased from 49 to 24 % with a decrease in the residence time. In the case of higher feed gas flow rate, the CO selectivity was the lowest among all the cases with a value of 52% and the CH_4 selectivity was reduced to 0.7%. A possible reason for the improved selectivity for liquid products when the residence time is lowered could be the prevention of the methanol decomposition by plasma. With the higher flow rates, the exposure of methanol (or formaldehyde) formed during the reaction to the plasma before leaving the discharge zone is less, and hence it could restrict the decomposition of methanol (or formaldehyde) [31–34]. This hypothesis is seconded by results from the burst mode application (Figure 5.6), where a 46% improvement is observed in the liquid product selectivities via reducing SEI by 50% (154 to 78 kJ/L). Moreover, the lesser SEI in the burst mode operation could restrict the probability of methanol (or formaldehyde) decomposition by plasma. It is seconded by the results of the burst mode operation, where liquid products selectivity increases from 9 to 21% and from 24 to 28% for empty and Pd-Au/γ-Al_2O_3 packed plasma reactor, respectively.

The measured power in the case of water electrode is found to be higher than that of a DBD reactor when the same electrical parameters were used. This result is coherent to what has been found concerning the performance in the CO_2 hydrogenation reactions carried with the water-electrode DBD reactor. The maximum energy yield was observed when a low residence time was used for the reaction with a maximum value of 141 mmol/kWh of the product.

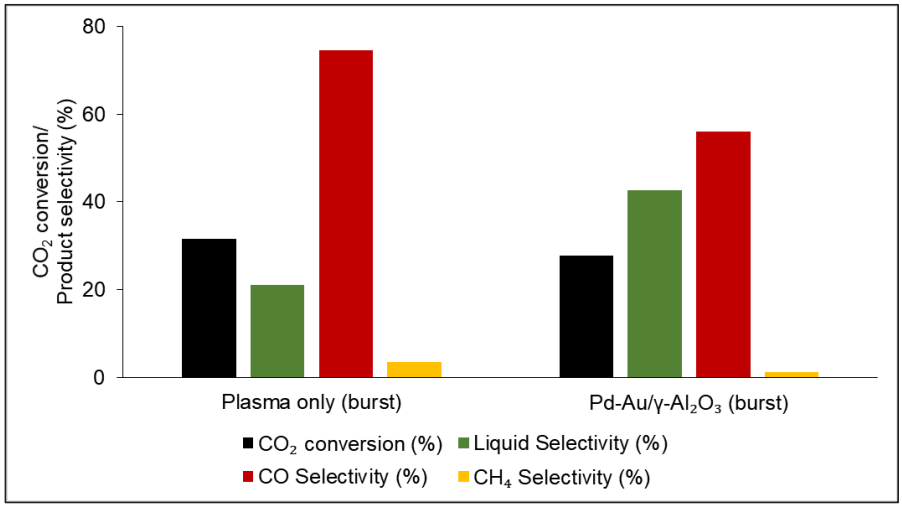

Figure 5.6: *Effect of the burst mode on the Pd-Au/γ-Al_2O_3 catalyst performance with respect to the CO_2 conversion and product selectivities; 3:1 ratio of H_2 and CO_2, 40 ml/min, 30 kHz, 15 kV_{p-p}, 100 ± 5 W*

5.4 Conclusions

The Pd-Au/γ-Al_2O_3 catalyst together with the plasma discharge generated by a water electrode DBD reactor showed that oxygenates molecules such as methanol and formaldehyde can be synthesised directly from CO_2 hydrogenation at ambient conditions; which was not possible without the application of plasma at the same reaction conditions. It is established that the importance of plasma reactor configuration is essential to achieve methanol synthesis directly from CO_2 and H_2 via the plasma process. Performing the plasma-catalytic CO_2 hydrogenation in a water-electrode DBD reactor substantially improved the selectivity of the liquid products containing mainly the methanol and the formaldehyde. The enhanced selectivities of the liquid products obtained were possible because of less heating of the DBD reactor itself. The improved reaction performance established the evidence of synergy between the plasma and the catalyst. The lower residence time and the application of burst mode have a significant positive effect on the liquid product selectivity at the expense of CO selectivity. The maximum liquid product

selectivity obtained is 47%. The energy yield of the reaction was found to be 147 mol/kWh of liquid products. This value is less than a value reported in the literature, and the liquid products composition is different (ethanol instead of formaldehyde [35]. The product formed via plasma catalytic activity might undergo decomposition through the plasma exposure, which justifies the observation that the liquid products selectivities are lowered at higher residence time. However, as the exact interactions between the catalyst and the plasma are as of yet relatively unknown, the reaction mechanism of direct the CO_2 hydrogenation to methanol is not yet completely developed. The late materialisation of the specialised water-DBD reactor did not allow the optimisation of this process. Yet, the first results showed promising prospects of the co-generation of industrially relevant formaldehyde and methanol from CO_2 [36]. Hence, future investigations exploring tailored catalysts for this reaction and optimisation of process and electrical parameters are necessary to further increase the yield of the liquid products.

References

[1] Marchal V, Dellink R, Vuuren D Van, Clapp C, Château J, Lanzi E, Magné B and Vliet J Van 2011 OECD environmental outlook to 2050: Climate change chapter *OECD* 90

[2] Olah G, Goeppert A and Prakash G K S 2009 Beyond Oil and Gas: The Methanol Economy: Second Edition (Wiley-VCH)

[3] Olah G, Prakash G K S and Goeppert A 2011 Anthropogenic chemical carbon cycle for a sustainable future *J. Am. Chem. Soc.* **133** 12881–98

[4] IHS Markit Formaldehyde- Chemical Economics Handbook 2017 (https://ihsmarkit.com/products/formaldehyde-chemical-economics-handbook.html, accessed on 28-8-2019)

[5] IHS Markit Online Newsroom (https://news.ihsmarkit.com/press-release/country-industry-forecasting/driven-china-global-methanol-demand-rises-23-percent-two-, accessed on 28-8-2019)

[6] Matsumoto H, Nagai H, Watanabe H, Morita K and Makihara H 1997 Advanced technology for large scale methanol plant *Technical Review - Mitsubishi Heavy Industries* **34** 58-62

[7] Studt F, Sharafutdinov I, Abild-Pedersen F, Elkjær C F, Hummelshøj J S, Dahl S, Chorkendorff I and Nørskov J K 2014 Discovery of a Ni-Ga catalyst for carbon dioxide reduction to methanol *Nat. Chem.* **6** 320–4

[8] Bernskoetter W H and Hazari N 2017 Reversible Hydrogenation of Carbon Dioxide to Formic Acid and Methanol: Lewis Acid Enhancement of Base Metal Catalysts *Acc. Chem. Res.* **50** 1049–58

[9] Suarez A, Leal-Quiros E and Gonzalez J 2015 From Inert Carbon Dioxide to Fuel Methanol by Activation in Plasma Atmosphere *J. Phys. Conf. Ser.* **591** 012058

[10] Puliyalil H, Lašič Jurković D, Dasireddy V D B C and Likozar B 2018 A review of plasma-assisted catalytic conversion of gaseous carbon dioxide and methane into value-added platform chemicals and fuels *RSC Adv.* **8** 27481–508

[11] Bill A, Wokaun A, Eliasson B, Killer E and Kogelschatz U 1997 Greenhouse gas chemistry *Energy Convers. Manag.* **38** S415–S422

[12] Bogaerts A and Neyts E C 2018 Plasma Technology: An Emerging Technology for Energy Storage *ACS Energy Lett.* **3** 1013–27

[13] De Bie C, Martens T, van Dijk J, Paulussen S, Verheyde B, Corthals S and Bogaerts A 2011 Dielectric barrier discharges used for the conversion of greenhouse gases: modeling the plasma chemistry by fluid simulations *Plasma Sources Sci. Technol.* **20** 024008

[14] Goede A and van de Sanden R 2016 CO_2 -Neutral Fuels *Europhys. News* **47** 22–6

[15] Hessel V, Anastasopoulou A, Wang Q, Kolb G and Lang J 2013 Energy, catalyst and reactor considerations for (near)-industrial plasma processing and learning for nitrogen-fixation reactions *Catal. Today* **211** 9–28

[16] Hessel V 2014 Special Issue: Design and Engineering of Microreactor and Smart-Scaled Flow Processes *Processes* **3** 19–22

[17] Wang Q, Shi H, Yan B, Jin Y and Cheng Y 2011 Steam enhanced carbon dioxide reforming of methane in DBD plasma reactor *Int. J. Hydrogen Energy* **36** 8301–6

[18] Eliasson B, Kogelschatz U, Xue B and Zhou L 1998 Hydrogenation of carbon dioxide to methanol with a discharge-activated catalyst *Ind. Eng. Chem. Res.* **37** 3350–7

[19] Klier K, Chatikavanij V, Herman R G and Simmons G W 1982 Catalytic synthesis of methanol from CO/H_2, The effects of carbon dioxide *J. Catal.* **74** 343–60

[20] Sahibzada M, Chadwick D and Metcalfe I S 1996 Hydrogenation of carbon dioxide to methanol over palladium-promoted $Cu/ZnO/Al_20_3$ catalysts *Catal. Today* **29** 367–72

[21] Chinchen G C, Denny P J, Parker D G, Spencer M S and Whan D 1987 Mechanism of methanol synthesis from $CO_2/CO/H_2$ mixtures over copper/zinc oxide/alumina catalysts: use of ^{14}C-labelled reactants *Appl. Catal.* **30** 333–8

[22] Melián-Cabrera I, Granados M L and Fierro J L G 2002 Effect of Pd on Cu-Zn catalysts for the hydrogenation of CO_2 to methanol: Stabilization of Cu metal against CO_2 oxidation *Catal. Letters* **79** 165–70

[23] Xu J, Su X, Liu X, Pan X, Pei G, Huang Y, Wang X, Zhang T and Geng H 2016 Methanol synthesis from CO_2 and H_2 over Pd/ZnO/Al_2O_3: Catalyst structure dependence of methanol selectivity *Appl. Catal. A Gen.* **514** 51–9

[24] Collins S E, Chiavassa D L, Bonivardi A L and Baltanás M 2005 Hydrogen Spillover in Ga_2O_3–Pd/SiO_2 Catalysts for Methanol Synthesis from CO_2/H_2 *Catal. Letters* **103** 83–8

[25] Liang X L, Dong X, Lin G D and Zhang H Bin 2009 Carbon nanotube-supported Pd-ZnO catalyst for hydrogenation of CO_2 to methanol *Appl. Catal. B Environ.* **88** 315–22

[26] Oyola-Rivera O, Baltanás M A and Cardona-Martínez N 2015 CO_2 hydrogenation to methanol and dimethyl ether by Pd–Pd_2Ga catalysts supported over Ga_2O_3 polymorphs *J. CO_2 Util.* **9** 8–15

[27] Chiavassa D L, Collins S E, Bonivardi A L and Baltanás M 2009 Methanol synthesis from CO_2/H_2 using Ga_2O_3-Pd/silica catalysts: Kinetic modeling *Chem. Eng. J.* **150** 204–12

[28] Lim H-W, Park M-J, Kang S-H, Chae H-J, Bae J W and Jun K-W 2009 Modeling of the Kinetics for Methanol Synthesis using Cu/ZnO/Al_2O_3/ZrO_2 Catalyst: Influence of Carbon Dioxide during Hydrogenation *Ind. Eng. Chem. Res.* **48** 10448–55

[29] Kawasaki M, Nakamura T, Morita T and Tachibana K 2016 Catalyst-Free One-Pot Plasma Chemical Conversion of Carbon Dioxide to Performic Acid by Water-Sealed Dielectric Barrier Discharge *Plasma Process. Polym.* **13** 1230–41

[30] Arakawa H, Dubois J-L and Sayama K 1992 Selective conversion of CO_2 to methanol by catalytic hydrogenation over promoted copper catalyst *Energy Convers. Manag.* **33** 521–8

[31] Sato T, Kambe M and Nishiyama H 2006 Analysis of a methanol decomposition process by a nonthermal plasma flow *JSME Int. J. Ser. B Fluids Therm. Eng.* **48** 432–9

[32] Rozovskii A Y and Lin G I 2003 Fundamentals of methanol synthesis and decomposition *Top. Catal.* **22** 137–50

[33] Derakhshesh M, Abedi J and Hassanzadeh H 2010 Mechanism of methanol decomposition by non-thermal plasma *J. Electrostat.* **68** 424–8

[34] Zhu X, Gao X, Qin R, Zeng Y, Qu R, Zheng C and Tu X 2015 Plasma-catalytic removal of formaldehyde over Cu-Ce catalysts in a dielectric barrier discharge reactor *Appl. Catal. B Environ.* **170–171** 293–300

[35] Wang L, Yi Y, Guo H and Tu X 2017 Atmospheric Pressure and Room Temperature Synthesis of Methanol through Plasma-Catalytic Hydrogenation of CO_2 *ACS Catal.* **8** 90–100

[36] Researchers want to produce formaldehyde from CO_2 (https://www.basf.com/global/en/media/news-releases/2016/09/p-16-312.html, accessed on 28-8-2019)

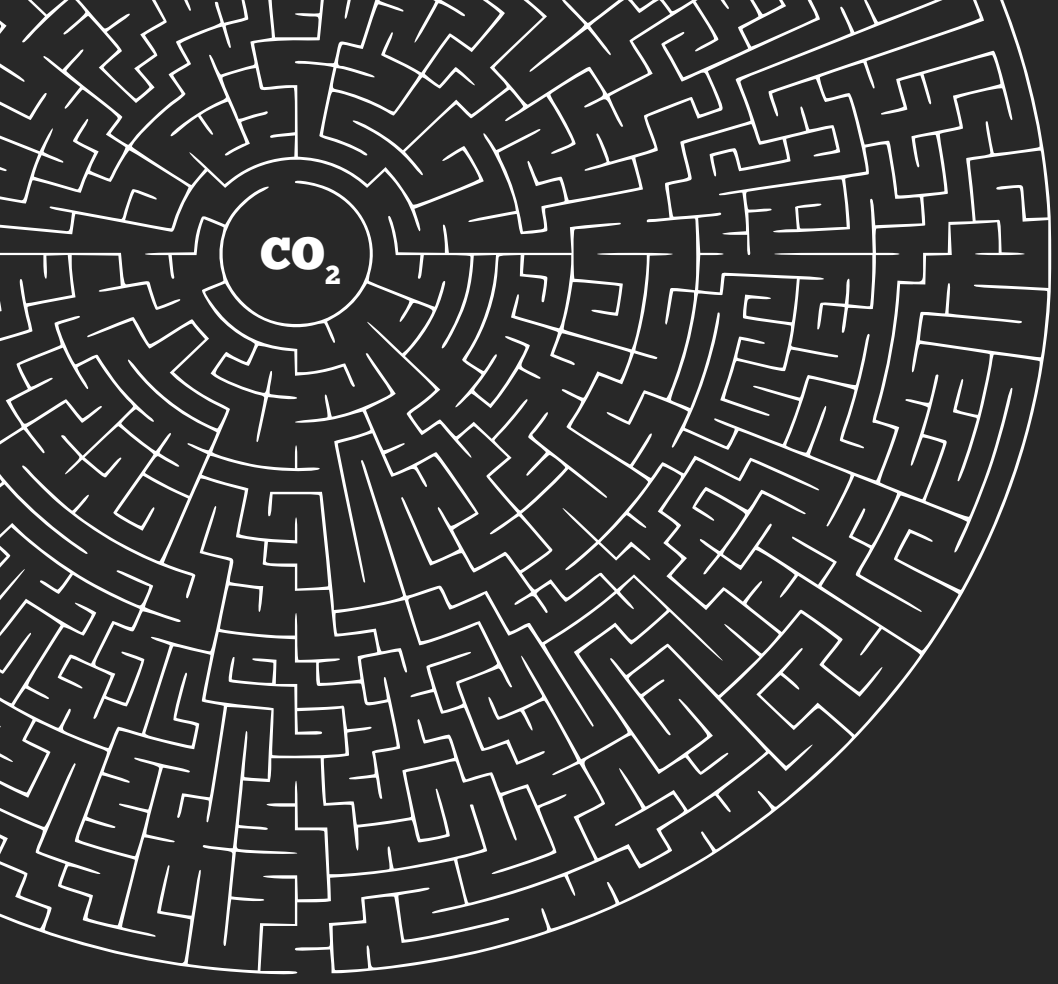
CO_2

Chapter 6

Techno-economic feasibility studies of plasma-assisted CO_2 hydrogenation processes

Based on: Techno-economic feasibility studies of plasma-assisted CO_2 hydrogenation processes, Chaudhary, R., Anastasopoulou, A., van Rooij, G., Li, S., van den Broeke, L.J.P., Hessel, V., in preparation.

Abstract

Reducing the environmental impact encourages humankind to move towards a society based on renewable energies. However, renewable energy sources such as solar and wind produce electricity which is intermittent, leading to surplus power, which can be stored via CO_2 hydrogenation processes carried out with the help of plasma reactors. The main costs of synthesis, in all cases, are hydrogen production and applied plasma power. The process models are made using Aspen Plus for process design of the plasma-assisted CO_2 hydrogenation at small-scale. These models consider H_2 production from water electrolysis and CO_2 procured via flue-gas capturing. The capacity of the process is defined through the CO_2 capture capacity data from chemical industries. Use of parallel reactor array of plasma reactor is assumed instead of scaling it up. Reverse water-gas shift, direct methanol synthesis, and methanation of CO_2 carried out at atmospheric pressure, are considered in this chapter for techno-economic evaluation. The mass and energy analysis based on the process simulations has revealed the plasma energy consumption of 22.5 GJ/t of CO for the RWGS process, 37.5 GJ/ton for the methanol synthesis process and 28 GJ/t for CO_2 methanation process. The operation costs and capital investment costs obtained for these processes are not compatible with the large-scale industrial production facilities as of now. The operating costs for the plasma-assisted RWGS, methanol synthesis and CO_2 methanation are 169, 911 and 649 € per ton of the product respectively, whereas the capital investments are 2.4, 4, and 3.4 k€ per ton of the product, respectively.

6.1. Introduction

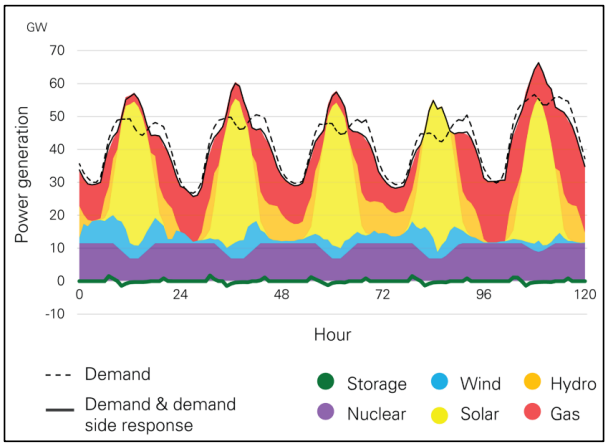

Figure 6.1: *Surplus power produced by the intermittency of the renewable energy sources, taken from BP Technology Outlook 2018 [16]*

Power-to-Gas and Power-to-Chemicals are the techniques comprising of various conversion routes of renewable electricity to chemicals and fuels which are easily stored and transported. Renewable electricity obtained by solar and wind sources is abundant but intermittent [1,2]. Such intermittency leads to the periods where the energy generation surpasses the demand producing surplus power, as shown in Figure 6.1. Power-to-gas and Power-to-chemicals technologies facilitate the storage of surplus energy [3]. In both of these pathways, in principle first electrolysis of water is carried out to produce hydrogen followed by its chemical conversion to desired products, such as syngas, methane and methanol. Syngas and methanol are enormously crucial feedstock in the chemical industry [4,5]. While methane can be directly used in the already established gas grid [6–8]. Use of recycled CO_2 as a carbon source for the synthesis of these molecules promotes CO_2 mitigation [9–12]. The current methods of use of CO_2 as a carbon resource in the chemical industry have a negligible positive effect on net CO_2 balance globally as it is approximately 1% of the total CO_2 emissions [13]. Hence such hydrogenation of recycled CO_2 to syngas, hydrocarbons or liquid oxygenates could have a higher positive effect on net CO_2 balance [14,15]. Reverse water-gas shift (RWGS), direct CO_2

hydrogenation to methanol, and CO_2 methanation provide raw materials as platform chemicals (syngas and methanol) and a directly implementable gas for already existing gas grid.

This chapter focuses on estimating the economics of these aforementioned processes carried out via a plasma pathway. The economic study provides the required capital investment and the operating costs. Moreover, it also highlights the focus areas of research needed to be explored to make the industrialisation possible for the process. Considering that similar industrial process has not been employed at an industrial scale, ex-ante process design for the novel plasma technology is necessary. Such preliminary process economics is essential to realise the feasibility of emerging plasma processes on a small scale installation. Small-scale production, even when operated at ideal efficiency, costs more than a centralised commercial practice. However, decentralised small-scale production facility can be set-up near the intended application of product, leading to cost savings on storage, reducing the total carbon footprint, as well as local jobs creation. In the chemical industry, the general idea has always been that bigger is better. Through upscaling, processes became more efficient and cheaper. Nowadays, there is a paradigm shift occurring towards small scale processes. The economy of scale is then obtained by increasing the number of plants instead of the capacity (i.e. mass production). The advantage of having a container-sized plant is that the supply of product can be located much closer to the demand. This way, either the cost for transport is reduced or transport losses are avoided. Another advantage is the ability to relocate the plant to another location if the profitability is jeopardized due to changes in the market. There are only a very few industrial users of plasma technology for chemical manufacture. For instance, Evonik Industries, which operates several small-scale industrial plasma plants for special chemistries. The new monosilane and aerosol plant was started up in 2010 in Yokkaichi and was with 150 Mio Euro the largest single project of Evonik in 2014. The preferred plasma equipment manufacturer for Evonik, U-W-E Company, has meanwhile installed > 150 industrial plasma plants worldwide.

The main objective of the plasma-assisted CO_2 hydrogenation is to use surplus renewable energy to valorise CO_2, obtained via capturing. Today supply of CO_2 (including sequestration) is 150 times higher than its demand (utilisation); hence we have no option but to store the excess CO_2 underground. Also there are several ways, proven in lab scale, by which CO_2 can be converted into other chemicals and fuels; however these methods are not practically employable owing to the fact that their incompetence with current large-scale industries. The current infrastructure is based on fossil fuels for supply of energy as well as raw materials; that is what makes them commercially viable. They have an enormous environmental impact with a large carbon footprint. Though the cost of production is small for these plants, the actual price can be higher than expected at some location due to transport/storage/handling charges. They do not have any problem like excess energy consumption, and hence it is not a case where we need to find new ways to save energy by substitute processes.

The idea of using plasma lies with the creation of new market where we intend to use the excess CO_2 which is being buried, to supply necessary chemicals (or fuels) at the point of demand; which may not be cheaper than the current commercial products, but they have substantially low environmental impact (low carbon footprint). This is creating a new parallel market for the carbon products. The aim is not to replace the current large-scale industry, but to increase the share of these "green carbon chemicals" in the market.

Let us take an example of methanol. Worldwide, over 90 methanol plants have a combined production capacity of about 110 million metric tons. The methanol plant we considered in our cases produces approximately 500-600 tpa, i.e. 0.0005% of global production. One hundred such plants would barely make 0.05% of the global capacity; however, they can be operated at multiple locations where there is demand for methanol. This will create local manufacturing infrastructure and jobs as well (additional benefit is less environmental impact including that from transport and storage).

Hence, through techno-economic study, we are trying to state the feasibility of setting up a plant using current technical advancements of the plasma processes. Furthermore, we provide a vision where we show the impact of improved performance of plasma reactions on the feasibility of the establishment of a small-scale plant. Hence the selling price of the methanol considering the container-sized approach is a crucial point here. In the case of methanol synthesis, the calculation of CAPEX/OPEX with the experimentally obtained results sets the benchmark for the current status of the plasma-assisted CO_2 hydrogenation reaction routes. Whereas CAPEX/OPEX calculations with the best case scenario provides potential improvement of the plasma-assisted CO_2 hydrogenation reaction routes.

6.2. Methodology

6.2.1 Process Design and Simulation

A modular methodology used for the process designing of the CO_2 hydrogenation routes under consideration is described in Figure 6.2. The essential feature of this approach is the use of plasma technology. In this method, it is considered that CO_2 is obtained from a CO_2 capture system, whereas hydrogen is obtained from water electrolysis using renewable energy. The design of this process is exclusively dependent on the amount of CO_2 produced by the CO_2 capture unit. Hence the capacity of the process is defined by the amount of CO_2 that needs to be processed per unit time. Depending on the type of hydrogenation reaction, the required quantity of hydrogen varies. The desired ratio of reactant gases, viz. CO_2 and H_2, is maintained before passing them through the plasma reactor. Subsequently, the products undergo several separation processes to obtain the pure product, and a recycle stream if necessary.

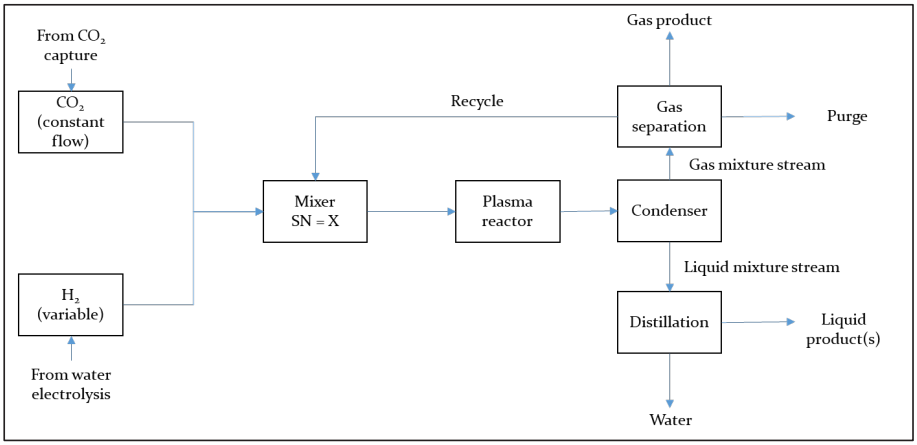

Figure 6.2: *Schematic representation of overall plasma-assisted CO_2 hydrogenation process*

Among all the cases, water electrolysis is the first phase of the overall process. Water electrolysis consists of converting electricity to (green) hydrogen and oxygen by dissociation of water [17]. Although the green hydrogen production process is well established over a century, it still occupies a tiny market share in the global production of hydrogen. However, a recent drop in the price of green hydrogen indicates that hydrogen production can become economical. At present, green hydrogen can be available from as low as 3.2 €/kgH_2 from a typical electrolyser operating about 50 kWh/kg capacity [18]. The second phase in these process designs is CO_2 capture to provide the CO_2 for plasma reaction. From the reports of International Energy Agency (IEA) and Global CCS Institute, today CO_2 capture units from 50 to 400 ktpa capacity are operating around the globe. The cost of CO_2 capture with new emerging technologies is estimated to be between 25 to 45 €/tCO_2 [19,20]. At present, the largest operating plant base on captured CO_2 producing methanol, by the 'Carbon Recycling International, Iceland' treats 5.5 ktpa of CO_2 [21]. Hence, to simulate small scale plant, the process designs of all three processes acknowledged in this chapter are intended for treating CO_2 captured by an industrial CO_2 capture unit operating at the rate of 2 ktpa. Today, among the processes producing synthetic fuel directly from CO_2, the syngas and methane

production processes, via direct CO_2 hydrogenations have exhibited the highest readiness level [22]. Moreover, direct synthesis routes of methanol from CO_2 to achieve a methanol economy have displayed ever-growing interest worldwide. Hence, the following three reactions are considered in this chapter for the techno-economic evaluation,

1. Reverse water-gas Shift (RWGS),
   $CO_2 + H_2 \leftrightarrow CO + H_2O$ $\Delta H_{25°C} = 41$ kJ/mol
2. Methanol synthesis
   $CO_2 + 3H_2 \rightleftarrows CH_3OH + H_2O$ ($\Delta H_{25°C} = -49.5$ kJ mol-1)
3. CO_2 methanation (Power-to-gas)
   $CO_2 + 4H_2 \leftrightarrow CH_4 + 2H_2O$ $\Delta H_{25°C} = -165$ kJ/mol

6.2.1.1 Plasma-assisted Reverse Water-Gas Shift

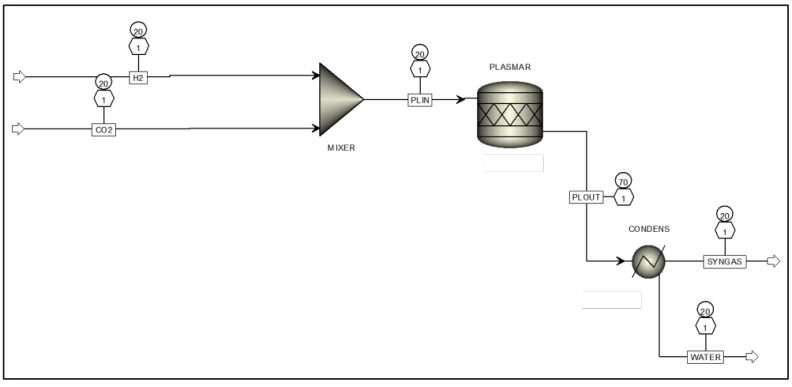

Figure 6.3: *Process flowsheet for plasma-assisted RWGS reaction*

The process design for plasma-assisted RWGS reaction is shown in Figure 6.3. The objective of the RWGS reaction is to produce syngas, which is suitable as raw material for further use in methanol synthesis (CAMERE reaction) or Fischer-Tropsch process [23,24]. From chapter 3, we learn that syngas can be synthesized directly from CO_2 and H_2 with 100% selectivity towards CO, without any carbon by-products. This indicates that the syngas without any contamination can be

successfully produced with the help of a plasma process. Moreover, it was found that the proportion of individual components in the syngas is acceptable for direct use in the methanol synthesis process and the Fischer-Tropsch process with the further addition of H_2 only, if desired. Hence, the output gas from the plasma process can be used in further processes as it is and any complex separation processes could be altogether avoided. The proposed plasma process is designed as a small scale plant with a capacity to treat 2 ktpa of CO_2, coming from a CO_2 capture unit, which defined the demand of H_2 as well. It is assumed that the process is operated 8200 hours per year. From operation point of view, plasma processes carried out are atmospheric pressure eliminate the use of compressors or vacuum systems, reducing the overall complexity of the process. Initially, the CO_2 is mixed with H_2, which is assumed to be obtained from the electrolysis unit while maintaining their temperature at 20 °C. The ratio of H_2:CO_2 needs to be maintained as 1:1 at the time it is fed to the gliding arc plasma reactor while keeping the pressure at 1 bar. The Aspen Plus software does not accommodate novel and state-of-the-art plasma reactor, hence a stoichiometric reactor is used to represent the gliding arc plasma reactor. From the experimental data, it was found that the outlet gas from the gliding arc plasma reactor has a temperature of 70 °C. Therefore, the temperature of the stoichiometric reactor is set at 70 °C. As the energy required to heat up the temperature in the plasma reactor is already considered in the energy consumption value of the plasma reactor, any extra heating duty is not considered for the plasma reactor. From chapter 3 the energy consumption value of the gliding arc plasma reactor is determined to be 2.4 mol/kWh, at 54% CO_2 conversion. The RWGS reaction, along with CO, produces an equivalent amount of water (equation 6.1). The water is separated from the syngas in the plasma reactor outlet stream via a condenser unit at 20 °C. The separated syngas is available at 20 °C and 1 bar pressure for further use.

6.2.1.2 Plasma-assisted Methanol Synthesis from CO_2

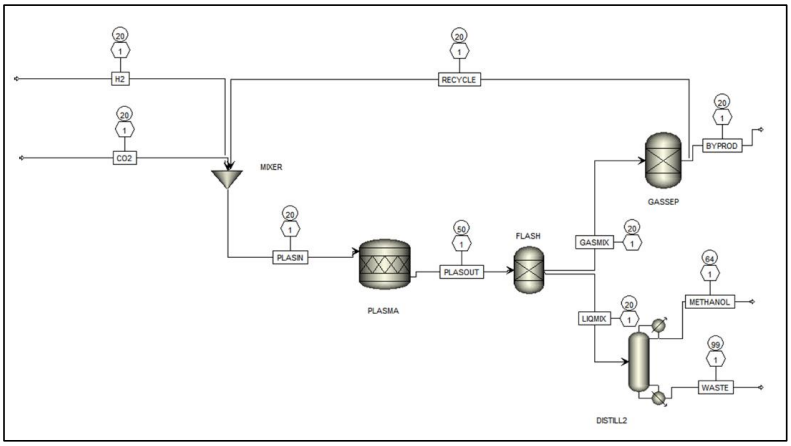

Figure 6.4: *Process flowsheet for plasma-assisted methanol synthesis*

The capacity of methanol synthesis process via plasma-assisted direct CO_2 hydrogenation is determined based on a CO_2 usage capacity of 2 ktpa. This CO_2 consumption by the plasma process determines the overall hydrogen uptake. Similar to the RWGS case a stoichiometric reactor is used in the process design of the Aspen software to represent the dielectric barrier discharge (DBD) reactor. The overall yield of the methanol which is 14% obtained from chapter 5 is used in the stoichiometric reactor along with the by-products, CO and CH_4. This DBD plasma reactor produces 0.3 moles of methanol per kWh of power applied. The reactor exit gas stream containing methanol, water, unreacted feed gases and the by-products (CO and CH_4) undergoes 3 steps of separation processes. In the first step, the gases are separated from the liquid products using a flash separator. The liquid stream containing water and methanol is fed to a distillation column to isolate the pure methanol. The gas stream contains unreacted CO_2 and H_2 along with CO and CH_4. As the H_2 is obtained via renewable energy sources, it is too valuable to be discarded hence its recycling is essential. A single step separation unit is mentioned in the process design to separate and recycle unreacted CO_2 and H_2. However, in the economic calculations, it is considered that this separation is carried out via 2 step processes, first, separation of H_2 then separation of CO_2. A membrane separation

technique is employed for separation of H_2, and the amine absorption technique is considered for CO_2 separation. The yield of CO is very high (32%) compared to that of methanol. This adds to the overall cost of methanol as important feed gases are consumed for unwanted reactions.

6.2.1.3 Plasma-assisted CO_2 Methanation

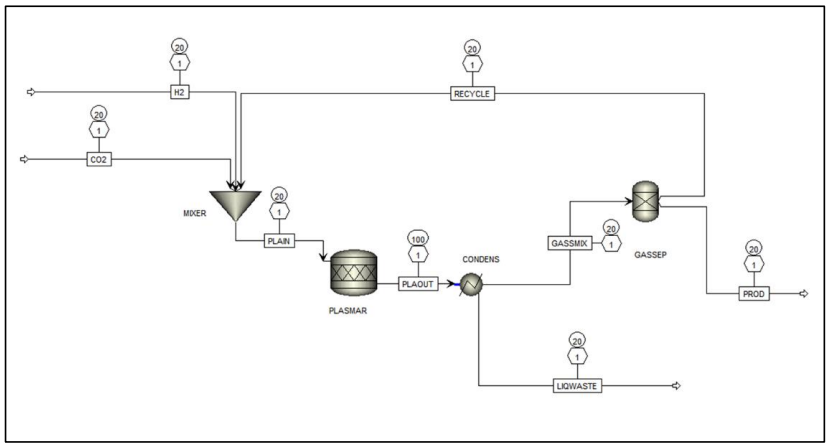

Figure 6.5: *Process flowsheet for CO_2 methanation via plasma route*

The elementary components of the CO_2 methanation process model are similar to that of the methanol synthesis process. The process flowsheet of CO_2 methanation processes is illustrated in Figure 6.5. The capacity of this process is established based on CO_2 uptake rate, similar to aforementioned cases, which is 2 ktpa of CO_2. The CO_2 and H_2 feed streams are mixed with the recycled stream, and resulting stream is fed to the stoichiometric reactor, representing a DBD plasma reactor. The CO_2 hydrogenation reaction shows 97% selectivity towards CH_4 and 3% towards CO. Although a few hydrocarbons are obtained in traces, they are not considered for the Aspen simulation. The molar ratio of H_2 and CO_2 is maintained at 3 in the stream 'PLAIN' via adjusting the flow rate of feed H_2 stream. This plasma reaction is carried out at 100 °C, and the product stream is condensed immediately to separate the water formed in the reaction. The dry product stream 'GASMIX' undergoes separation process to recover and recycle the CO_2 and H_2. The 'PROD' stream

containing CH_4, CO and unrecovered feed gases is available at 20 °C. In the calculations of recovery of CO_2 and H_2 a similar approach is adopted as the methanol synthesis case. The energy requirement for the formation of CH_4 via plasma-assisted process is considered as 2 moles/kWh obtained from chapter 4.

6.2.2 Sensitivity Analysis

The power consumption of the plasma reactor is humungous among overall energy requirements of the processes mentioned above [25–27]. Hence, in all the three cases, the different scenarios for energy consumption were considered to understand their effect on the overall cost. In case of the RWGS reaction 3, 4 and 5 moles/kWh were considered, and in case of the methanol synthesis, 1, 2 and 3 moles/kWh were considered, while in case of the methanation reaction 3, 4 and 5 moles/kWh were considered. Apart from energy considerations, different design alternatives have also been taken into account to identify the optimum operating conditions which would lead to making the overall process more energy efficient. In the RWGS case, a sensitivity analysis is carried out with respect to overall CO_2 conversion. Along with the aforesaid 54% conversion case, the scenarios involving 60, 70 and 80% conversion are also assessed. As the product from the RWGS case is directly acceptable, it does not have the energy-intensive downstream processes, unlike the other two cases. In the case of methanation 65% yield and in the case of methanol synthesis 20% yield scenarios were evaluated to observe their impact on subsequent downstream processes.

6.2.3 Economic Evaluation

The economic evaluation comprises of estimation of capital expenditures (CAPEX) and operating expenditures (OPEX). Such a cost analysis of the process attempts to predict the attractiveness of capital investments in the project. Although plasma techniques are not mature and contemporary in nature, the economic evaluation benchmarks the current processes, provide their competitiveness with respect to conventional processes and directs the research of scientific community in the direction to make these processes feasible. The latter is the most important, as it

allows a process-options analysis, when including optimistic future performance assumption besides considering the immature present technology status quo.

The CAPEX involves direct and indirect costs, along with the initial working capital. Direct costs contain instrument purchase cost, their installation, instrumentation controls, piping, electrical systems, buildings, site development and utilities, while indirect costs cover engineering and supervision, contractors and construction payments, legal expenses and contingency amount. Moreover, the OPEX consists of the cost of raw materials, fixed costs, maintenance, labour, supervision, plant overheads, laboratory charges, insurance and taxes and sales expenses. The CAPEX and OPEX analysis have been performed using the factorial approach [28,29]. In this methodology, various cost elements of CAPEX such as installation, piping, electrical systems, instrumentation, and civil work are considered to be varying fraction of 'purchased equipment cost' (PCE). The factorial approach data used in this study is explained in Tables 6.1 and 6.2. The purchase cost of green H_2, recycling cost of H_2 and CO_2 are directly used for calculation of OPEX. The lack of literature data for chemical reactions employing plasma techniques prompts to assume for the calculation of the plasma reactor. Therefore, in this evaluation studies, a cost of € 1M is considered for a 1 MW plasma system including the plasma reactor and the power supply [31]. The power rating required by the plasma system is calculated based on energy consumption value and mass flow analysis provided by the process simulations.

Table 6.1: *Capital cost factors for estimation [28,29]*

Direct costs	**%**
Total purchase cost (PCE)	Actuals (€)
Purchase equipment installation	25% of PCE
Instrumentation controls installed	6% of PCE
Piping installed	10% of PCE
Electrical systems installed	10% of PCE
Buildings, process	4% of PCE
Site development	(-)% of PCE
Utilities / Services	6% of PCE
Total	Direct costs
Indirect costs	
Engineering and supervision	5% of Direct costs
Construction expenses	6% of Direct costs
Legal expenses	(-)% of PCE
Contractor's fee	(-)% of PCE
Contingency	5% of FCI
Fixed Capital Investment (FCI)	Direct Costs + Indirect Costs
Working Capital Investment (WCI)	15% of TCI
Total Capital Investment (TCI)	WCI + FCI

Table 6.2: *Operating cost factors for estimation*

Variable costs	**%**
Raw materials	Actuals ($)
Utilities	Actuals ($)
Catalysts	Actuals ($)
Fixed costs	%
Maintenance	2% of FCI
Operation labour	Actuals ($)
Supervision	(-)% of operating labour
Plant overheads	50% of operating labour
Laboratory charges	10% of operating labour
Insurance	0.4% of FCI
Local taxes	1% of FCI
Royalties	(-)% of direct costs
Total	Variable + Fixed costs
Sales expenses	10% of (Variable costs + Fixed costs)
Total operating costs	Variable costs + Fixed costs + Sales expense

6.3 Results and Discussion

6.3.1 Process Simulation Results

The Aspen simulation results for the RWGS, methanol synthesis and CO_2 methanation are presented in Tables 6.3-6.5. As the capacity of the aforementioned processes is pre-determined with respect to uptake rate of the CO_2, the process simulations provide the quantity of H_2 required for each process. The mass and energy flow data from the Aspen simulations is used for further calculation of the CAPEX and the OPEX for the economic evaluation of these processes.

Table 6.3: *Material and energy data obtained via process simulation of plasma-assisted RWGS process*

Material	Value	Unit
H_2 input rate	11.1	kg/h
CO production rate	83.8	kg/h
Hydrogen	132	kg/tCO
Energy for water electrolysis	23843	MJ/tCO
Plasma energy	48913	MJ/tCO
Cooling and Heating	150	MJ/tCO

Table 6.3 lays out the mass and the energy portfolio for the plasma-assisted RWGS process obtained via Aspen simulations. The composition of the syngas obtained via RWGS reaction is 31.5, 31.5 and 37% of H_2, CO_2 and CO respectively, which makes this process suitable to be used in conjunction with the conventional methanol synthesis process or Fischer-Tropsch process. The productivity of this process is realized to be 83.8 kg/h of CO. The hydrogen is required at the rate of 11.1 kg/h to produce 83.8 kg/hr of CO, which leads to total 132 kg of H_2 to produce a ton of CO. To provide this amount of H_2 via water electrolysis, 23843 MJ of electricity is needed, considering the performance of the electrolyser to be 50 kWh/kg [17]. The water electrolysis is approximately half of the electrical energy consumed by the plasma reaction. The plasma reaction requires 48913 MJ of electrical energy to produce a

ton of CO gas. The high energy consumption in the plasma reaction dictates the overall energy performance of the plasma process and establishes itself as the most crucial factor. A similar trend is observed in the plasma-assisted methanol synthesis process, where a humungous 367647 MJ of electricity is required to produce a ton of methanol. Along with electricity required to provide hydrogen via water electrolysis (65935 MJ) for a ton of product, it can be inferred that the energy utilisation of remaining unit operations is substantially outweighed. From the process engineering point of view, it can be argued that to optimize the process, an adequate improvement in the energy performance of the plasma reactor is necessary.

The mass and energy balances for the plasma-assisted methanol production are shown in Table 6.4. The hydrogen input rate of 19 kg/h yields 58.1 kg/h of Methanol alongside the 103 kg/h of CO as a by-product. Since per pass yield of methanol is lower than that of CO, valuable H_2 is not being used sufficiently for the desired reaction of methanol synthesis. The amount of H_2 required for the production of one ton of methanol is found to be 366 kg, which is approximately double compared to the stoichiometric requirement. The recycled quantity of H_2 gas is 2.6 times that of the input quantity, and 4.5 times for CO_2 gas. Such high recycle quantities necessitate a high investment in separation processes.

Table 6.4: *Material and energy data obtained via process simulation of plasma-assisted CO_2 hydrogenation to methanol*

Material	Value	Unit
H_2 input rate	19	kg/h
Methanol production rate	58.1	kg/h
CO production rate	103	kg/h
Recycled H_2	50.1	kg/h
Recycled CO_2	261.4	kg/h
Hydrogen per t Methanol	366.3	kg/tCH_3OH
water electrolysis electricity per t Methanol	65935	MJ/tCH_3OH
Plasma energy required per t Methanol	367647	MJ/tCH_3OH
Cooling and Heating	800	MJ/tCH_3OH

Table 6.5 depicts material and energy flow data involved in the plasma-assisted CO_2 methanation reaction. To achieve 85 kg/h production rate of methane, 43 kg/h input rate of hydrogen is to be maintained. Alongside the methane, 4.6 kg/h of the CO is also produced. The amount of H_2 and CO_2 recycled is 14.8 and 179 kg/h, respectively. Further investigation illustrates that per ton of methane produced 506 kg of hydrogen gas is consumed, which is very close to the stoichiometric requirement. This is due to the very high selectivity of the plasma process towards methane (>97%). 91750 MJ of electricity is demanded from renewable sources for the water electrolysis. The calculated plasma energy needed for the methanation reaction is significant, i.e. 54878 MJ per ton of methane. In this case, the energy required for water electrolysis is almost 1.6 times higher than the energy required for the plasma reaction. The energy consumption of the water electrolysis is about 4 times more than that of methanation reaction for the P2G process using a conventional catalytic reactor for methanation [32]. Which indicates that the performance of the novel and contemporary plasma process is following the right footsteps. Compared to electrical energy required to produce per ton methane the cooling and heating energy requirements are insignificant.

Table 6.5: Material and energy data obtained via process simulation of plasma-assisted CO_2 hydrogenation to methane

Material	Value	Unit
H_2 input rate	43	kg/h
Methane production rate	87	kg/h
CO production rate	4.6	kg/h
Recycled H_2	14.8	kg/h
Recycled CO_2	179	kg/h
Hydrogen per t methane	506	kg/tCH_4
water electrolysis electricity per t methane	91750	MJ/tCH_4
Plasma energy required per t methane	54878	MJ/tCH_4
Cooling and Heating	554	MJ/tCH_4

The impact of the electrical energy required on the overall energy performance for the processes mentioned above is illustrated in Figure 6.6. In all the cases, the electrical energy eclipses the energy requirements of heating and cooling of the process. In the plasma-assisted RWGS case, more than 70% of the total electrical energy is consumed by the plasma reactor. While in the plasma-assisted methanol synthesis and plasma-assisted CO_2 methanation the energy accounts for about 85% and 65% respectively.

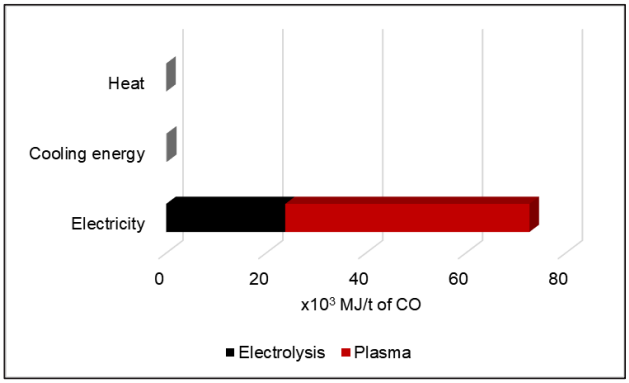

(a)

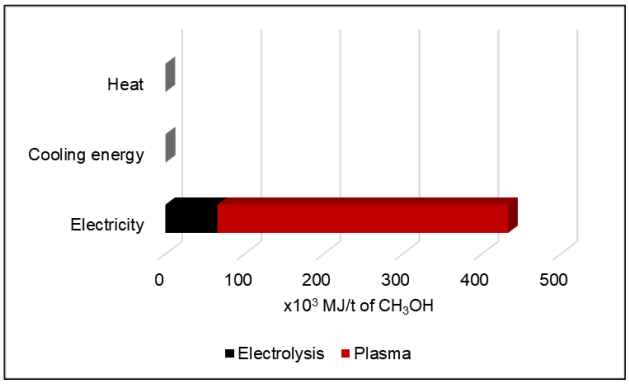

(b)

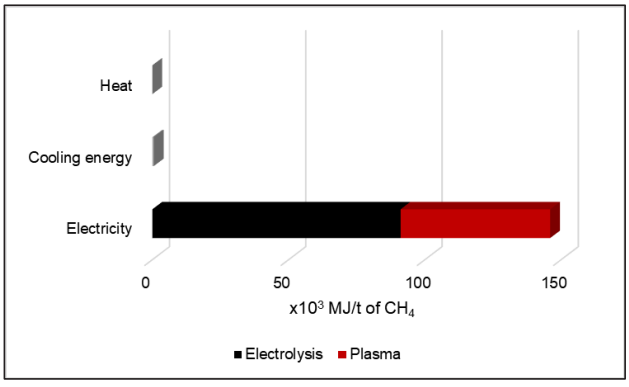

(c)

Figure 6.6: *Distribution of energy requirement of plasma-assisted (a) RWGS process, (b) Methanol synthesis, (c) CO_2 methanation process*

6.3.2 Sensitivity Analysis

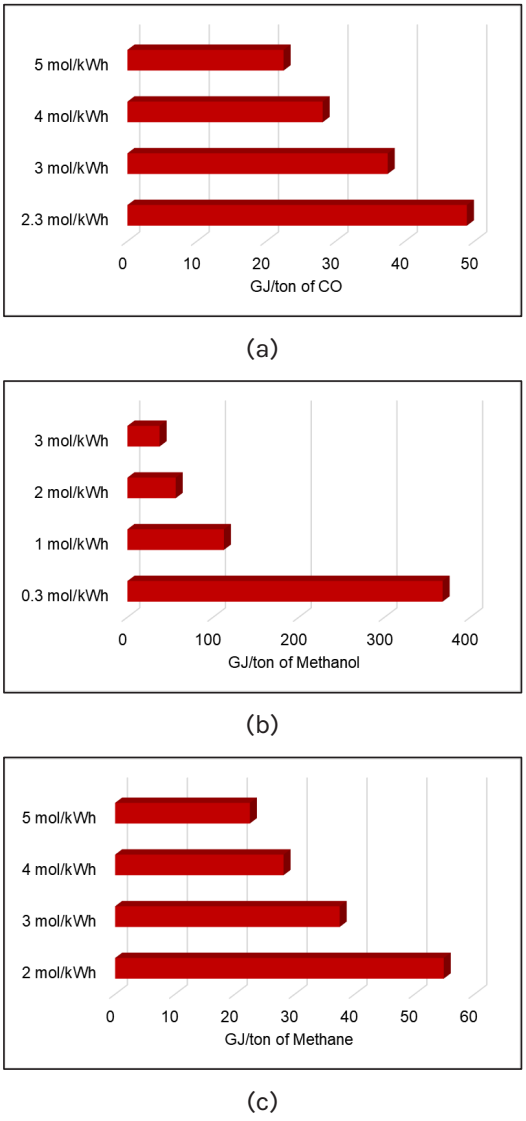

Figure 6.7: *Analysis illustrating the effect of plasma power consumption on the plasma energy requirements for the plasma-assisted (a) RWGS process, (b) methanol synthesis, and (c) CO_2 methanation process*

The sensitivity analysis for all the three processes is carried out to investigate the effect of the energy consumption and product yield on the process performance. A general trend of improved energy efficiency of plasma process yielding better overall energy consumption by the process is observed in all three cases (Figure 6.7). However, it is observed that for RWGS, methanol synthesis and methanation process, when the plasma energy consumptions are 5, 3 and 4 mol/kWh, respectively, the energy consumption obtained is close to the energy consumptions required for a conventional process. In other terms, theoretically plasma process could show compete with the conventional catalytic process if this energy efficiency is achieved. Although it should be noted that the cost of the plasma reactor is calculated based on the energy rating of the process, hence improving the energy efficiency giving low purchase cost of plasma reactor does not entirely describe the scenario of effect on capital expenditures.

The yield used in the RWGS process simulations was 54%. Figure 6.8 shows the effect on the product composition by varying the yield to 60, 70, and 80%. As yield increases, the ratio of CO:CO_2 also improves, from almost 1:1 to 4:1.

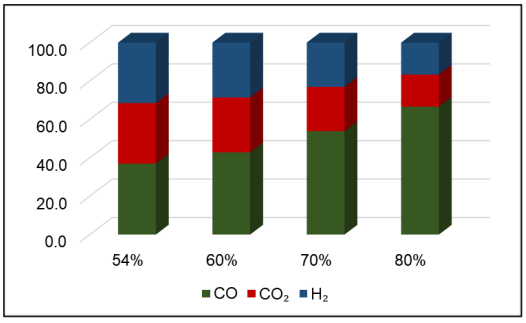

Figure 6.8: *Yield sensitivity analysis, showing the effect on product composition for plasma-assisted RWGS reaction*

The effect of the yield variation on the outcome of the other two cases is shown in Table 6.6. For the plasma-assisted methanol synthesis process, a 20% yield scenario is compared with the original 14% yield scenario. The overall CO_2

conversion is kept constant, and it is assumed that the yield improvement is solely the result of enhanced selectivity towards methanol. It is directly reflected in the product flow rate as it increases from 51.8 to 73.1 kg/h, and the CO flow rate decreases from 103 to 83.6 kg/h. The improved selectivity towards methanol is positively reflected in the hydrogen requirement of the process, from 366 to 299 kg of H_2 to produce a ton of methanol. The recycle of H_2 is lower while CO_2 is a bit higher in the case of 20% yield scenario. The total energy requirement also went down from 434 to 422 GJ. The apparent effect for the CO_2 methanation case is not very prominent by varying the methane yield. As the original process was operating very close to the stoichiometry of the reaction, owing to the high selectivity of the methane, the effect on improvement with respect to methane productivity and hydrogen uptake rate is minute. The major improvement is observed with the recycle streams of the process. The desired recycle rate of hydrogen declined by 58% of the original value, while for CO_2 it declined by 33% of the original value.

Table 6.6: *Effect of yield variation on methanol synthesis and methanation process*

	Methanol		Methane		Unit
	14% Y	**20% Y**	**55% Y**	**65% Y**	
Product flow rate	51.8	73.1	85.0	86.0	kg/h
Recycled H_2	50.2	47.9	14.8	6.3	kg/h
Recycled CO_2	261.4	264.1	179.7	118.8	kg/h
By-product (CO)	103.0	83.6	4.6	4.2	kg/h
Total energy	434.0	422.0	146	146	GJ/t of product
Hydrogen requirement	366.0	299.0	43.2	43.6	t/t of product

6.3.3 Economic Evaluation

The distribution of various factors amongst CAPEX and OPEX is illustrated in Figure 6.9, 6.10, 6.11 and 6.12 for plasma-assisted RWGS process, plasma-assisted methanol synthesis process and plasma-assisted CO_2 methanation process, respectively. In the case of the plasma-assisted RWGS process, the share of purchased cost equipment dominates the overall capital cost with 47%. Out of the total purchased cost equipment, the contribution of the cost of the plasma reactor system (€ 0.52M) dominates the cost of the other purchased equipment. The share of the raw materials purchase cost is 44%, while electricity required for plasma reaction contributes to 26% of the entire OPEX. The total CAPEX and OPEX values are estimated to be € 1.1M and € 0.6M, respectively. The CAPEX value translates to € 2.4k of capital investment per ton of CO produced. Similarly, the operating cost of 169 €/ton of CO is determined. The simplicity of the RWGS process saves costs on expensive downstream process units, as the product syngas can be directly implemented.

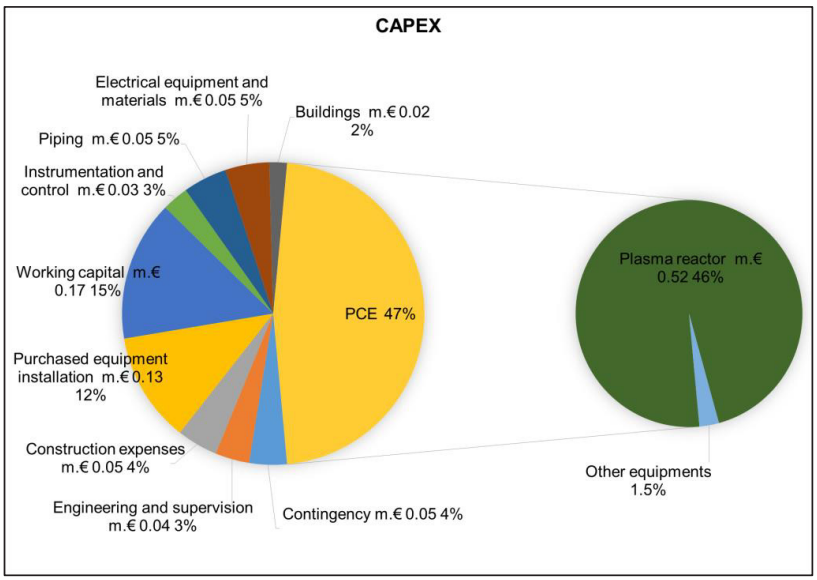

(a)

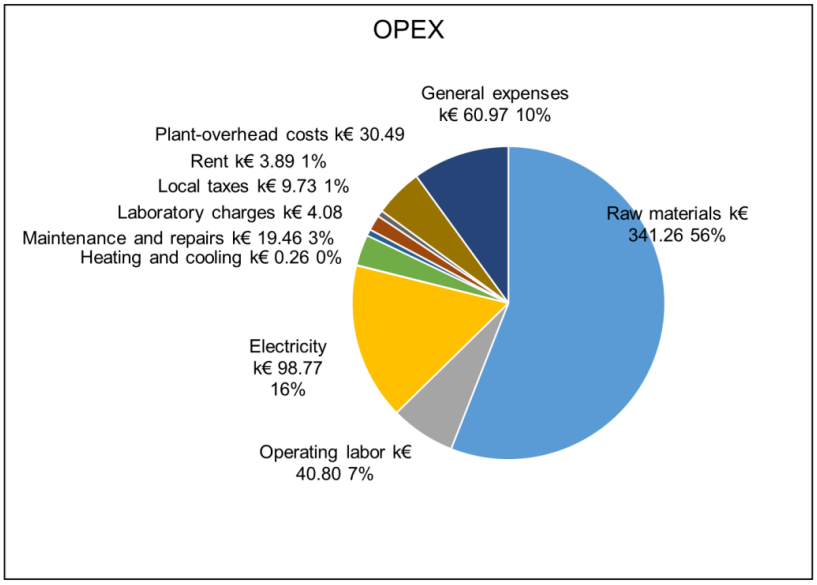

(b)

Figure 6.9: *(a) CAPEX and (b) OPEX for the RWGS reaction (ideal energy case)*

In the case of the plasma-assisted methanol synthesis from CO_2, the purchased cost equipment dictates the total CAPEX with a contribution of 46%, out of which 72% comes from the plasma reactor assembly cost. The total CAPEX estimated is € 1.61M, and capital investment per ton of methanol is € 3.4k. Owing to the fact that a low-per-pass yield of methanol is given, recycling cost dominates the OPEX with a share of 36% and a value of almost € 1.5M. The electricity required for plasma-process has the second largest fraction of the OPEX (2%) accounting for € 0.91M. The total operating cost is estimated to be about € 3.21M resulting in a production cost of 911 €/t of methanol. The high operating cost via the plasma-assisted process obtained resonates the findings in prior cost estimation studies of plasma-assisted nitrogen fixation processes, where the operating cost for the conventional route was found to be multiple times lesser [31]. The low selectivity towards methanol causes two issues, low per pass yield, which requires a high rate of recycling, and high by-products formation, which consumes expensive green hydrogen. These issues are reflected in high OPEX. Here the ratio of CAPEX to OPEX

is very low (0.5) which means that even a less investment plant requires excessive operating cost, making it less attractive for investors.

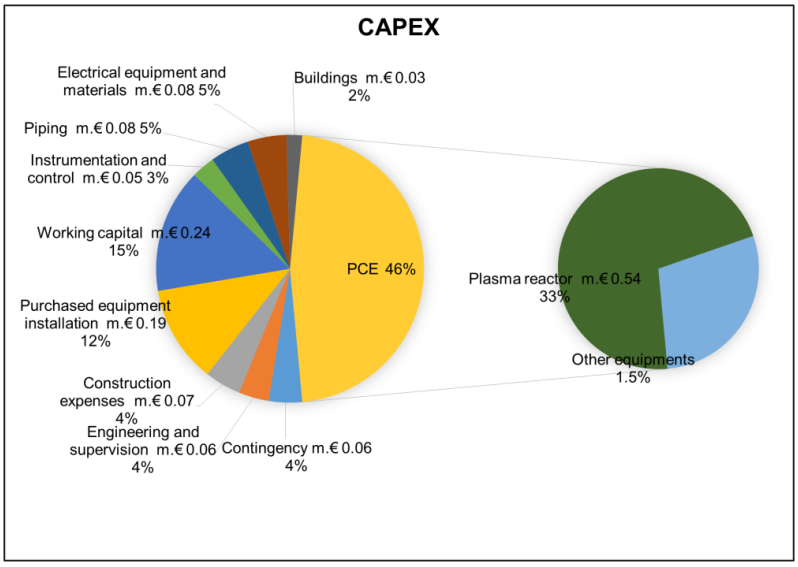

(a)

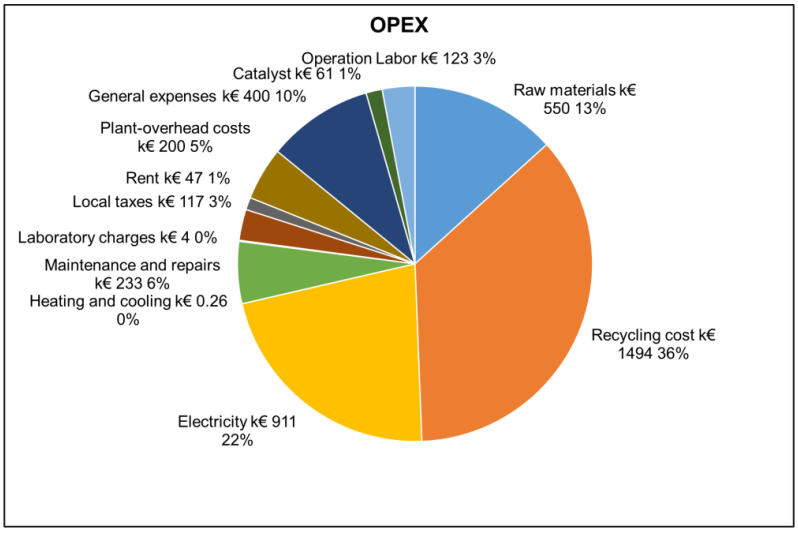

(b)

Figure 6.10: *(a) CAPEX and (b) OPEX, for the methanol synthesis (ideal energy case)*

In the cases of RWGS and methanation the energy considered for the expenditure calculations is not very far from the ideal case energy. However, in the case of methanol synthesis, the ideal case energy is a magnitude low. This will not forecast a reasonable cost estimation. Hence it is important to consider the experimental energy value of the cost analysis as well and then compare them both of them. In the case of plasma-assisted methanol synthesis considering the experimental energy consumption, purchased cost equipment contains a big share from the total CAPEX with a contribution of 47%, out of which 97% comes from plasma reactor assembly cost. The total CAPEX estimated is €11.7M, and capital investment per ton of methanol is € 24k. Owing to the fact that low per pass yield of the methanol, recycling cost dominates the OPEX with a share of 37% and a value of almost € 1.5M. Electricity required for plasma-process has the second largest fraction of the OPEX (23%) accounting for € 0.91M. The total operating cost is estimated to be about € 3.8M resulting in production cost of 1072 €/t of methanol. Comparing both cases of methanol it is clear that the operating cost does not change by a huge margin, even when the energy consumption considerations are a magnitude apart.

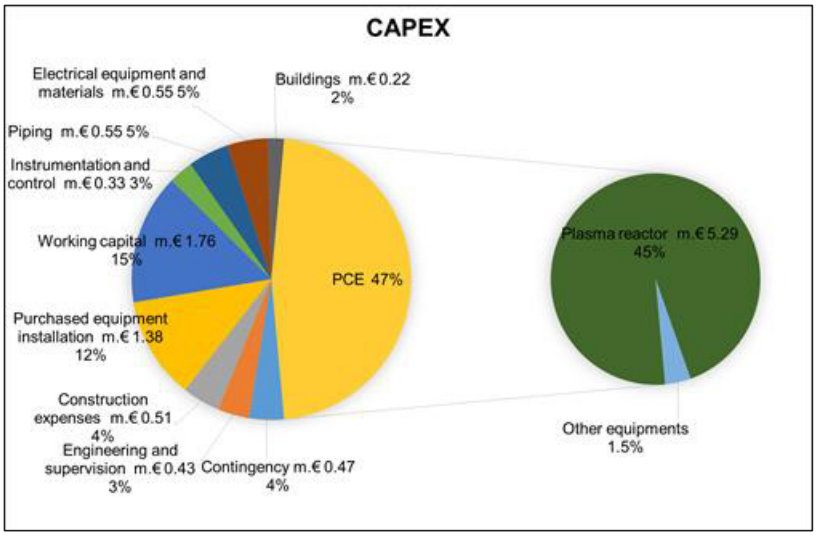

(a)

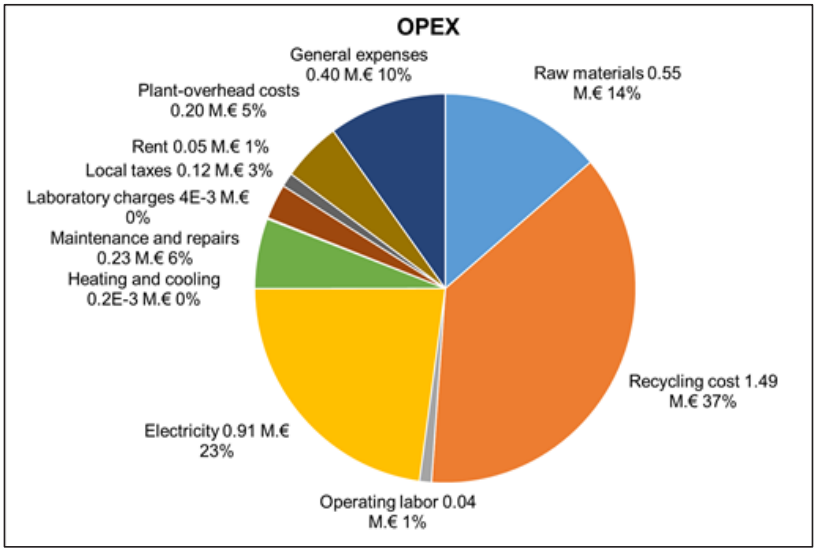

(b)

Figure 6.11: *(a) CAPEX and (b) OPEX, for the methanol synthesis (experimental case)*

The economic assessment of the plasma-assisted CO_2 methanation process estimates the total capital expenditure as € 1.88M. The main contributor to this CAPEX value is the plasma reactor system itself costing € 0.67M alone. The amount of hydrogen required for the direct CO_2 methanation is quite high, which reflects the considerable share of raw material costs among the total OPEX (54%). Besides, the electricity cost occupies 11% share of the whole OPEX which is determined to be € 2.29M. The estimated values of CAPEX and OPEX provides capital investment cost and operating cost as € 4k and €649 per ton of methane, respectively. Again, in this case, OPEX is much higher that CAPEX, which represents an investment to create useful assets for the business.

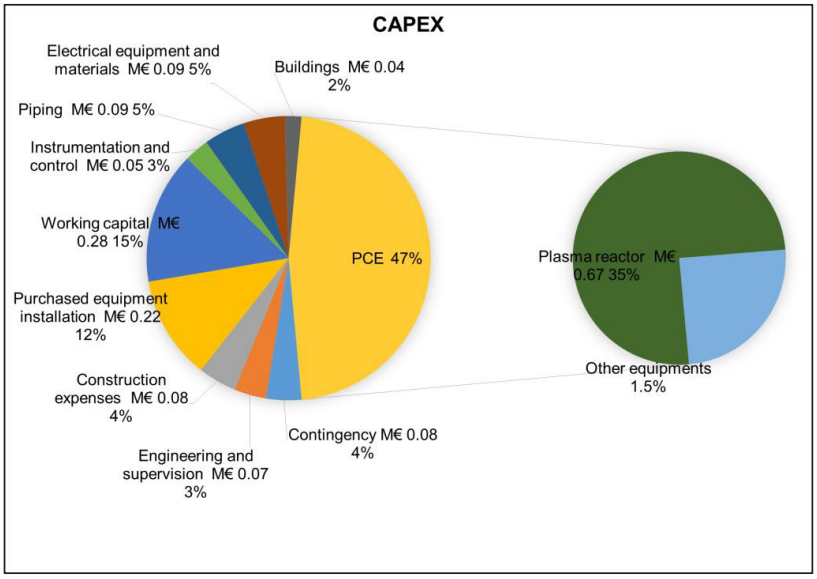

(a)

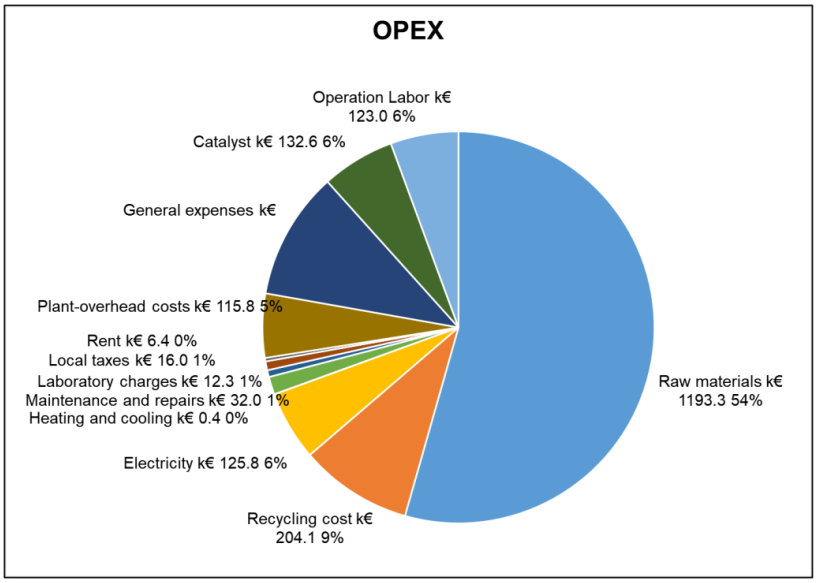

(b)

Figure 6.12: *(a) CAPEX and (b) OPEX, for the plasma-assisted CO_2 methanation. (Ideal energy case)*

The sensitivity analysis of the process simulations establishes that the improvement of the energy consumption by the plasma reaction which reflects heavily on the required amount of electricity. The experimentally obtained energy consumption is compared with the ideal scenario energy consumption case for each of these three cases. Here the plasma reactor costs, which contributes to the CAPEX, and electricity expenditures, which contributes to the OPEX, are calculated. The improved energy efficiency of the plasma process has an enormous impact on the reduction of the CAPEX and OPEX directly. The fraction of amount saved on the plasma reactor will reflect on overall CAPEX as it will reduce the purchase cost and as the factorial approach is used in determining the CAPEX, the other elements of the CAPEX will also reduce consequently. A 50% saving on the cost of the plasma reactor will effectively save about 35-40% from the total CAPEX. For RWGS and methanol synthesis cases, the share of plasma electricity cost on overall OPEX is approximately 25%; hence a 50% saving on the plasma electricity cost will save 12.5% of the OPEX. However, in methanation case the share of electricity of plasma process is only 11%; hence a 22 % savings in cost would result in merely 2-3% of total OPEX. In case of methanol and methane formation, the contribution of the recycling cost to the OPEX is quite significant. From sensitivity analysis with respect to overall product yield, it is established that the improvement in per pass yield of the product reduces the recycle rate (Table 6.6). Reduced recycle rate has two significant implications, first is proportional cost-cutting in the OPEX. Furthermore, second is more critical, as the rate of recycling reduces, the per pass material flow also reduces, Since we assume a parallel flow numbering up of plasma reactors, the reduced material flow will require fewer plasma reactor units. Savings on the purchase price of the reactor units would consequently lower the overall CAPEX.

6.4 Conclusions

A preliminary techno-economic assessment for three different plasma-assisted CO_2 hydrogenation processes described in this chapter provides primary benchmarking of these plasma processes. The mass and energy flow data obtained via Aspen simulations are used to estimate the cost of these plasma processes. The basis of the process design is determined by the desired rate of CO_2 treatment obtained via a CO_2 capture plant. The energy consumption for the plasma-assisted RWGS, methanol synthesis and CO_2 methanation, considering the experimental data, is found to be 73, 434, and 146 GJ/t of the desired products respectively. To get a perspective on these values, let's consider methanol synthesis, where the calculated energy consumption value is about 10 times more than that of a large-scale commercial facility [33]. Hence an ex-ante cost evaluation is performed considering ideal energy consumption by the plasma reactor. The economic evaluation also provides the operating cost for the plasma-assisted RWGS, methanol synthesis and CO_2 methanation 169, 911, and 649 € per ton of the product. These operating costs are monumental compared to current large scale industrial production facilities. However, it is worth noting that the plasma-assisted CO_2 hydrogenation processes are intended to represent the small-scale, decentralised chemical industry. The small-scale, decentralised process allows the production of desired chemicals to be possible near its intended application site, minimising the handling, transport and storage costs. A case study shows that the conventional methanol process in small scale in Nigeria would be profitable for local use of methanol [34]. Likewise, case of the nitrogen–fixation via plasma process, it is demonstrated that though the process is bit expensive, if implemented in a right place, for example, away from the centralised industrial cluster (in Africa) [25], a profitable business case could be built. It is essential to adopt an identical approach in case of CO_2 hydrogenation routes as well. Moreover, considering that the environmental impact of plasma processes is much less than current industrial processes, classifying them as green synthesis processes [35]. Considering the economic estimations, the direct CO_2 methanation followed by

RWGS process stand a reasonable chance for commercial exploitation for on-site supply of syngas as a raw material.

The sensitivity analysis has identified the pathway to improving the overall cost of the process via improving the energy efficiency of the plasma reaction. Thereby, considering the best-case scenario of the energy consumption, approximately 35-40% savings of CAPEX and 12-15% savings on OPEX could be achieved for RWGS and methanol synthesis cases. Whereas in case of methanation, improved energy efficiency only reflects significantly (~40%) in overall savings on the CAPEX. Nonetheless, improved plasma energy efficiency has a minimal effect on the OPEX, and hence it is important to achieve lower costs for procuring renewable hydrogen to make this process more economical. This provides another angle to industrialise the plasma processes, i.e., production of cheaper plasma reactors and power supply. Besides that, improved energy efficiency could be achieved via enhancing the plasma reaction performance and also via different configuration and design of a plasma reactor and its source. The reaction performance of a 2-dimensional gliding arc reactor was considered in this study for techno-economic evaluation. In the literature it is mentioned that using a 3-dimensional arc reactor would improve the energy performance significantly than a 2-dimensional gliding arc reactor [36–38]. Similarly, microwave plasma processes are reported to exhibit a high energy efficiency which could bring down cost as mentioned above [39–41]. The role of consumed electricity is enormous on the overall cost of the plasma processes. Hence it has been recognized that the type of electricity source, location of the plant installation will have a significant impact on operating cost as the price of electricity depends on these parameters. Since, the CO_2 hydrogenation using green hydrogen involves two high electricity consuming operations, viz. water electrolysis and plasma reaction smart operating process should be implemented based on the surge in the electricity prices. For instance, consideration of the fluctuations in electricity prices, which are lower during nights and weekends for operating procedure of the plant. To decrease the cost of products the energy-intensive processes can operate at reduced capacity during those periods of higher

electricity prices and at full capacity during lower electricity prices. The outcome of the sensitivity analysis also suggests that the capital expenditure could be minimized given the improvement in per-pass yield of the product. Nevertheless, plasma processes manifest few advantages over conventional production facilities, in terms of mild operation conditions, a green environmental profile and suitability for decentralized production. By virtue of identifying the economic and sustainability targets and windows of opportunity, the theoretical potential of the technology could be transferred to the chemical industry.

References

[1] Rahman F, Baseer M A and Rehman S 2015 *Assessment of Electricity Storage Systems* (Elsevier)

[2] Oberschmidt J, Klobasa M and Genoese F 2013 *Techno-economic analysis of electricity storage systems* (Woodhead Publishing)

[3] Sternberg A and Bardow A 2015 Power-to-What?-Environmental assessment of energy storage systems *Energy Environ. Sci.* **8** 389–400

[4] Rostrup-Nielsen J R 2002 Syngas in perspective *Catal. Today* **71** 243–7

[5] Olah G A 2013 Towards oil independence through renewable methanol chemistry *Angew. Chemie - Int. Ed.* **52** 104–7

[6] Bailera M, Lisbona P, Romeo L M and Espatolero S 2017 Power to Gas projects review: Lab, pilot and demo plants for storing renewable energy and CO_2 *Renew. Sustain. Energy Rev.* **69** 292–312

[7] Buchholz O S, Van Der Ham A G J, Veneman R, Brilman D W F and Kersten S R A 2014 Power-to-Gas: Storing surplus electrical energy a design study *Energy Procedia* **63** 7993–8009

[8] Götz M, Lefebvre J, Mörs F, McDaniel Koch A, Graf F, Bajohr S, Reimert R and Kolb T 2016 Renewable Power-to-Gas: A technological and economic review *Renew. Energy* **85** 1371–90

[9] Olah G , Prakash G K S and Goeppert A 2011 Anthropogenic chemical carbon cycle for a sustainable future *J. Am. Chem. Soc.* **133** 12881–98

[10] Artz J, Müller T E, Thenert K, Kleinekorte J, Meys R, Sternberg A, Bardow A and Leitner W 2018 Sustainable Conversion of Carbon Dioxide: An Integrated Review of Catalysis and Life Cycle Assessment *Chem. Rev.* **118** 434–504

[11] Mikkelsen M, Jørgensen M and Krebs F C 2010 The teraton challenge. A review of fixation and transformation of carbon dioxide *Energy Environ. Sci.* **3** 43–81

[12] Li D, Rohani V, Fabry F, Ramaswamy A P, Sennour M and Fulcheri L 2020 Applied Catalysis B : Environmental Direct conversion of CO_2 and CH_4 into liquid chemicals by plasma-catalysis **261** 2–9

[13] IEA 2019 Putting CO_2 to Use (www.iea.org/publications/reports/PuttingCO2touse/, accessed on 28-8-2019)

[14] Peters M, Köhler B, Kuckshinrichs W, Leitner W, Markewitz P and Müller T 2011 Chemical technologies for exploiting and recycling carbon dioxide into the value chain *ChemSusChem* **4** 1216–40

[15] Kondratenko E V., Mul G, Baltrusaitis J, Larrazábal G O and Pérez-Ramírez J 2013 Status and perspectives of CO_2 conversion into fuels and chemicals by catalytic, photocatalytic and electrocatalytic processes *Energy Environ. Sci.* **6** 3112–35

[16] 2018 *BP Technology Outlook* (https://www.bp.com/technologyoutlook2018, accessed on 28-8-2019)

[17] IRENA 2018 *Hydrogen From Renewable Power: Technology outlook for the energy transition*

[18] Glenk G and Reichelstein S 2019 Economics of converting renewable power to hydrogen *Nat. Energy* **4** 216–22

[19] IEA 2010 CO_2 Capture and Storage *IEA ETSAP: Technology Brief E14*

[20] Bietz H 2012 The global status of CCS: 2012 *29th Annu. Int. Pittsburgh Coal Conf. 2012, PCC 2012* **2** 1519–26

[21] George Olah Renewable Methanol Plant - Industrial scale production of renewable methanol from CO_2 — CRI - Carbon Recycling International (https://www.carbonrecycling.is/projects#project-goplant, accessed on 12-11-2019)

[22] Daza Y A, Kent R A, Yung M M and Kuhn J N 2014 Carbon Dioxide Conversion by Reverse Water – Gas Shift Chemical Looping on Perovskite-Type Oxides *Ind. Eng. Chem. Res.* **53** 5828–37

[23] Joo O S 2000 Camere process for carbon dioxide hydrogenation to form methanol *ACS Div. Fuel Chem. Prepr.* **45** 686–7

[24] Yao Y, Hildebrandt D, Glasser D and Liu X 2010 Fischer-tropsch synthesis using $H_2/CO/CO_2$ syngas mixtures over a cobalt catalyst *Ind. Eng. Chem. Res.* **49** 11061–6

[25] Anastasopoulou A, Butala S, Patil B, Suberu J, Fregene M, Lang J, Wang Q and Hessel V 2016 Techno-Economic Feasibility Study of Renewable Power Systems for a Small-Scale Plasma-Assisted Nitric Acid Plant in Africa *Processes* **4** 54

[26] Yamamoto T, Yang C-L, Beltran M R and Kravets Z 2000 Plasma-assisted chemical process for NO_x control *IEEE Trans. Ind. Appl.* **36** 923–7

[27] Bromberg L, Cohn D R, Rabinovich A and Alexeev N 1999 Plasma catalytic reforming of methane *Int. J.*

Hydrogen Energy **24** 1131–7
[28] Kobe K A 1958 Plant Design and Economics for Chemical Engineers *J. Chem. Educ.* **35** A506
[29] Towler G and Sinnot R 2013 *Chemical Engineering Design* (Elsevier)
[30] Chemical Engineering Plant Cost Index: 2018 Annual Value - Chemical Engineering (https://www.chemengonline.com/2019-cepci-updates-january-prelim-and-december-2018-final/ accessed on 25-8-2019)
[31] Anastasopoulou A, Hessel V and Rooij G J van 2018 *Conceptual process design of plasma-assisted nitrogen fixation through energy, environmental and economic assessment* (Eindhoven University of Technology)
[32] Baier J, Schneider G and Heel A 2018 A cost estimation for CO_2 reduction and reuse by methanation from cement industry sources in Switzerland *Front. Energy Res.* **6** 1–9
[33] Holm-Larsen H 2001 CO_2 reforming for large scale methanol plants - an actual case *Studies in Surface Science and Catalysis* **136** 441–6
[34] Stokes C A and Stokes H C 2002 the Economics of Methanol Production in Nigeria based on large low-cost gas resources *Toyo Engineering Corporation*
[35] Anastasopoulou A, Butala S, Lang J, Hessel V and Wang Q 2016 Life Cycle Assessment of the Nitrogen Fixation Process Assisted by Plasma Technology and Incorporating Renewable Energy *Ind. Eng. Chem. Res.* **55** 8141–53
[36] Nunnally T, Gutsol K, Rabinovich A, Fridman A, Gutsol A and Kemoun A 2011 Dissociation of CO_2 in a low current gliding arc plasmatron *J. Phys. D. Appl. Phys.* **44** 274009
[37] Ramakers M, Medrano J A, Trenchev G, Gallucci F and Bogaerts A 2017 Revealing the arc dynamics in a gliding arc plasmatron: a better insight to improve CO_2 conversion *Plasma Sources Sci. Technol.* **26** 125002
[38] Kalra C S, Cho Y I, Gutsol A, Fridman A and Rufael T S 2005 Gliding arc in tornado using a reverse vortex flow *Rev. Sci. Instrum.* **76** 025110
[39] van Rooij G, Akse H N, Bongers W A and van de Sanden R 2018 Plasma for electrification of chemical industry: a case study on CO_2 reduction *Plasma Phys. Control. Fusion* **60** 014019
[40] Hessel V, Anastasopoulou A, Wang Q, Kolb G and Lang J 2013 Energy, catalyst and reactor considerations for (near)-industrial plasma processing and learning for nitrogen-fixation reactions *Catal. Today* **211** 9–28
[41] Bongers W, Bouwmeester H, Wolf B, Peeters F, Welzel S, van den Bekerom D, den Harder N, Goede A, Graswinckel M, Groen P W, Kopecki J, Leins M, van Rooij G, Schulz A, Walker M and van de Sanden R 2017 Plasma-driven dissociation of CO_2 for fuel synthesis *Plasma Process. Polym.* **14** 1600126

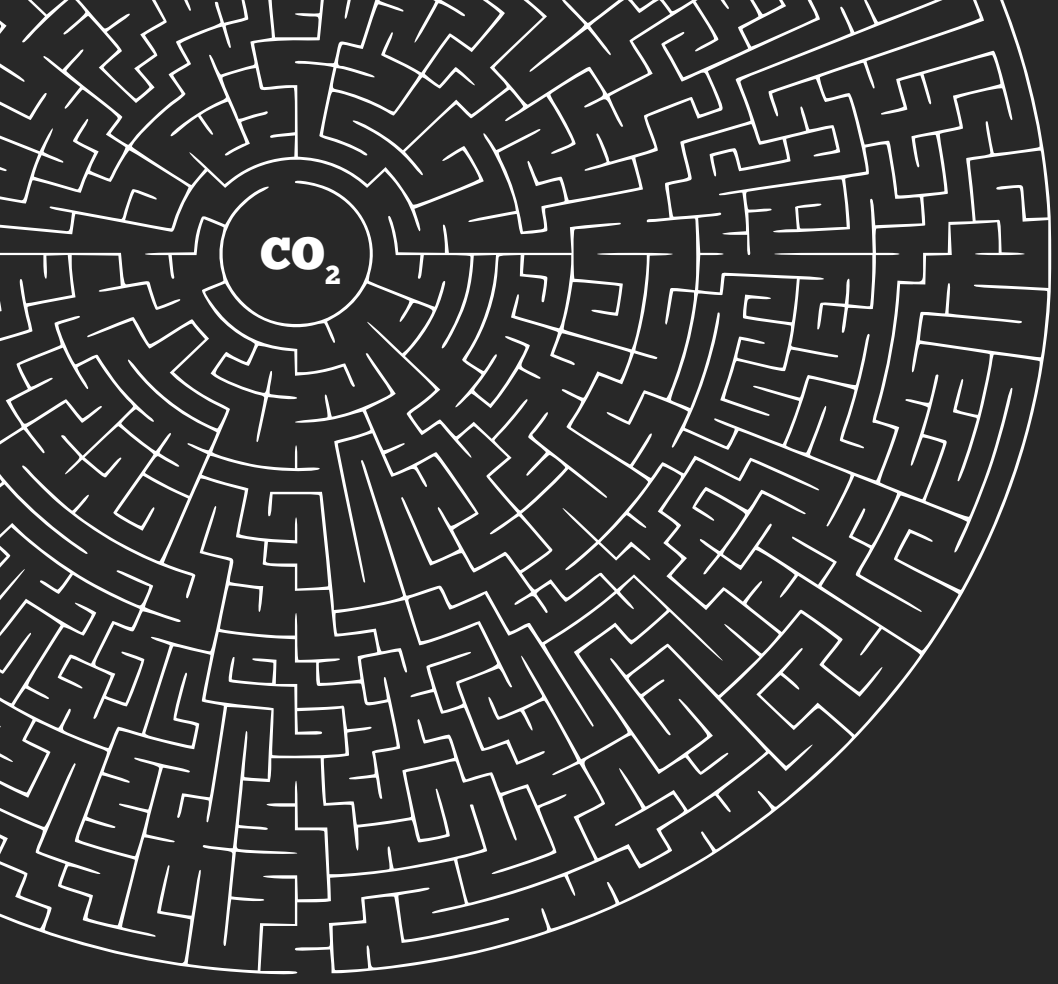
CO_2

Chapter 7

Conclusions and Outlook

Abstract

The Overview of the results, for plasma-assisted CO_2 hydrogenation, presented in this thesis is illustrated as follow with a graphical abstract.

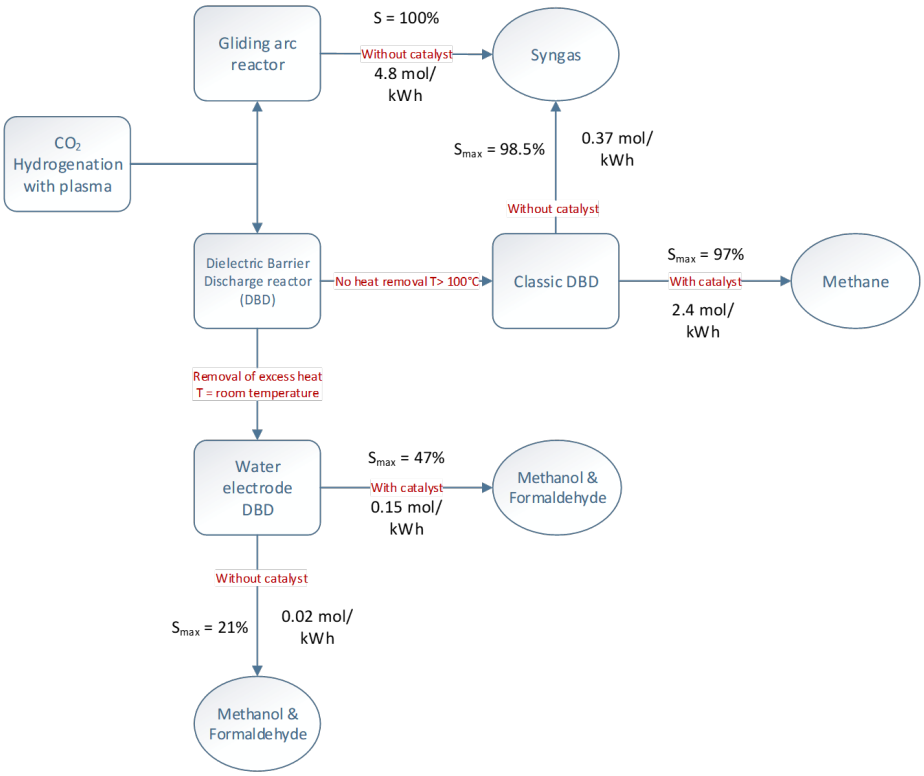

The hydrogenation of CO_2 at atmospheric pressure is an intriguing research topic as it offers various routes to obtain several key industrially relevant chemicals. On the same subject line, the three routes for CO_2 hydrogenation to desired products via a plasma discharge were studied. The present thesis explores different plasma reactor and reactor configurations along with the application of catalysts, in order to steer the selectivity towards the desired product. The product channels identified and explored within the scope of this thesis are syngas, methanol/formaldehyde and methane. A techno-economic evaluation of these three CO_2 hydrogenation plasma processes was also carried out to analyse the status quo of these processes from being industrialised.

7.1 Conclusions

Being a thermodynamically stable molecule, CO_2 does not readily react with hydrogen at atmospheric pressure and low temperatures. Investigation of CO_2 hydrogenation at atmospheric pressure plasma was performed to realise that the multiple reaction pathways to different valuable products can be undergone, depending on the type of plasma reactor, process parameters and a catalyst. The main conclusions from the study are compiled below.

7.1.1 Reverse Water-Gas Shift Reaction (RWGS)

The RWGS reaction was performed via a dielectric barrier discharge (DBD) reactor and a gliding arc reactor to produce CO, which is free of oxygen and hence can be directly implemented in further chemical synthesis.

DBD reactor for RWGS

CO_2 splitting is widely explored pathway by plasma processes to form CO molecules. However, the co-existence of O_2 makes it challenging to implement it directly in further relevant chemical processes. Hence the RWGS reaction was studied in a DBD reactor, which provides an opportunity to use the CO plasma exhaust gas streams of this study as feed to industrial processes, which use syngas for chemical synthesis. The introduction of H_2 into CO_2 feed stream showed a significant effect

on the CO_2 conversion as it forms the stable water molecules, which suppresses the backward reactions from intermediate species and facilitates the forward RWGS reaction. Several process parameters were studied such as feed gas ratio, residence time, discharge gap, and operating frequency, to optimise the reaction performance. A higher fraction of H_2 in the feed gas and higher residence time showed the higher CO_2 conversions. Reducing discharge gasp and operating frequency saw lower CO_2 conversion but better energy consumption. Further, the application of burst mode demonstrated the increase in energy efficiency. A maximum CO_2 conversion of 50% was achieved, and the maximum selectivity obtained was 98%, with 2% of methane as a by-product. It was established that 337 mmol/kWh was the optimum value of energy required for CO molecule formation in this study.

- Higher content of H_2 in feed gas mixture gives improved CO_2 conversion
- Lowering operating frequency results in improved energy efficiency
- Highest conversion obtained: 50% with 94% CO selectivity.
- Burst mode: best selectivity 98.7%, best energy consumption 337 mmol/kWh

Gliding arc reactor for RWGS

The reverse water-gas shift reaction was also performed using an alternate current sinusoidal gliding arc plasma reactor at ambient conditions, which saw 100% CO selectivity and significantly improved energy efficiency. The maximum conversion of CO_2 was established as 54% when operating at 3:1 ratio of H_2 to CO_2, whereas the best energy efficiency value obtained was 4459 mmol/kWh when operating at 1:1 ratio. Plasma parameters calculated using optical emission spectroscopy (OES) are used to interpret the reaction mechanism of the RWGS in a gliding arc reactor. The electron density calculated using H_α emission was in the range of 10^{15} cm^{-3} and the rotational temperature calculated using OH (A-X) band was 3250 K, which represents a typical gliding arc discharge. From OES of the gliding arc discharge, the diminished chemiluminescence signifying CO oxidation to CO_2 was observed as

compared to DBD discharge for the same reaction, which explains the high energy efficiency of gliding arc plasmas.

- The selectivity of CO is 100%
- At 3:1 ratio of H_2 to CO_2, highest conversion obtained: 54%
- At 1:1 ratio of H_2 to CO_2, highest energy efficiency: 4.46 mol/kWh
- OES results: $n_e \sim 10^{16}$ cm^{-3}, T_{rot} is 3250 K

7.1.2 Direct CO_2 Methanation in DBD Plasma Reactor

The effects of different support materials and Rh/γ-Al_2O_3 catalyst in plasma discharge using a DBD reactor were investigated. The plasma discharge packed with support materials showed improved CO_2 conversion compared to an empty reactor with plasma discharge, but no significant effect on CH_4 selectivity and high selectivity towards CO were observed. These selectivities were completely inverted by the implementation of Rh/γ-Al_2O_3 catalyst in the plasma discharge with 97% and 2%. By implementation of burst mode, it can be inferred that CO_2 conversion decreases and CH_4 selectivity increases by a small margin. However, a humungous improvement in the energy efficiency was obtained, 2.1 mol/kWh of CH_4 being produced. The results of Rh/γ-Al_2O_3 catalyst plasma reaction were used to predict a reaction mechanism for plasma-catalytic direct CO_2 methanation, considering characteristic CO and H_2 adsorption on Rh surface. It was demonstrated that by using the plasma in conjunction with a catalyst allows the CO_2 to get activated and additionally accelerates the overall reaction to occur at the atmospheric pressure and lower temperatures.

- Blank reactor and only support material with plasma: S_{CO} >92%, S_{CH4} <7%
- Rh/γ-Al_2O_3 with plasma: S_{CO} <4%, S_{CH4} >95%
- Highest CH_4 yield obtained (Rh/γ-Al_2O_3 with plasma): 65% (S_{CH4} = 96%)
- Lowering residence time improved selectivity and energy efficiency

- Burst mode (Rh/γ-Al_2O_3 with plasma): highest energy efficiency obtained 2.1 mol/kWh, highest S_{CH4} 97.3%

7.1.3 Water-Electrode DBD for Methanol/ Formaldehyde Synthesis

Reactor design and configuration are fundamental parameters to the DBD reactor. With the traditional DBD configuration, it is challenging to produce methanol at ambient conditions; however using a new design of water-electrode DBD, methanol synthesis was achieved at ambient conditions. This is evident by the 21% selectivity towards liquid products when the reaction was carried out without any catalyst using a burst mode plasma. When the plasma discharge was packed with Pd-Au/γ-Al_2O_3 catalyst, methanol along with the formaldehyde showed a maximum total selectivity of 47%. It shows that the use of water-electrode reactor can be used to direct the selectivity towards desired methanol and formaldehyde. The energy consumption of the reaction was found to be 147 mol/kWh of liquid products. This value is less than a value reported in the literature; however simultaneous synthesis of formaldehyde makes this methanol synthesis process an attractive route to explore further.

- Methanol and formaldehyde identified in the liquid product
- Blank reactor with plasma : 9% liquid product selectivity
- Blank reactor with plasma (burst mode): 21% liquid product selectivity
- Highest CO_2 conversion by Pd-Au/γ-Al_2O_3 with plasma: 49% (S_L = 29%)
- Highest liquid product selectivity by Pd-Au/γ-Al_2O_3 with plasma: 47% (X_{CO2} = 24%)

7.1.4 Techno-Economic Evaluation

The techno-economic evaluation was performed to realise the aforementioned plasma-assisted CO_2 hydrogenation processes for a small-scale plant operating to treat 2kt of captured CO_2 annually. A model is made using Aspen Plus for process design of the plasma-assisted CO_2 hydrogenation. This model considers H_2 production from water electrolysis and CO_2 production from capturing. The capacity of the process is defined through the CO_2 capture capacity data from chemical industries. Use of parallel reactor array of plasma reactor is assumed instead of scaling it up. The mass and energy analysis based on the process simulations has revealed the plasma energy consumption considering experimental data is 49 GJ/t of CO for the RWGS process, 367 GJ/t for the methanol synthesis process and 55 GJ/t for CO_2 methanation process. Moreover, the plasma energy consumption considering best case scenario (ideal plasma energy efficiency) is 22.5 GJ/t of CO for the RWGS process, 37.5 GJ/t for the methanol synthesis process and 28 GJ/t for CO_2 methanation process. It was found that the main costs of synthesis, in all cases, are hydrogen production and applied plasma power. Cost-analysis was performed using an ex-ante approach where ideal plasma energy efficiency was considered. The operating costs for the plasma-assisted RWGS, methanol synthesis and CO_2 methanation are 169, 911 and 649 € per ton of the product respectively, whereas the capital investments are 2.4, 4 and 3.4 k€ per ton of the product, respectively.

- Plasma energy consumption (experimental): 49 GJ/tCO, 367 GJ/tCH_3OH, 55 GJ/tCH_4
- Plasma energy consumption (ideal): 22.5 GJ/tCO, 37.5 GJ/tCH_3OH, 28 GJ/tCH_4
- Operating cost: 169 €/tCO, 911 €/tCH_3OH, and 649 €/CH_4
- Capital investment: 2.4 k€/tCO, 4 k€/tCH_3OH, and 3.4 k€/CH_4

7.2 Outlook

In the light of the present results, it seems that the hydrogenation of CO_2 at low temperature could be a realistic solution for the control of increasing emissions of CO_2, in spite of the fact that more research should be carried out in order to reach the optimal reaction conditions to improve the catalytic performances It was demonstrated that a steady RWGS reaction could be performed using a GA reactor. As it is mentioned in the literature that using a 3-D geometry for the arc discharge improves energy efficiency [1,2]. Therefore, a six electrode gliding arc reactor was designed and fabricated based on a 3-phase 6-electrode design [3]. Preliminary tests with Ar confirm the randomness of arc formations. A simple electrical circuit operated with AC sinusoidal power supply, which is already being used commercially for plasma treatments, can make its implementation easy.

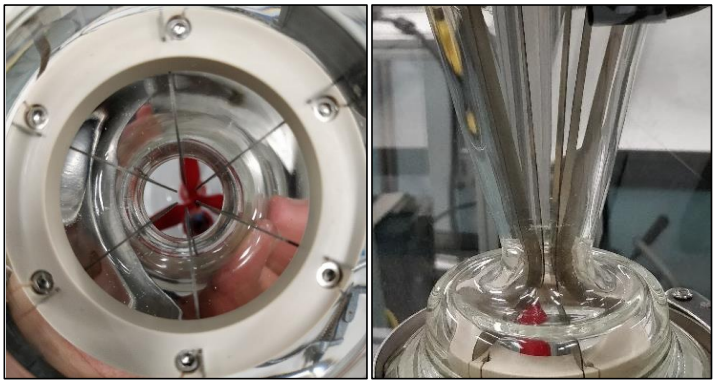

Figure 7.1: *Geometry of a six electrode gliding arc plasma reactor*

In this thesis, utilisation possibilities for the carbon dioxide-to syngas, methanol and methane processes were outlined, following traditional channels and new windows of opportunity [4,5]. This is now somewhat refined with the aid results and has led to point 2. Yet, we found that we can make a number of products with our approach and not only methanol. Most promising seems to be the pure CO manufacture through the RWGS reaction. This has led to the statement of point 3.

1) *Market potential*

- A literature check has been performed to get the net potential for CO_2 emissions reduction. It is reported that the anthropogenic CO_2 release amounts to 36 Gt of CO_2 in 2016 [6]

2) *Niche / future markets*

- We identified the RWGS reaction to pure CO as a promising route and are optimistic to improve the present performance (54% yield). Therefore, we like to check if this opens a market perspective. An ex-ante cost analysis performed gives an insight. By coupling it to the catalysed hydrogenation of CO to methanol (without plasma) there is a chance to achieve the goal of methanol formation via CAMERE process. As we have already a process simulation on the fully plasma-based methanol synthesis, a refined techno-economic evaluation by a combined plasma and non-plasma two-step process will help to realise the status quo.

3) *Proposal for new Windows of Opportunity: suited (niche) business cases*

- Apart from using the CO gained by the RWGS reaction for methanol as given in 2, there might be another process channel to be connected to. Gas fermentation has been identified as a suitable method to process RWGS products, i.e. a mixture of CO_2-CO-H_2 gas [7,8].

- The syngas fermentation process has advantages over a chemical process since it takes places at lower temperature and pressure, has higher reaction specificity, tolerates higher amounts of sulphur compounds, and does not require a specific ratio of CO to H_2.

- A disadvantage of gas fermentation is the slow speed of reaction. Yet, this can be changed by combination with established chemical processes. Besides, this helps to diversify the product spectra and value, as, e.g. renewable aviation fuels and synthetic rubber are reported as possible products.

References

[1] Ramakers M, Medrano J A, Trenchev G, Gallucci F and Bogaerts A 2017 Revealing the arc dynamics in a gliding arc plasmatron: a better insight to improve CO_2 conversion *Plasma Sources Sci. Technol.* **26** 125002

[2] Kalra C S, Cho Y I, Gutsol A, Fridman A and Rufael T S 2005 Gliding arc in tornado using a reverse vortex flow *Rev. Sci. Instrum.* **76** 025110

[3] Baba T, Takeuchi Y, Stryczewska H D and Aoqui S 2012 Study of 6 electrodes gliding arc discharge configuration *Prz. Elektrotechniczn* **88** 86–8

[4] Hessel V 2014 Special Issue: Design and Engineering of Microreactor and Smart-Scaled Flow Processes *Processes* **3** 19–22

[5] Hessel V, Anastasopoulou A, Wang Q, Kolb G and Lang J 2013 Energy, catalyst and reactor considerations for (near)-industrial plasma processing and learning for nitrogen-fixation reactions *Catal. Today* **211** 9–28

[6] Baumgarten S 2007 Trinidad methanol-run power fills niche needs - ICIS Explore (https://www.icis.com/explore/resources/news/2007/10/18/9071304/trinidad-methanol-run-power-fills-niche-needs/, accessed on 6-8-2019)

[7] Peters G P, Andrew R M, Canadell J G, Fuss S, Jackson R B, Korsbakken J I, Le Quéré C and Nakicenovic N 2017 Key indicators to track current progress and future ambition of the Paris Agreement *Nat. Clim. Chang.* **7** 118–22

[8] Liew F M, Martin M E, Tappel R C, Heijstra B D, Mihalcea C and Köpke M 2016 Gas Fermentation-A flexible platform for commercial scale production of low-carbon-fuels and chemicals from waste and renewable feedstocks *Front. Microbiol.* **7** 694

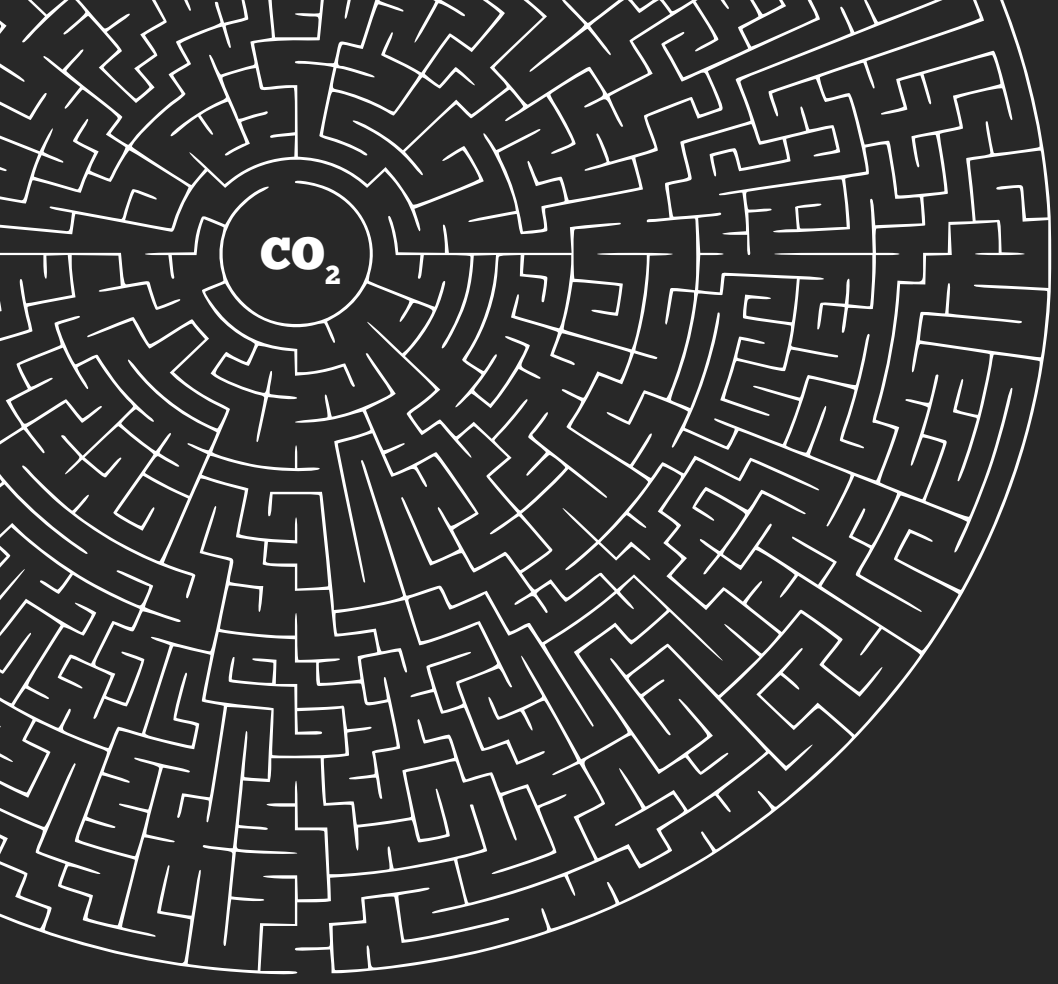
CO_2

Appendices

Appendix A1

1. Selection of dielectric barrier thickness.

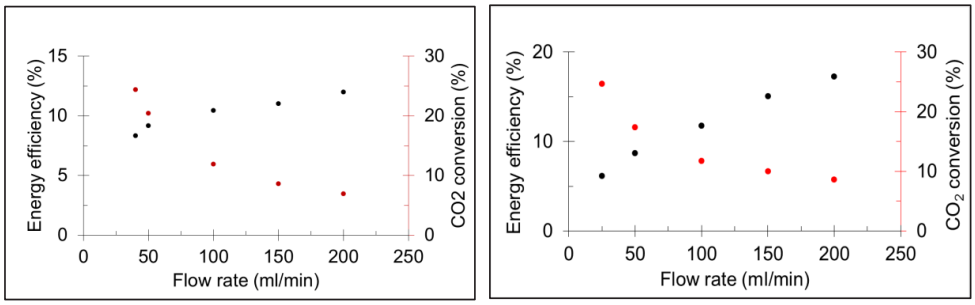

(a) (b)

a) Old reactor: applied voltage: 15kV$_{p-p}$, frequency: 50kHz, barrier thickness: 2mm, discharge gap: 1.4 mm, power 105 ± 5W

b) New reactor: applied voltage: 15kV$_{p-p}$, frequency: 30kHz, barrier thickness: 1.5mm, discharge gap: 1 mm, power 105 ± 5W

2. Selection of ground electrode for DBD reactor.

Type	Conversion %	Energy efficiency %
Mesh	7.7	9.0
Al foil	7.7	9.0
Ag paint	9.2	11.7

*corona outside the reactor is eliminated by Ag paint as the ground electrode

3. CO_2 Splitting

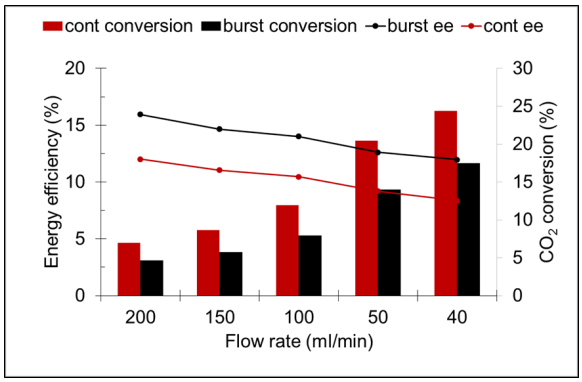

CO_2 splitting: applied voltage: 15kV, frequency: 50kHz, barrier thickness: 2mm, discharge gap: 1.4 mm

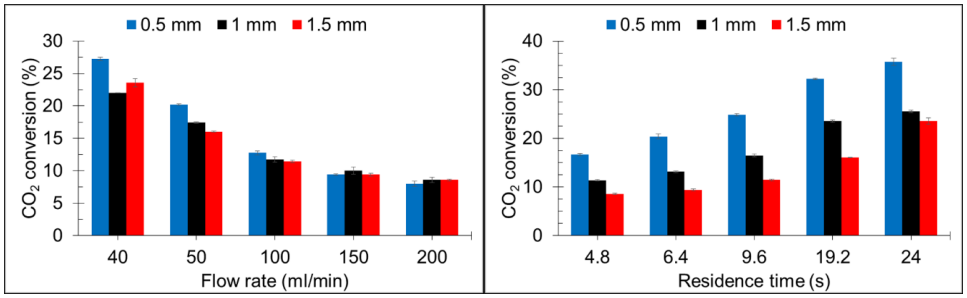

CO_2 splitting: applied voltage: 15kV, frequency: 30kHz, power 100 W (±5%)

Appendix A2

PnID: experimental setup:

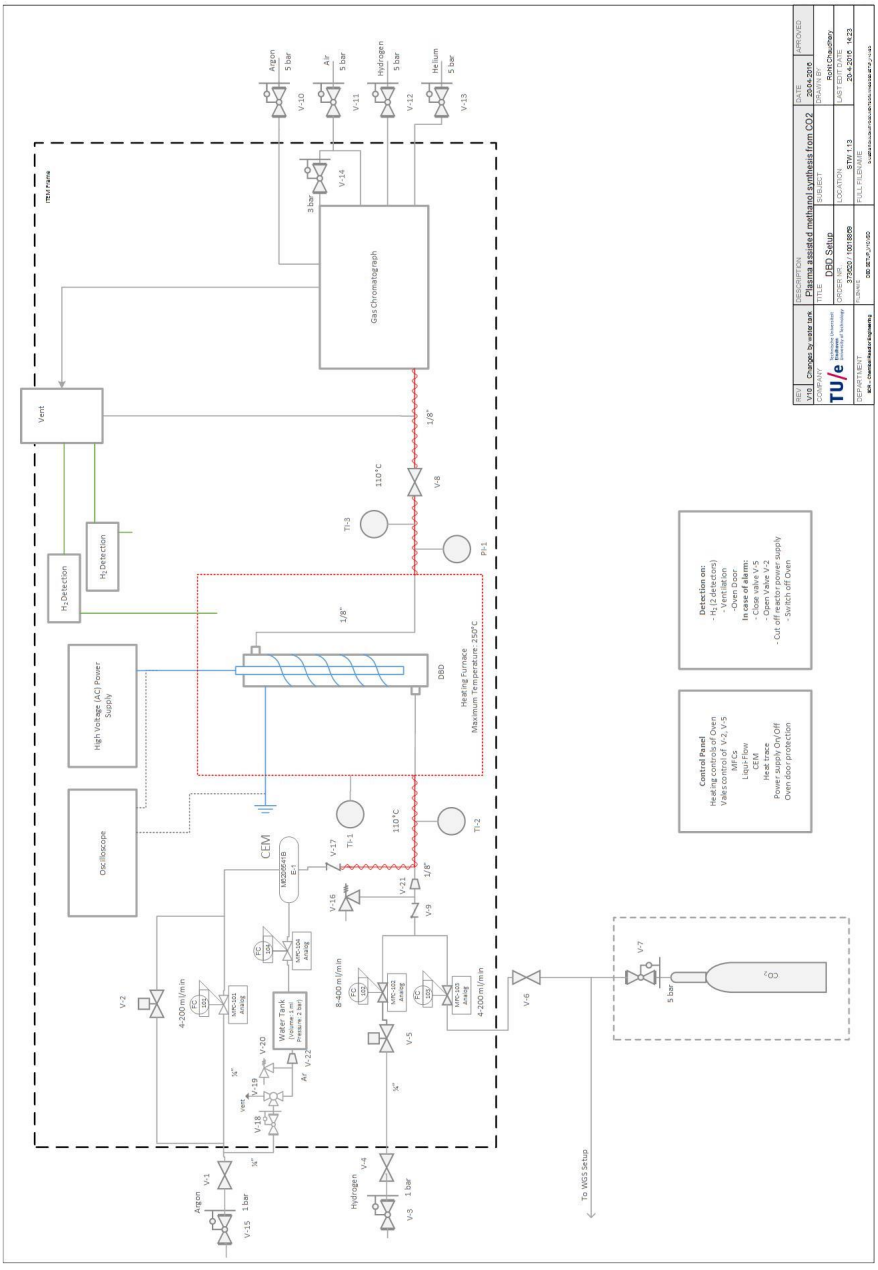

Appendix A3

Thermal image DBD

Appendix A4

OES-DBD

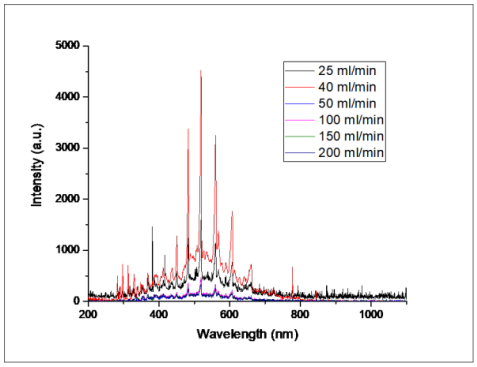

Effect of flow rate, Voltage: 15kV_{p-p}, frequency: 30kHz, CO_2 only

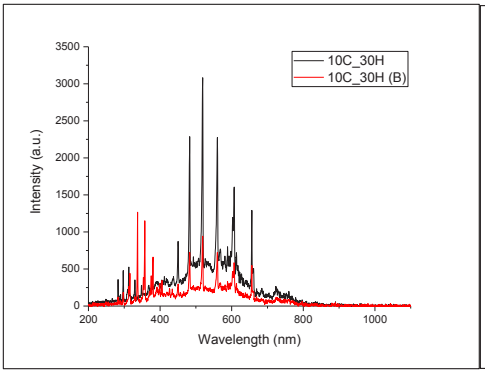

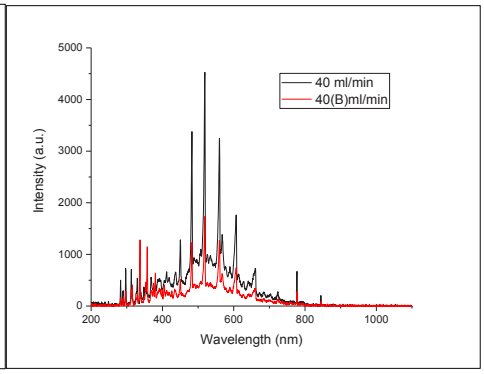

Effect of H_2 addition and burst mode, Total Flow: 40 ml/min, Voltage: 15kV_{p-p}, frequency: 30kHz

A

Appendix A5

OES calibration

I_{plasma} (λ) : actual experimental measurements with OES

f_{cal} (λ) : $\frac{Calibration\ curve\ (\lambda)}{I_{meas,cal}-I_{dark}}$ → $\frac{(data\ from\ the\ lamp)}{(\ from\ measurement\ of\ lamp)}$

$I_{plsama,cal} = I_{plasma}$ (λ). f_{cal} (λ)

Absolute Y-Axis:

Cal curve (λ) is in (MJ/cm²/nm)

$I_{meas,cal}$ (λ) is in [counts] (more accurate → [count/pixel])

f_{cal} (λ) should be in MJ/(counts/pixel) … (A certain number of counts on a pixel corresponds to a certain number of photons)

f_{cal} (λ) = $\frac{cal\ curve\ (\lambda)}{(I_{meas,cal}-I_{dark})/(A_{fiber}.t_{integration})} x(\frac{nm}{pixel})$ … A_{fiber} (um²), $t_{interaction}$ (s)

Appendix A6

T_e determinations

$$\frac{E_{ion}}{kT_e} = \ln(k_0 n_a \tau_{loss})$$

In this equation only E_{ion} is significant affected by the gas composition, hence roughly it can be stated as $E_{ion} \propto T_e$

Appendix B

Appendix B1

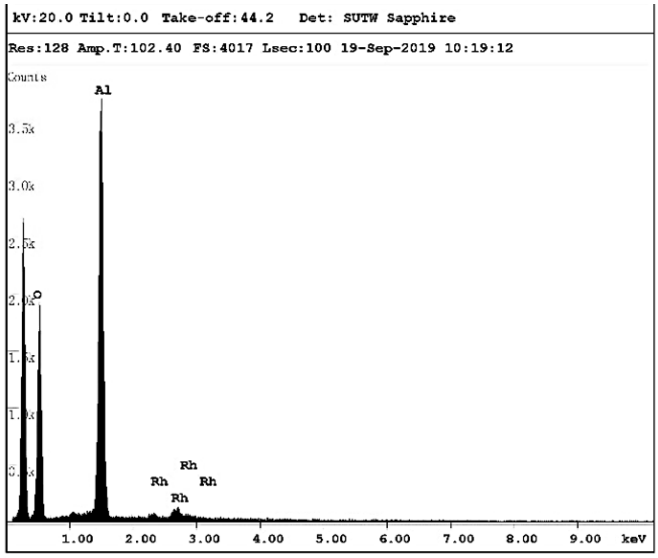

EDAX ZAF Quantification (Standardless)
Element Normalized
SEC Table : Default

Element	Wt %	At %	K-Ratio	Z	A	F
O K	47.52	62.03	0.1892	1.0425	0.3818	1.0007
AlK	47.85	37.03	0.3529	0.9707	0.7594	1.0005
RhL	4.64	0.94	0.0345	0.7944	0.9378	1.0000
Total	100.00	100.00				

Element	Net Inte.	Bkgd Inte.	Inte. Error	P/B
O K	97.65	1.50	1.03	65.10
AlK	245.08	2.96	0.65	82.80
RhL	7.56	3.24	4.96	2.33

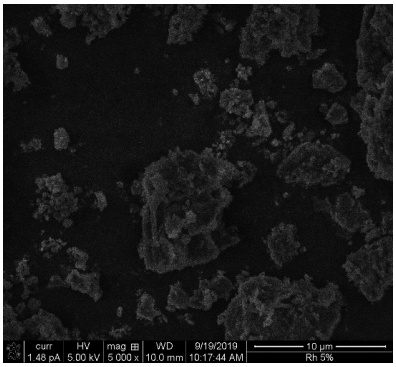

SEM –EDX for 5% Rh/γAl_2O_3

Appendix B2

Support	Support size fraction [µm]	Pressure drop [mbar]	Conversion [% CO_2]
Al_2O_3	500-630	73	12.8
	630-850	84	13.1
TiO_2	500-630	56	2.70
	630-850	28	3.18

Appendix B3

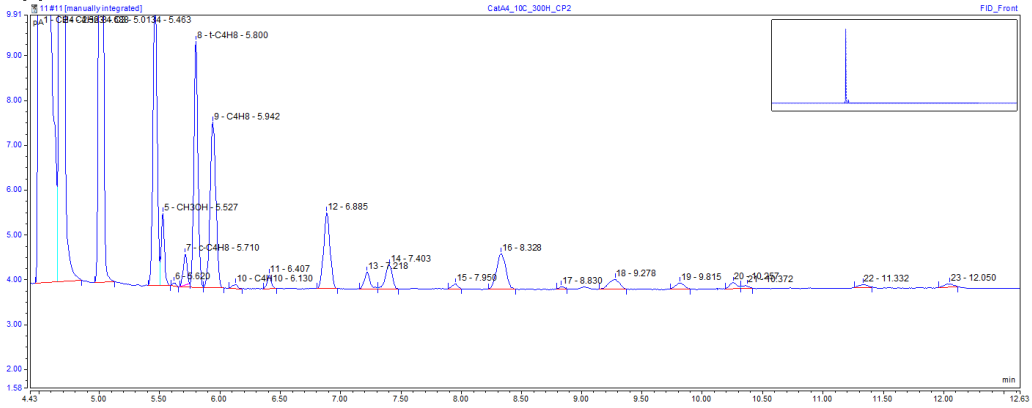

Gas chromatograph shows 20+ products on FiD detector, Rh-Ag/γ-Al_2O_3; 200ml/min; 30kHz, 15kV

A

Appendix B4

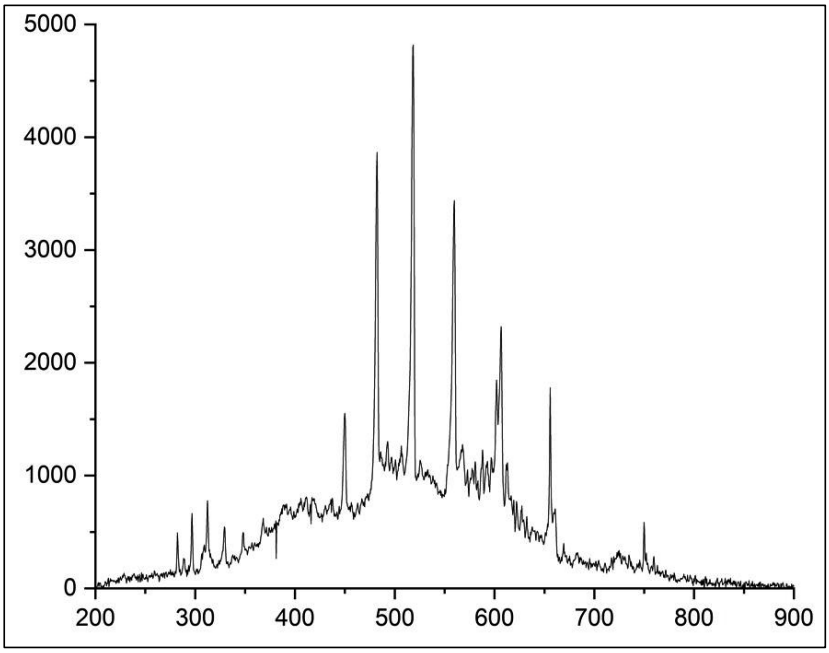

OES spectra: water electrode DBD, CO_2 hydrogenation, 15kVp-p, 30 kHz, 40 ml/min, 3:1 ration of H_2 and CO_2

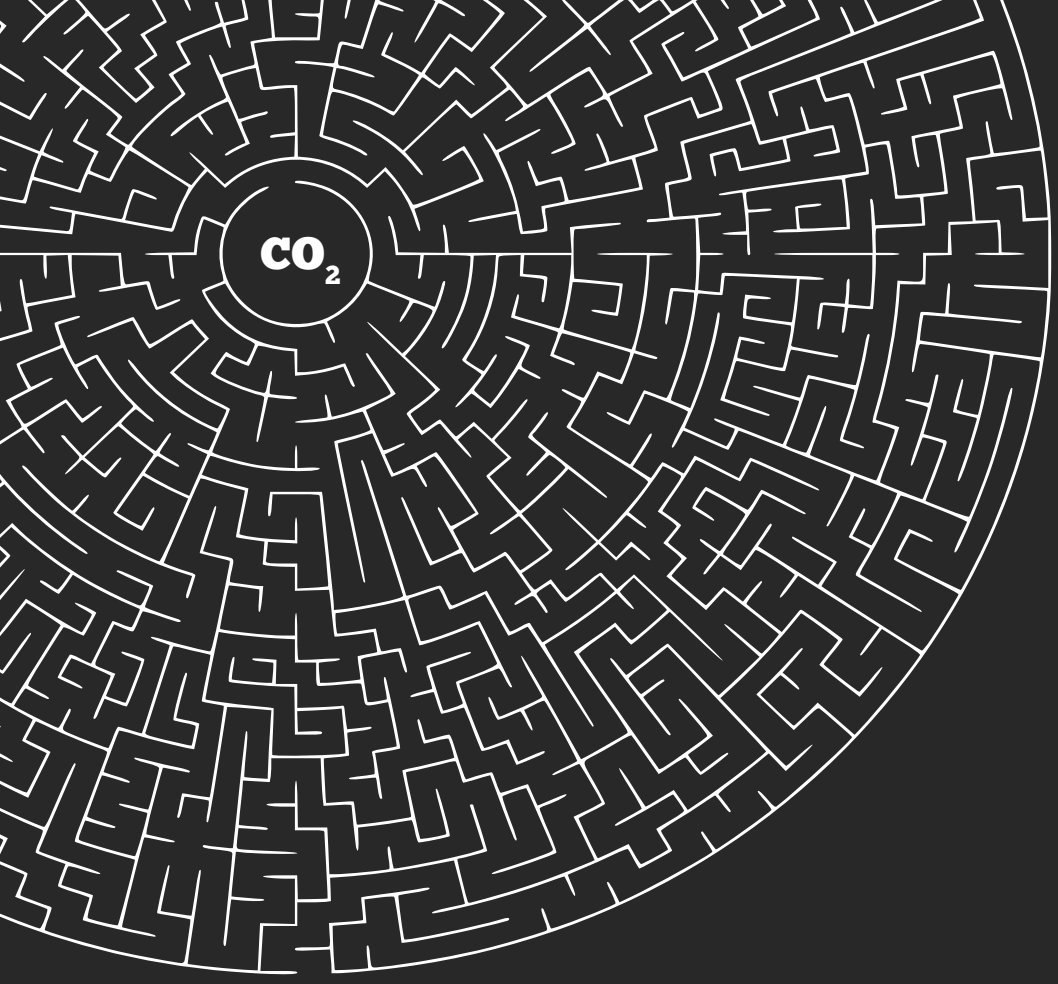
CO_2

Research output

Journal Publications

- **Chaudhary, R.**, van Rooij, G., Li, S., Wang, Q., Hensen E., Hessel, V., Low-temperature, atmospheric pressure reverse water-gas shift reaction in dielectric barrier plasma discharge, with outlook to use in relevant industrial processes, Submitted to Chemical Engineering Science.
- Ma, X., Li, S., Ronda-Lloret, M., **Chaudhary, R.**, Lin, L., van Rooij, G., Gallucci, F., Rothenberg, G., Raveendran Shiju N. & Hessel, V., Plasma Assisted Catalytic Conversion of CO_2 and H_2O Over Ni/Al_2O_3 in a DBD Reactor, 2018, Plasma Chemistry and Plasma Processing, 39(1), 109-124.
- **Chaudhary, R.**, van Rooij, G., Peeters, F. Li, S., Hessel, V., Ambient pressure Reverse water-gas shift reaction non-equilibrium gliding arc plasma discharge, in preparation.
- **Chaudhary, R.**, van Rooij, G., Li, S., van den Broeke, P., Hessel, V., Techno-economic feasibility studies of plasma assisted CO_2 hydrogenation processes, in preparation.
- **Chaudhary, R.**, van Rooij, G., Li, S., Hessel, V., CO_2 methanation reaction using an atmospheric pressure plasma with $Rh/\gamma\text{-}Al_2O_3$ catalyst, in preparation.
- **Chaudhary, R.**, van Rooij, G., Li, S., Hessel, V., Prospects of ambient condition plasma-assisted direct CO_2 hydrogenation to methanol, in preparation.

Oral Publications

- **Chaudhary R.**, Li, S., Peeters F. , van Rooij G., Hessel V., Conference On Cold Plasma Sources and Applications, Ypres, Belgium, from 19-23 November 2018.
- **Chaudhary R.**, Li, S., van Rooij G., Hessel V., 23rd International Symposium on Plasma Chemistry, Montréal, Canada, 30 July – 4 August, 2017.
- **Chaudhary R.**, Li, S., van Rooij G., Hessel V. Renewable Energy Driven Chemistry at DIFFER in Eindhoven on 5 April 2017.

Poster Publications

- **Chaudhary R.**, van Rooij G., Hessel V., Chemistry as Innovating Science 2016 (CHAINS 2016), 6-7 December 2016, Veldhoven, Netherlands.
- **Chaudhary R.**, Wang Q., Hessel V., Chemistry International Workshop on Plasmas for Energy and Environmental Applications (IWPPEA) 21-24 August 2016, Liverpool.
- **Chaudhary R.**, Wang Q., Hessel V.NWO symposium 'Research challenges in harvesting and converting solar energy, September-2015, DIFFER.

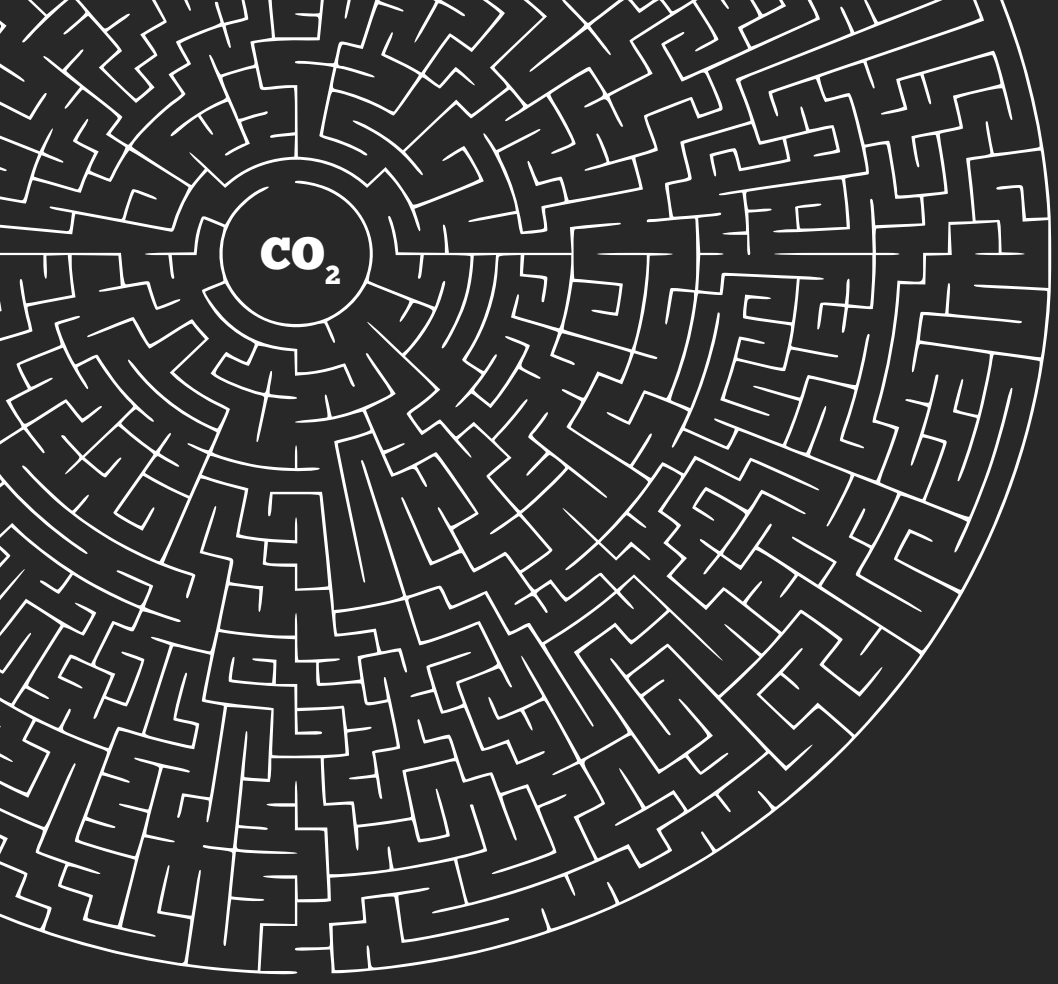
CO_2

Acknowledgements

The journey through PhD has been a genuinely life-changing experience. It would not have been possible to finish this journey without the support, assistance and guidance from so many people around me.

First and foremost, I express my deepest gratitude and appreciation to my promoter, Prof. Volker Hessel. I thank you cordially for providing me the opportunity to pursue PhD under your guidance. You always backed my ideas and proposals with the trust and confidence which proved to be driving force behind the success of the results we obtained from the research. I personally and professionally learned a lot from you during my time at TU/e. Despite being in Australia during my last year at TU/e, the time difference was never a problem for our Skype meetings and discussions. I learned a lot about firm dedication to the work from your example, as you helped me even though it was 3 am in Australia. It was a great pleasure to work with you.

I would like to express my gratitude to Dr. Qi Wang, who was my first contact at TU/e and who selected me for this position. Dear Qi, I am thankful for your supervision during my early stages of my PhD. Your support and encouragements during these times helped me build and develop the whole structure of my PhD research.

I am deeply indebted to Prof. Gerard van Rooij who was my co-promoter. Discussions with you have been insightful. I benefited a lot from them as you helped me see the same issue from different vantage points. Your immense knowledge and experience helped me grow my interest and understanding of plasma chemistry.

I am extremely grateful to Prof. Emiel Hensen for giving encouragement and sharing insightful suggestions. You have been very helpful in providing advice and supporting me many times during my PhD. I would also like to thank the STW-Alliander committee members for their continuous constructive feedback and inputs. I want to thank Dr. Jürgen Lang for always providing valuable comments and suggestions from the industrial perspective. I want to thank Michiel Geurds for having productive discussions regarding the techno-economic assessments. I am grateful to Prof. Gunther Kolb for your comments and suggestions.

I would like to extend my sincere thanks to Dr. Peter van den Broeke. Dear Peter, it's been a great pleasure working with you for the collaboration. Conducting the study regarding such a difficult topic could not be as simple as you made this for me with your industrial experience and knowledge.

I would also like to extend my gratitude to my other committee members Prof. Whitehead, Prof. Bogaerts, Prof. van de Sanden and Prof. Gallucci, for taking the time to review my thesis and providing thorough and valuable feedback.

I am thankful to Dr. Floran Peeters for our collaborative work. I really enjoyed our long and productive discussions/ calculation sessions, where, every time I learned something new and exciting things from you. Your practical suggestions were also crucial for the optimisation of the plasma reactors. I wish you all the best on the latest professional endeavour in your life. An exceptional thanks to Dr. Sirui Li, with whom I worked during my last two years of PhD. Thank you for mentoring me daily. Your unwavering support and motivation were what I needed during the rough periods. We had many discussions on various topics which resulted in numerous new ideas, designs, and concepts. I appreciate your interest in my work and your help in the timely conclusion of my thesis. I would also like to thank Dr. N. R. Shiju, Maria and Alexander for the collaboration and knowledge sharing. I also wish to thank Tesfaye for helping me with the laser measurements with the optical emission spectroscopy.

I would like to thank Jose for all the help and support you provided during my first two years. All the formal processes were made easy because of you. I am extremely grateful to Denise for helping me with everything, especially during the submission of the thesis. I wish to thank Jannelies for having many friendly conversations especially the ones which we scheduled during morning coffee just to share our thoughts.

Now, I would like to gratefully acknowledge the help and assistance provided by Carlo, Marlies, Erik and Peter for helping me materialise my ideas into a functioning setup. Thank you, Carlo, for SEM-EDX measurements as well and Erik for always helping me with modification of the setup or with fixing the problems in the setup. Thank you Marlies for your assistance with the GC-analysis and Peter for being generously helpful towards any issue in the lab. Many thanks to all of you for helping me solve all the problems I had in the lab throughout my PhD and making my life (in the lab) much

easier. I would also like to thank Paul Aendenroomer, Paul Beijer and Peter Minten for technical assistance.

I would like to thank my SCR (now SPE) group and all the group members, current as well as past, with whom I had pleasure sharing the time, especially Vishnu, Jasper, Amin, Alexi, Arnab, Arturo, Jose, Teresa, Ria, Stefan, Lakshmiprasad Pala, Pia, Anke, Mytro, Slavisa, Hamid, Chenyue, Arash and Alejo. I will cherish the special moments we had during the coffee time and group outings. I would like to thank Dr. M. F. Neira d'Angelo, Dr. Timothy Noël and Dr. John van der Schaaf for their advice during our short conversations.

I genuinely admire and appreciate my best friend Liang for being an ideal officemate during my PhD tenure. I was very fortunate to share the office with you. We shared numerous moments from lunch to coffee break, from attending borrels to going on trips, from sharing our problems to helping each other in the lab, and I enjoyed all of them. I learned a lot from you during this time, mainly from the way you work, non-stop! Along with the professional relationship we formed during this period, the friendship we developed will be cherished forever by me. I wish you every success in your life and in your research and academic career.

Thanks to Smitha and Shamayita for always accompanying me during the coffee breaks (or should I say chai pani breaks ☺). We had many funny moments while discussing any random topic, and I remember most of those topics were focused on Indian food. This lead to another kind of breaks, which were a bit prolonged and included snacks as well. Apart from all the lighter moments we had, we also had quite a lot of technical discussions. I thank you, Smitha, for helping me with my process simulations doubts and thank you Shamayita for helping with my catalysis doubts. I would also like to thank Shamayita's husband Shauvik, the calmest/ most relaxed person I ever met. A very special thanks to my dear friend Katerini, you are one of the nicest and most polite people I know. I like the way you explain any topic, calmly but thoroughly. Thank you for taking out the time from your busy schedule to have discussions for our collaboration.

I am also thankful to my former and current SPF group members Olivia, Xintong, Vetrivel, Radka, Elnaz, Carlos and Marc. Xintong, it was a pleasure working with you in

the lab and experimenting with various plasma reactor configurations. Thanks, Olivia, for the technical discussions and casual conversations we had. I wish both of you all the best. I like to extend my appreciation to Radka. We worked very closely in the lab for two years, where I learned a lot from you. Also, thank you for helping me do the XRD analysis. I wish you all the imaginable success in your future endeavour. A special thank to Carlos whose help cannot be overestimated. I really admire your approach towards the research with attention to every detail. I really liked the initiative you started with Shamayita of having a catalyst group meeting, that was certainly helpful to all the members in our group doing research on catalysis. Thank you Vetrivel for the memorable moments we had while working in the lab. It was a great pleasure knowing and working alongside all of you.

Many thanks to the people with whom I shared the office during my PhD, Nathan, Brandon, Rodrigo, David and Parimala for always maintaining a comfortable office environment. A special thanks to Nathan for helping me by translating the Dutch documents and offering me advice for many things which helped me integrate better with the Dutch culture. Brandon and Rodrigo, as you joined in my very last phase of the PhD, we did not spend much time together. However, I like the positive energy you brought to the office, and I wish you all the best for your PhD.

I would also like to thank Fardous and OGO-energy course students for their hard work. I was extremely fortunate that I got a chance to supervise your projects.

I would like to thank my friends from VNIT who are currently staying in the Netherlands; Raj, Disha, Kartik, and Kamlesh. We spent a lot of time together in Eindhoven, mostly for just hanging out, getting nostalgic or having a meal together. I couldn't have imagined a few years ago that our lives will have another chapter together in another country. An extended thanks to Kamlesh for always being there for me, also all the best for your PhD.

To my friends in Eindhoven; Sayli, Riddhi, Sagar, Charu, Anuj, Chetna, Shubhendu, Carlo and Shreynal, thank you for making me feel like home in a foreign country. The Mumbai group, thank you for our unforgettable trip to Gran Canaria and all the time-pass we do on weekends. I want to specially mention my 'little' friends, Aavya and Chendu, with whom I can relive my childhood. I appreciate the time spent with you all. Moreover, I

would like to extend my gratitude to my international family in Eindhoven, Carola, Audrey, Flo, Giulia, Francesco, Musarrat, Tahsin, Megha and Saurab. It is a great pleasure having you in my life, we have shared fond memories together during many outings, barbeques and GIT events. Carola, nothing beats your warm heart and kindness, you showed to me and my wife.

No journey starts without the first step, and Prof. G. D. Yadav was the person who encouraged me to take that first step towards my journey of PhD. I am extremely grateful to Prof. Yadav for not only teaching me valuable lessons about catalysis but life in general. I was extremely fortunate for having Prof. Yadav as a guide during my graduation project. I would also like to thank Prof. S. S. Bhagvat, Prof. A. W. Patwardhan and Prof. A. V. Patwardhan for inspiring me to take a more profound interest in the Chemical Engineering research, which is helping me shape my career. I am also grateful to Dr. S. Mandavgane for his immense belief in my abilities and for his valuable advice.

I would like to thank my childhood friends Amit, Kalpesh, Aditya, Omkar, Ashwin, Viren, Shaunak, Kaustubh and my VNIT friends (Baru, Mani, Afnan, Aniruddha, Rathi, Chando, Eshana, Sathya, Arora, Laksh, Mundra, Moorjani, Patre, Somani, Rohit, Shrishail, Suharto, Suryansh, Pant, Sai, Utsav, Tanmay and Aneesh) for always being there for me. I wish to thank (Dr.) Saikiran for continually motivating me throughout my PhD tenure. I also like to express my gratitude towards my friends from ICT, Rahul, Saurabh, Gunjan and Moreshwar for the wonderful time we had in the GDY lab, and also for teaching me various aspects of catalytic research.

Finally, I would like to express my deepest gratitude to my family for unconditional love, eternal belief in me and absolute support. My mother and father provided me with a stimulating environment in our home and encouraged me to chase my dreams. My grandmother always told me to pursue happiness. I cannot express my appreciation in words towards my family. I would also like to thank all my dear relatives in India whom I always miss; Utkarsh, Anurag, Tai and Jiju, Nikhil and Ashu Dada, Madhavi and Shital Vahini, Mavshi-Kaka, Mama, Mami, Kaka-Kaku and my in-laws, especially Praju. I would also like to thank those who influenced me but are not here amongst us; my grandparents, uncles and aunts.

And last but not least, I would like to thank my wife, my soulmate and my best friend, Swapnali. You have been a dependable and great supporter of me and loved me unconditionally during my highs and lows. You were phenomenal in instilling confidence in me. You are the order to my randomness. I thank you for being my inspiration, proofreader and editor. We have travelled this far together accomplishing this milestone, and I wish to achieve many more milestones together. Again thanks for having my back during this PhD, undoubtedly, all the credit goes to you.

About the Author

Rohit Chaudhary was born on June 28th 1989 in Mumbai, India. He obtained his Bachelor in Technology in Chemical Engineering in 2011 from Visvesvaraya National Institute of Technology, Nagpur. During this period he worked on the project 'Synthesis of bio-ethanol from lignocellulose' and did an internship at 'Rashtriya Chemicals and Fertilizers, Mumbai' studying high-pressure nitric acid plant. After obtaining bachelor's degree, he joined the Master of Chemical Engineering programme at the Institute of Chemical Technology in Mumbai, India. For his graduation research project, he synthesised heterogeneous bi-metallic nano-catalysts supported on silica nanotubes and studied their application for selective glucose hydrogenation to sorbitol in a super-critical carbon dioxide medium. In June 2013 he defended his thesis 'Development of green and smart chemical processes' under the guidance of Prof. G. D. Yadav. From February 2015 he joined Micro Flow Chemistry, and Process Technology group at Eindhoven University of Technology, Netherlands under the guidance of Prof. Volker Hessel, where he worked on 'Plasma enabled Chemical Value-Product Pathways from CO_2 and H_2, Including Methanol Synthesis'. His PhD research was funded by STW (Foundation for Technical Sciences, the Netherlands)-Alliander Program on Plasma Conversion of CO_2. The results of this research are presented in this dissertation.

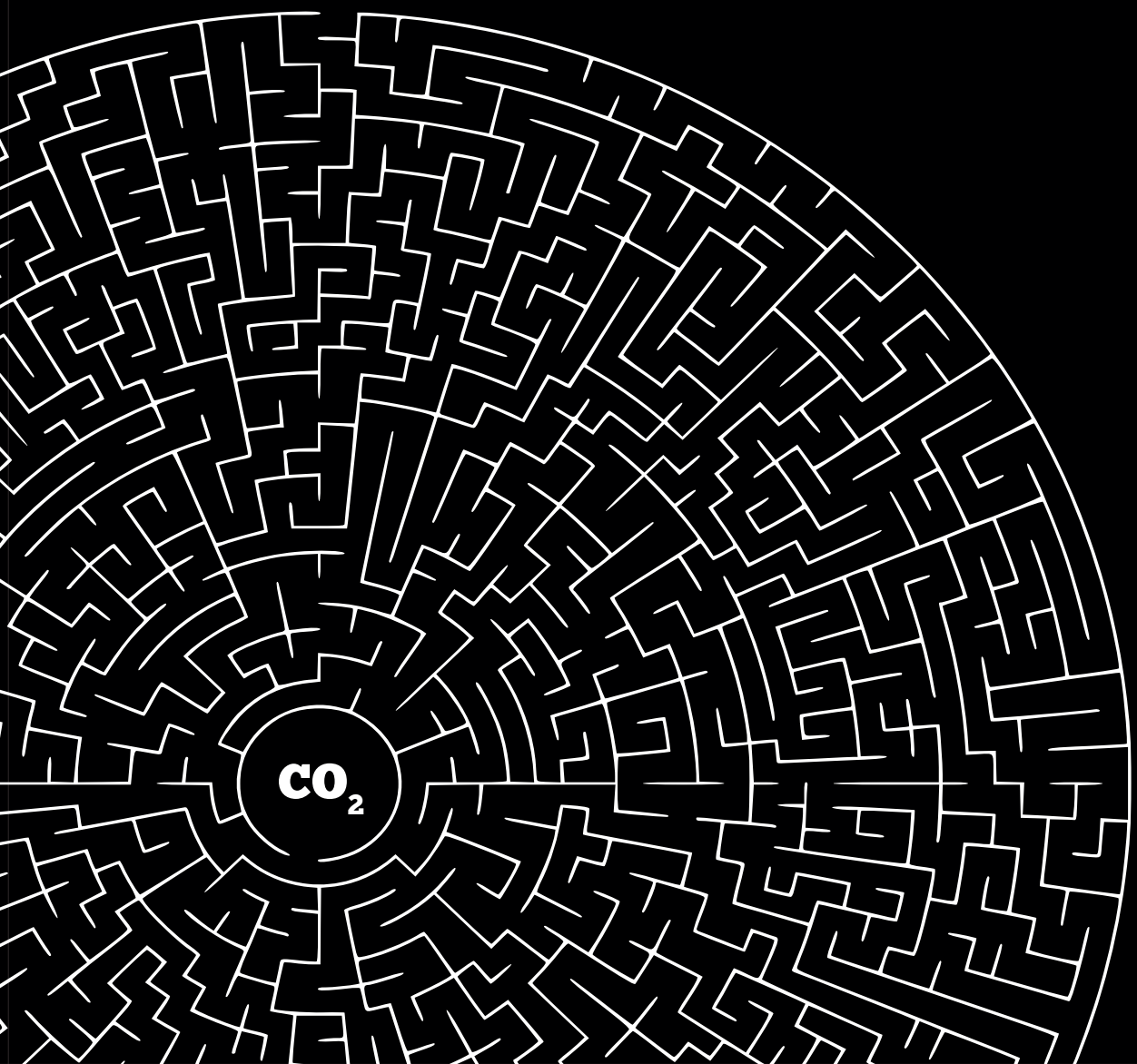
CO_2